Longitudinal changes in subcortical morphology in Huntington Disease and the relationship with clinical, motor and neurocognitive outcomes

Fiona Anne Wilkes

December 2020

A thesis submitted for the degree of Doctor of Philosophy of

The Australian National University

ANU Medical School

College of Health and Medicine

The Australian National University

© Copyright Fiona Anne Wilkes 2020

All Rights Reserved

Candidate statement

I certify that, to the best of my knowledge, the content of this thesis is my own work, unless otherwise specified, and that this thesis complies with The Australian National University Research Award Rules and has not been previously accepted for award of a degree or diploma to any other institution of higher learning. The research presented in this thesis was supported by an ANU University Research Scholarship.

Word count: 42, 474

Signed:

Date: 13/05/2021

Acknowledgements

Dedicated with thanks to my primary supervisor Jeffrey Looi, whose unwavering support and encouragement meant that I continued even when I didn't think I could, who indulged my many sidesteps along the way, and who led me by example rather than coercion into a field I didn't think possible.

Thank you also to my co-supervisors Professors Mark Walterfang, Dennis Velakoulis and Nellie Georgiou-Karistianis, who have been unfailingly kind, generous and patient. Further thanks are due to my numerous co-authors and collaborators, listed in full in the various chapters and papers, but in particular to David Jakabek, Conor Owens-Walton and Lauren Turner.

To my entire extended network of friends and family and colleagues (clinical and research), who have given so much time and love and support.

To Justin, who loved.

To my grandfather, who died more than a decade ago but in whose name I started research into neurodegenerative disease and in whose life I take inspiration for kindness, intelligence and dignity.

Finally, thank you to the people living with Huntington disease who so generously gave their time to be involved in the IMAGE-HD study.

Funding

The IMAGE-HD study was supported by the CHDI Foundation, Inc. (USA) (grant number A – 3433) and the National Health and Medical Research Council (NHMRC) (grant number 606650).

This thesis was supported by an ANU PhD scholarship, the RANZCP New Investigator Grant 2013, as well as the University of Melbourne for computer and software support.

Abstract

Huntington disease (HD) is a devastating inherited neurodegenerative disease which causes progressive motor, psychiatric and cognitive disturbances as well as neurodegeneration. Mapping the spatiotemporal progression of neuroanatomical change in HD is fundamental to developing biomeasures suitable for prognostication and to aid in development and testing of potential treatments. The neostriatum is central to HD and is known to start to degenerate more than a decade before observable motor onset. It is central to a number of frontostriatal re-entrant circuits which regulate motor control and other forms of behaviour. Changes in striatal morphology can consequently be correlated with observable clinical, motor and cognitive outcomes. However, the neostriatum is merely one part of the "hubs and spokes" of neural circuitry and neurodegeneration in HD also occurs in other areas of the brain. The hippocampus has been less fully studied in HD and has implications for neural plasticity, particularly given neurogenesis continues into adulthood in this region. Furthermore, thickness of the corpus callosum may be used as a proxy for cortical changes that are known to occur later in HD.

This thesis uses data from the IMAGE-HD study to characterise neuroanatomical changes in HD, with the aim to improve knowledge of HD-associated neurodegenerative pathways and to provide further insight to relate quantitative measures of morphology to function. A number of analytical techniques are used to investigate changes in size and shape of neuroanatomical structures and to correlate these with clinical, motor and neurocognitive outcomes.

This thesis demonstrates that shape changes in the neostriatum in HD and pre-symptomatic HD correlate with functional measures subserved by corticostriatal circuits, and identifies significant longitudinal differences in putaminal and caudate shape. Only the putamen has a significant group by time interaction, suggesting that it is a better marker for longitudinal change in pre-symptomatic HD and HD. While HD has its most marked effects on the neostriatum, it also has more subtle effects on other subcortical areas. This thesis shows surface contraction occurring in HD in the hippocampus compared to controls, although without correlations to functional measures or significant longitudinal change. Unlike these "hubs", this thesis finds that the large "spoke" of the corpus callosum is not impacted early in the HD process but becomes affected after symptom onset, highlighting the spread of neurodegeneration in other structures.

This is the first time that such robust statistical analysis of longitudinal shape change in HD has been able to be performed and shows the neostriatum, particularly the putamen, as a potentially useful structural basis for the characterisation of an endophenotype of HD. This thesis provides a more comprehensive picture of neuroanatomical change in HD by using a "hubs and spokes" approach to analyse key areas, increasing knowledge about neurodegenerative pathways and functional outcomes.

Table of Contents

List of Manuscripts

The following manuscripts were published during my PhD candidature, derived from research project material presented in this thesis:

Study One: Wilkes F.A., Abaryan, Z., Ching, C.R.K., et al. (2019) Striatal morphology and neurocognitive dysfunction in Huntington disease: The IMAGE-HD study. *Psychiatry Research: Neuroimaging 291,* 1-8.

The following manuscripts were published during my PhD candidature, derived from research project material directly related to this thesis:

Turner, L., Jakabek, D., Wilkes, F.A., et al. (2016). Striatal morphology correlates with frontostriatal electrophysiological motor processing in Huntington's Disease: An IMAGE-HD study. *Brain and Behaviour.* 2016 Jul 27;6(12):e00511. doi: 10.1002/brb3.511

The following manuscripts were published during my PhD candidature, derived from research project material indirectly related to this thesis:

Owens-Walton C., Jakabek D., Li X., Wilkes F.A., et al. (2018) Striatal changes in Parkinson disease: An investigation of morphology, functional connectivity and their relationship to clinical symptoms. *Psychiatry Research: Neuroimaging 275,* 5-13

Power B.D., Jakabek D., Hunter-Dickson M., Wilkes F.A., et al. (2017) Morphometric analysis of thalamic volume in progressive supranuclear palsy: In vivo evidence of regionally specific bilateral thalamic atrophy. *Psychiatry Research: Neuroimaging 265*,65-71

Power, B.D., Wilkes, F.A., Hunter-Dickson, M., et al. (2015). Validation of a protocol for manual segmentation of the thalamus on magnetic resonance imaging scans. *Psychiatry Research: Neuroimaging 232*, 98-105

Macfarlane, M., Jakabek, D., Walterfang, M., et al. (2015). Striatal atrophy in the behavioural variant of frontotemporal dementia: correlation with diagnosis, negative symptoms and

disease severity. *PLOS One*, DOI:10.1371/journal.pone.0129692

Looi, J.C.L., Velakoulis, D., Walterfang, M., et al. (2014). AUSSIE – the Australian United States Scandinavian Imaging Exchange: an innovative virtual integrated health research network embedded in health care. *AustPsychiatry, 22,* 260-265

List of Figures

List of Tables

List of Abbreviations

Abbreviation	Full form/explanation
ACC	Anterior cingulate cortex
AC-PC plane	Anterior commissure- posterior commissure plane
BDI-II	Beck Depression Inventory score, Version II
BDNF	Brain derived neurotrophic factor

CA1-4	Cornus ammonis subfields 1-4, cytoarchitecture of the hippocampus
CAG (triplet) repeat	Genetic change coding for polyglutamine repeat, in this document generally referring to the CAG triplet expansion within the *huntingtin* gene, although expansions also occur in other genes/disorders
CAP score	An index of degree of exposure to toxic polyglutamine repeats, based on CAG repeat length and age.
CC	Corpus callosum
CSF	Cerebrospinal fluid
DBS	Disease burden score, a marker of Huntington disease burden based off CAG repeat length and age
DG	Dentate gyrus
DLPFC	Dorsolateral prefrontal cortex
DTI	Diffusion tractography imaging
EEG	Electroencephalogram
FA	Fractional anisotropy
FDR	False discovery rate
FEF	Frontal eye fields
FIRST	FMRIB (Oxford Centre for Functional MRI of the Brain) Integrated Registration and Segmentation Tool
fMRI	Functional magnetic resonance imaging
FrSBe	Frontal Systems Behaviour Scale
FSL	FMRIB Software Library
HADS A	Hospital Anxiety and Depression Scale, Anxiety subscale
HADS D	Hospital Anxiety and Depression Scale, Depression subscale
HD	Huntington disease
Htt	Huntingtin protein
ICC	Intraclass correlation
ICV	Intracranial volume
ITI	Inter-tap interval, related to ITIPTAP and ITISTAP below
ITIPTAP	Variance in inter-trial interval in participant passed tapping,

	assess at two speeds, fast (3Hz) and slow (1.8Hz)
ITISTAP	Variance in inter-trial interval in speeded tapping
IQ	Intelligence quotient, in this thesis estimated from the National Adult Reading test
JD	Jacobian determinant
LDDMM	Large Deformation Diffeomorphic Metric Mapping
MANCOVA	Multivariate analysis of covariance
MC	Motor cortex
MD	Mean diffusivity
mHtt	Mutant huntingtin protein
MRI	Magnetic resonance imaging
MSNs	Medium spiny neurons
OCD	Obsessive compulsive disorder
OFC	Orbitofrontal cortex
PPC	Posterior parietal cortex
pre-HD	Presymptomatic Huntington disease
SCOPI	Schedule of Compulsions Obsessions and Pathological Impulses
SD	Standard deviation
SDMT	Symbol Digit Modalities Test
SGZ	Subgranular zone
SMA	Supplementary motor area
SPHARM-PDM	Spherical Harmonic Description- Point Distribution Models
SSC	Somatosensory cortex
SSRI	Selective serotonin reuptake inhibitor
symp-HD	Symptomatic Huntington disease
SVZ	Subventricular zone
UHDRS	Unified Huntington Disease Rating Scale
UPSIT	University of Pennsylvania Smell Identification Test

When once it begins it clings to the bitter end.

George Huntington

1. Introduction

1.1 Overview

Huntington disease (HD) is a devastating neurodegenerative disease, famously described by George Huntington, an American physician who wrote an account of the hereditary movement disorder in 1872 (Wexler, et al. 2016). It causes a clinical triad of progressive motor, cognitive and psychiatric symptoms, as well as observable in vivo imaging and post-mortem neurodegeneration. While the causative gene was eventually characterised in 1993 (The Huntington's Disease Collaborative Research Group 1993), unfortunately disease modifying treatments remain elusive. There is a concerted international effort to develop treatments for HD and to develop a clinical biomarker to aid in monitoring treatments and preventative measures.

Endophenotypes are "biological measures that correlate with, or predict, clinical features of brain dysfunction" (Looi, et al. 2014b). The concept was popularised in psychiatry due to the complexity of small changes in multiple genes and varying outcomes in psychiatric disorders, related to the interplay between environment and propensity, nurture and nature (Looi, et al. 2014b). This thesis uses a "hubs and spokes" neuroanatomical approach (Looi, et al. 2014b) to investigate key structures within the brain in HD with the view to developing an endophenotype and relate changes within the brain to observable clinical, motor and neurocognitive outcomes. Here, the neostriatum and hippocampus are investigated as "hubs" within the brain, followed by the major "spoke" of the corpus callosum, to develop a better understanding of the progression of neuroanatomical and related changes in HD.

Morphological analysis of these structures may provide insight into the pathophysiology and progression of HD and help with staging and monitoring progression, measuring treatment response, and targeting novel treatments.

1.2 Background/context

1.2.1 Huntington disease epidemiology and course

HD is a lethal autosomal dominant, fully penetrant neurodegenerative disease caused by an expansion of the CAG triplet (polyglutamine) repeat in the gene *huntingtin* (The Huntington's Disease Collaborative Research Group 1993). It affects approximately 6 people per 100,000 population in Australia, with prevalence in the rest of the world ranging from 0.4 per 100,000 in Asia to 7 per 100,000 in North America (Rawlins, et al. 2016). HD is characterised by progressive motor, cognitive and psychiatric disturbances, as well as considerable brain atrophy, particularly of the neostriatum (Vonsattel, et al. 1985). The adult-onset subtype of HD is most common (>90% of cases (Koutsis, et al. 2013)), where onset usually occurs in midlife and death occurs 12 to 15 years later (Vonsattel and DiFiglia 1998), most frequently by aspiration pneumonia due to motor impairment (Heemskerk and Roos 2012; Sørensen and Fenger 1992). Throughout this thesis, "HD" refers to the adult-onset form of HD.

When HD becomes clinically manifest, it frequently causes a motor disorder in the form of a chorea, dance-like movements which are uncontrolled and cause spasmodic jerking, as well as other deficits with motor coordination (Young, et al. 1986). Prior to this motor manifestation more subtle changes can be seen in cognition and motor control (Biglan, et al. 2009; Paulsen, et al. 2017; Walker 2007). As motor processes degenerate, chorea can become less

pronounced and rigidity and dyskinesia develop, eventually leading to a loss of fine and gross motor skills. There is also a decline in cognitive capacity, particularly in executive function (Walker 2007; Young, et al. 1986). Neuropsychiatric symptoms are common throughout the course of HD, including dysphoria, irritability, agitation, apathy and anxiety (Paulsen, et al. 2001), with a higher rate of depression and suicide in both premanifest and symptomatic HD (Kachian, et al. 2019) (Table 1.1). There are no disease-modifying treatments, only symptomatic treatments such as antidepressants and antipsychotics for psychiatric and behavioural symptoms and dopamine-modulating agents to attenuate chorea (Table 1.1) (Bachoud-Levi, et al. 2019; Loi, et al. 2018; Ross and Tabrizi 2011).

Table 1.1: Symptoms in HD and current treatment options (Bachoud-Levi, et al. 2019; Ross and Tabrizi 2011).

Symptoms	Treatments	Notes
Motor		
- **Chorea** - **Myoclonus** - **Dystonia, rigidity** - **Akathisia (frequently iatrogenic)** - **Gait and balance disorders** - **Swallowing disorders**	Dopamine depleting agents (or dopamine agents, depending on symptoms), anticonvulsants, benzodiazepines, muscle relaxants Cease medication if thought to be causing side effects.	Important to optimise medications due to side effects. Occupational therapy and physiotherapy extremely important. Advanced swallowing disorders may require consideration of percutaneous endoscopic gastrostomy tube.

Cognitive		
- **Reduced executive function** - **Slowed information processing** - **Language and communication disorders** - **Social cognition impairments** - **Memory disorders** - **Disorientation** - **Visuospatial and visual perceptual disorders**	No pharmacological treatment is currently recommended for cognitive symptoms. Some medications used to treat motor and psychiatric symptoms can negatively affect cognition.	Rehabilitation strategies are key. Treatment of psychiatric conditions such as depression may improve cognitive symptoms.
Psychiatric		
- **Depression** - **Anxiety** - **Obsessive compulsive behaviour** - **Irritability** - **Apathy** - **Psychosis** - **Mania** - **Impulsivity** - **Suicidal ideation and attempts**	Antidepressants, antipsychotics (also affect dopamine), anticonvulsants, mood stabilisers	Prevention of suicide includes treating risk underlying risk factors.

1.2.2 Pathogenesis of HD

CAG (polyglutamine) repeats exist in normal copies of the *huntingtin* gene, but more than 35 copies confer a risk for the development of HD, and more than 40 copies are generally associated with disease onset before the age of 65 (Chaganti, et al. 2017; Langbehn, et al. 2004; Rubinsztein, et al. 1996). Of note, although 27-35 CAG repeats are in the normal range, they are considered intermediate or unstable alleles and may expand or contract during reproduction (Sun, et al. 2017). However, while the genetic alteration accounts for approximately 50-70% of the age of motor onset, it has less to do with the later progression. A large proportion of age of onset and progression is likely related to environmental factors and other modifier genes conferring risk or protection (Rosenblatt, et al. 2006; Wexler, et al. 2004). As the gene is passed down the generations there is not infrequently an expansion of the unstable polyglutamine repeat, leading to a more severe form of the disease and an earlier age of onset. This phenomenon is known as anticipation and also occurs in other genetic diseases with similar triplet repeats, such as Fragile X syndrome and myotonic dystrophy (Teisberg 1995).

Theories as to the cause of neurodegeneration include a direct toxic effect of the mutant huntingtin protein (mHtt), as well as loss of its normal function in healthy neuronal tissue (Figure 1.1) (Morigaki and Goto 2017; Saudou and Humbert 2016). Wild-type huntingtin (Htt) is important as a major protein interaction hub and an orchestrator of converging intracellular trafficking and signalling pathways (Ratovitski, et al. 2012), has anti-apoptotic properties (Rigamonti, et al. 2000; Rigamonti, et al. 2001) and is essential for normal embryonic development (Nasir, et al. 1995)

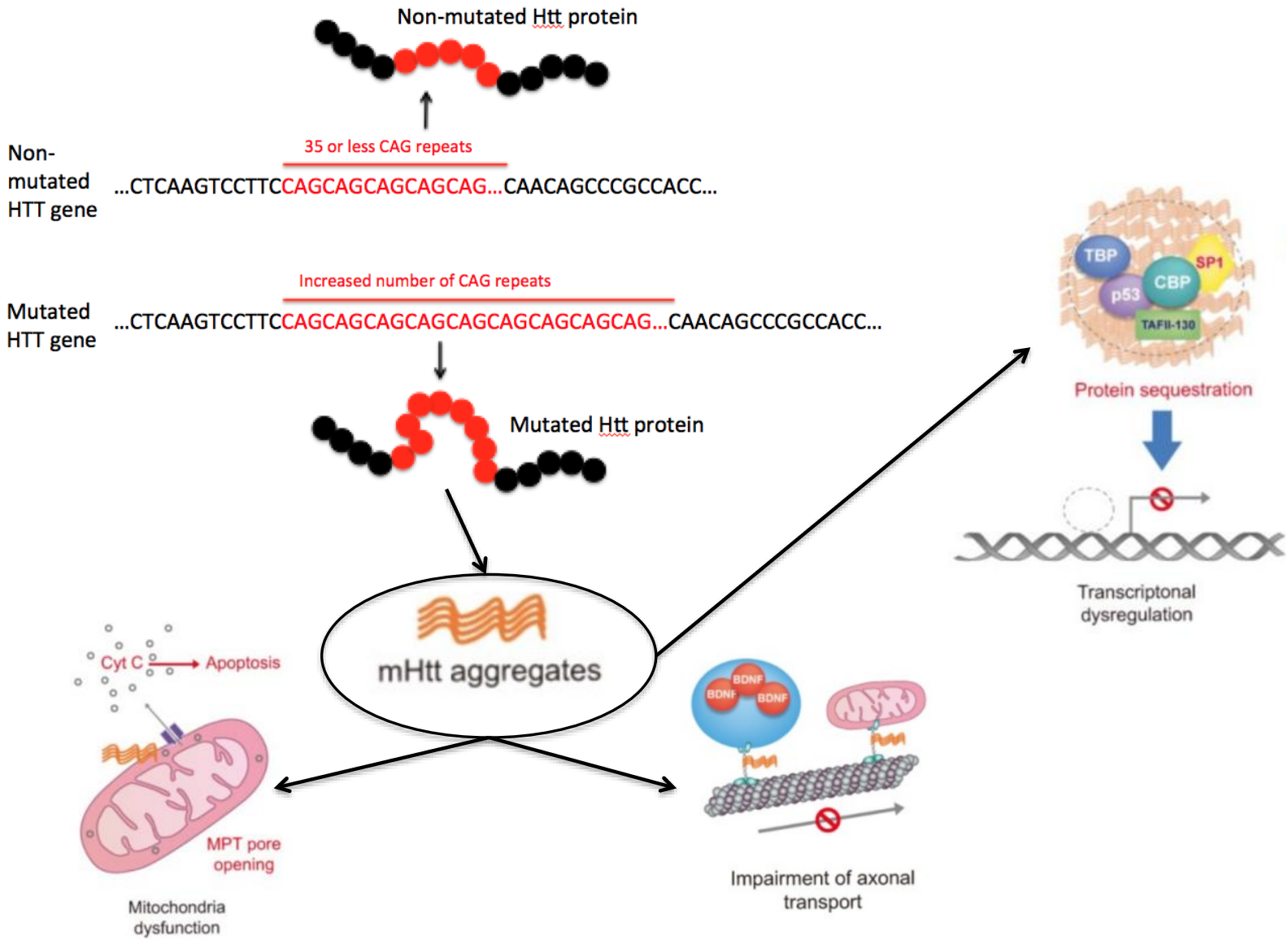
Non-mutated Htt protein
35 or less CAG repeats
Non-mutated HTT gene
...CTCAAGTCCTTCCAGCAGCAGCAGCAG...CAACAGCCCGCCACC...
Increased number of CAG repeats
Mutated HTT gene
...CTCAAGTCCTTCCAGCAGCAGCAGCAGCAGCAGCAG...CAACAGCCCGCCACC...
Mutated Htt protein
mHtt aggregates
TBP
SP1
p53
CBP
TAFII-130
Protein sequestration
Transcriptonal dysregulation
Cyt C
Apoptosis
MPT pore opening
Mitochondria dysfunction
BDNF
BDNF
BDNF
Impairment of axonal transport

Figure 1.1: Pathogenesis of HD. Adapted from (Kim and Kim 2014). Huntingtin gene (HTT), huntingtin protein (Htt), Mutant huntingtin (mHtt), cAMP response element binding protein (CREB) binding protein (CBP), TATA-binding protein (TBP), specificity protein 1 (SP1) and TBP-associated factor, 135 kDa (TAFII-130), brain-derived neurotrophic factor (BDNF), mitochondrial permeability transition (MPT), Cytochrome c (Cyt c).

An expanded polyglutamine sequence causes the normal huntingtin protein to misfold. These misfolded proteins build up in the cell nucleus as aggregates, which may cause altered cellular metabolism, neurotransmitter dysfunction, oxidative stress, microglial activation, and reactive astrogliosis (Andre, et al. 2016; Bates 2003; DiFiglia, et al. 1997; Lee, et al. 2007; McColgan and Tabrizi 2018; Tabrizi, et al. 2000). mHtt also causes alterations in transcription and epigenetic pathways (Ament, et al. 2018; Hervas-Corpion, et al. 2018; Seredenina and Luthi-Carter 2012). Although proteosomal degradation of mHtt prevents cytotoxicity early in life, this function is decreased with ageing and is at least partially responsible for the manifestation of disease later in life (Li and Li 2011).

Medium spiny neurons (MSN) are the striatal cell population predominantly affected in HD (Ferrante, et al. 1987a; Ferrante, et al. 1987b), despite the fact that *huntingtin* is expressed in almost all tissues (Sassone, et al. 2009). MSN have a number of characteristics which may make them more susceptible to the toxic effects of Htt (Morigaki and Goto 2017), including requiring high amounts of energy to maintain hyperpolarised states (Wilson and Kawaguchi 1996), containing lower levels of superoxide free radical scavengers (Medina, et al. 1996), and having alterations in glutamate transmission and response (Calabresi, et al. 1999; Calabresi, et al. 1998; Rossi, et al. 2006). While expression of mHtt itself is not increased in the striatum, there is increased expression of Rhes, a guanine nucleotide-binding protein that binds to mHtt and increases its toxicity (Subramaniam, et al. 2009). Striatal projection

neurons require Htt for synaptic plasticity and survival (Burrus, et al. 2020), as well as brain derived neurotrophic factor (BDNF) (Canals, et al. 2004; Li, et al. 2012; Zuccato, et al. 2008), which depends on Htt for its production and transport to the striatum (Gauthier, et al. 2004; Zuccato and Cattaneo 2007; Zuccato, et al. 2001; Zuccato, et al. 2003). Growing evidence such as this points to HD as causing neurodevelopmental disruption as well as neurodegeneration (Lee, et al. 2012; Mangin, et al. 2020; Nopoulos, et al. 2011; Zuccato, et al. 2008).

1.2.3 Overview of neuroanatomical changes in HD

Changes in the striatum in HD have been observed since the late 19th century and were further characterised by Vonsattel in the 1980s into five neuropathological grades of disease which correlated with reported clinical disease severity (Figure 1.2) (Vonsattel, et al. 1985). This study was based on post-mortem brain specimens of 163 clinically diagnosed cases of HD, and divided changes into grade 0, where there was a clinical diagnosis of HD but no discernible brain changes (note this occurred in 5 people only), through microscopic changes only (grade 1- 50% of neurons lost in the caudate) to gross changes in the caudate and putamen. The earliest changes were seen in the medial paraventricular portions of the caudate, in the caudate tail, and in the dorsal part of the putamen. In grades 3 and 4 changes were seen in other brain regions including the thalamus, sub-thalamic nucleus, white matter and cerebellum. By grade 4, 95% of neurons were lost in the caudate (Vonsattel, et al. 1985).

Extending this work, neuroimaging studies have shown neostriatal (caudate and putamen) volume is reduced in individuals with premanifest HD more than a decade before predicted disease onset (van den Bogaard, et al. 2011a), while more pronounced atrophy is apparent in patients the closer they are to onset (van den Bogaard, et al. 2011b). Caudate atrophy rates

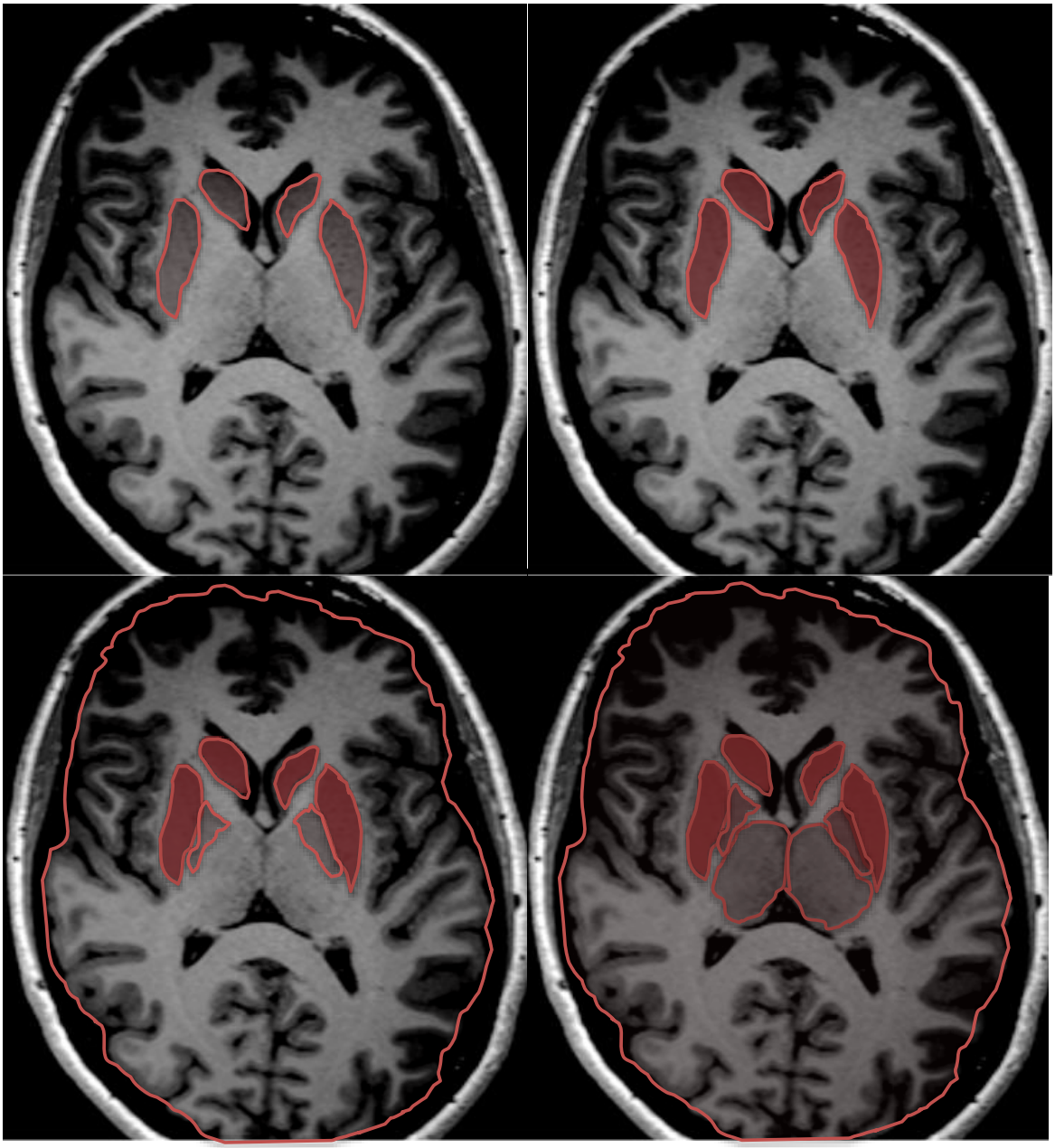

Figure 1.2: Gross neuroanatomical changes in HD. Progression of HD via Vonsattel grades, from grades 1-4 (top left to bottom right) (Vonsattel and DiFiglia 1998). Affected areas represented in red, overlaid on an axial MRI slice of a normal brain from our study. Top images show changes in the caudate and putamen alone, while bottom images progress to include cortex and pallidum (bottom left and right), then thalamus (bottom right).

have been found to be 1-4% per year (Aylward, et al. 2011b; Aylward, et al. 2003; Hobbs, et al. 2009; Kipps, et al. 2005; Tabrizi, et al. 2011), while putaminal atrophy rates are as high as 3-7% (Tabrizi, et al. 2011) and may be the better predictor in whether an individual will develop the motor symptoms of HD in the next one to four years (Aylward, et al. 2012). Neurodegeneration in later stages of HD spreads out from the striatum, locally into other areas of the basal ganglia but also distally into cortex, particularly sensorimotor, insular and opercular cortices as well as frontal, cingulate, and visual cortex (Poudel, et al. 2019; Reiner and Deng 2018; Wijeratne, et al. 2018). White matter changes also occur, largely but not exclusively in corticostriatal white matter pathways (for overview see (Poudel, et al. 2019; Poudel, et al. 2014b)).

When investigating morphology using neuroimaging techniques, the striatum shows the earliest and largest amount of shape change in pre-symptomatic HD (pre-HD) and symptomatic HD (symp-HD) (Faria, et al. 2016; Kim, et al. 2017; Tang, et al. 2019; van den Bogaard, et al. 2011b; Wijeratne, et al. 2018; Younes, et al. 2012). Changes are also described in other areas in pre-HD closer to disease onset, including in the nucleus accumbens, globus pallidus, thalamus, hippocampus and amygdala, although results are less consistent (Faria, et al. 2016; Tang, et al. 2019; Younes, et al. 2012). Small areas of striatal shape displacement are seen in people with premanifest HD more than a decade from predicted disease onset, with more pronounced changes occurring in the medial caudate nucleus and putamen in those closer to predicted onset (van den Bogaard, et al. 2011b). Using an index of degree of exposure to the toxic polyglutamine repeats (a so-called “CAP-score”, based on CAG repeat length and age [CAG-Age Product]), significant shape differences are seen in caudate and putamen in people with high CAP scores, and in left putamen in the mid CAP scores group

(Younes, et al. 2012). These changes spare the dorsal caudate and show no clear gradient in putamen, although the most rostral portion of putamen is spared (Younes, et al. 2012).

1.3 The subcortical connectome: role of the striatum and other subcortical areas involved in HD

The neostriatum, the hippocampus, and the corpus callosum are the structures of interest in this thesis, investigated together as part of the subcortical connectome, with the view towards using this as an endophenotype of HD. By quantitative mapping of neuroanatomical changes in HD, specifically with respect to subcortical structures, we relate the topography of these maps to the contours of the circuits affected by disease, and according to symptomatic dysfunction (Looi, et al. 2014b).

1.3.1 The neostriatum

The neostriatum, composed of the caudate nucleus and putamen, is a critical relay in frontostriatal re-entrant circuits involved with cognitive, emotional, behavioural and motor functions (Draganski, et al. 2008) (Figure 1.3). In general, these originate in the relevant area of cortex, then travel through, and are modified in, the neostriatum, globus pallidus, thalamus, and back to originating cortex. Structural changes in the striatum may disrupt these frontostriatal pathways and, as well as the obvious motor sequelae, also lead to measurable changes in related cognitive and neuropsychiatric outcomes (Looi and Walterfang 2012). In both Parkinson's disease and HD, abnormalities, particularly, but not exclusively in movement, are related to damage to this circuitry: in Parkinson's disease because of a lack of the neurotransmitter dopamine, while in HD this is related to neuronal loss (eg (Reiner and Deng 2018)).

There are five frontostriatal re-entrant circuits which are generally described (Figure 1.3). Two of these are frontostriatal motor circuits: the first is the well-known motor circuit originating in the supplementary motor area (SMA) and central to many movement disorders, including Parkinson's disease and HD (Alexander, et al. 1986; Cummings 1993). The other frontostriatal motor circuit originates in the frontal eye fields (FEF) and regulates visual attention and eye movements. HD patients have deficits in the voluntary control of saccadic eye movements, which is attributed to damage to this frontro-striatal loop (Peltsch, et al. 2008; Winograd-Gurvich, et al. 2003). There are three "cognitive loops", named for the area of cortex in which they originate: the dorsolateral prefrontal circuit is required for executive function such as problem solving, the orbitofrontal circuit mediates inhibition and impulse control, and the anterior cingulate circuit mediates motivation and initiation of behaviour (Alexander, et al. 1986; Cummings 1993). The striatum is structurally and functionally organised in a topographic pattern with more anterior portions receiving connections from more anterior parts of the cortex and more posterior parts from more posterior cortex (Bohanna, et al. 2011a).

The striatum is highly topographically organised (Figure 1.4), with the caudate head and body receiving connections on the lateral aspect from dorsolateral prefrontal cortex (DLPFC), inferior orbitofrontal cortex (OFC) and posterior parietal cortex (PPC) and on the medial aspect from the anterior cingulate cortex (ACC). The caudate tail meanwhile receives input from the FEF. The putamen receives more motor input, receiving on its medial aspect connections from the motor cortex (MC) and somatosensory cortex (SSC), and on the lateral from the FEF. The putamen receives more motor input, receiving on its medial aspect connections from the motor cortex (MC) and somatosensory cortex (SSC), and on the lateral

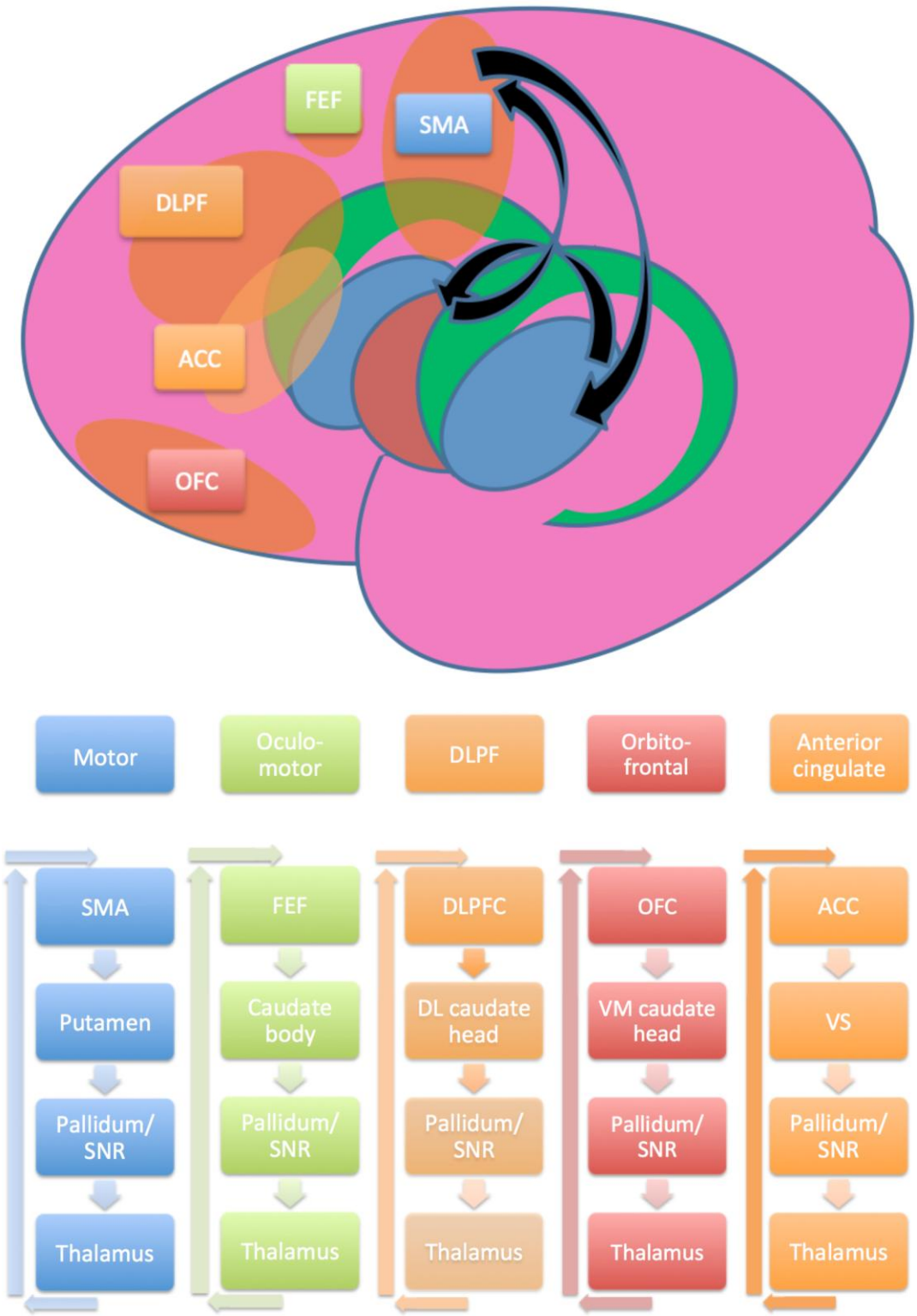

Figure 1.3: Central position of the striatum and schematic view of fronto-striatal re-entrant circuits. Based on Alexander, 1986 (Alexander, et al. 1986). SMA, supplementary motor area; SNR, substantia nigra pars reticulata; FEF, frontal eye fields; DLPF/C, dorsolateral prefrontal/cortex; DL, dorsolateral; OFC, orbitofrontal cortex; VM, ventromedial; ACC, anterior cingulate cortex; VS, ventral striatum.

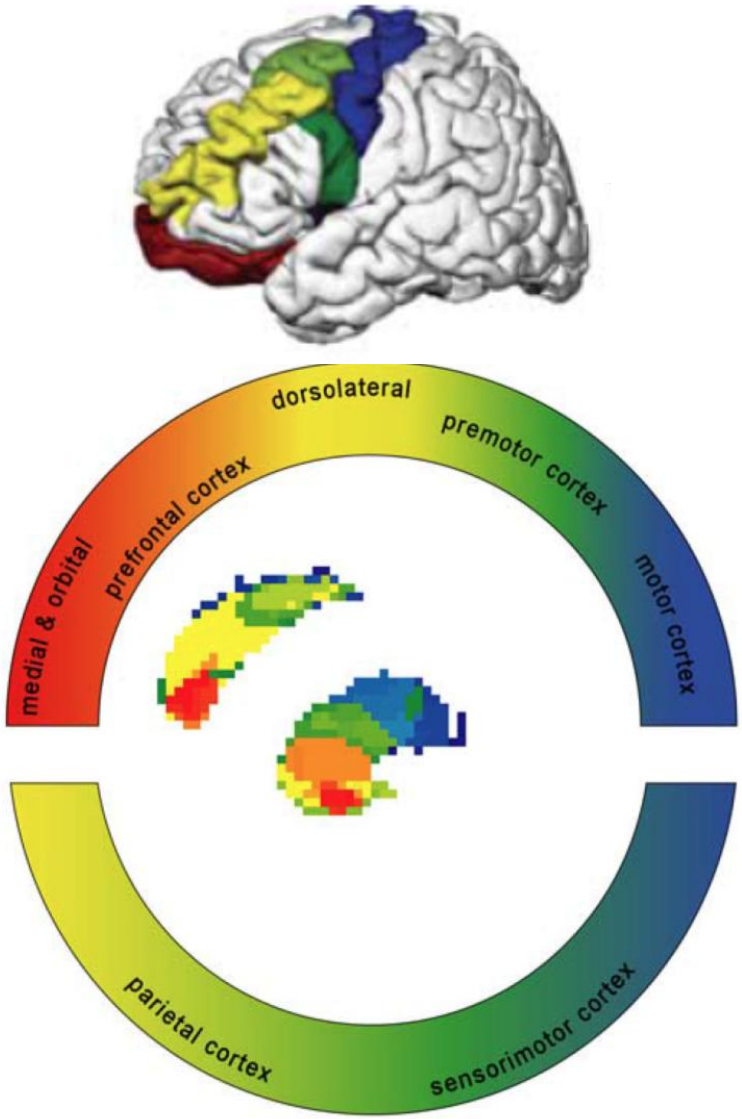
dorsolateral
premotor cortex
motor cortex
prefrontal cortex
medial & orbital
parietal cortex
sensorimotor cortex

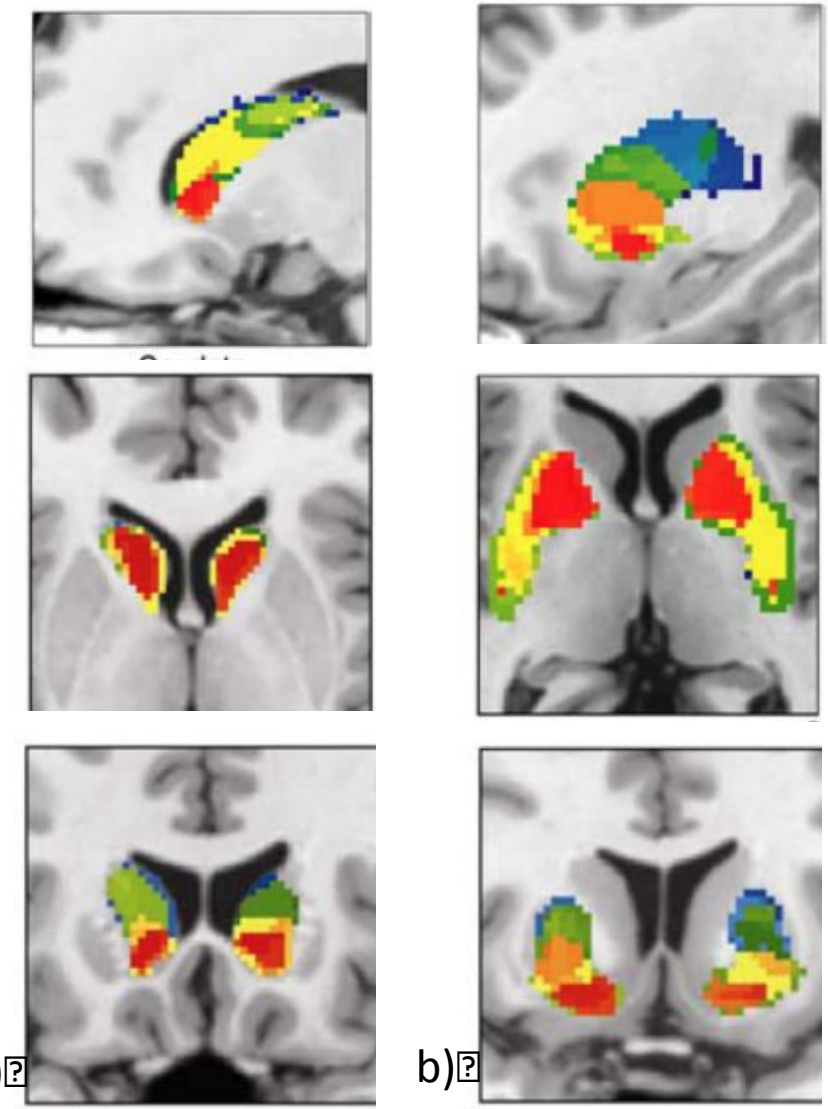

a)

b)

Figure 1.4: Topographic arrangement of the neostriatum. "Rostrocaudal gradient" of frontal cortical connectivity in caudate and putamen. a) Caudate connectivity to different areas of cortex, represented in primary colours, visualised in sagittal, axial and coronal planes. b) Putamen connectivity to same, also visualised in sagittal, axial and coronal planes. Adapted from (Draganski, et al. 2008), after (Haber 2003).

aspect connections from the SMA. On its ventral aspect the putamen also receives input from the DLPFC, while both caudate and putamen are also linked directly through fibres traversing the internal capsule (Alexander, et al. 1986; Draganski, et al. 2008; Haber 2003; Haber, et al. 2000). In general, both caudate and putamen are topographically organised along an anterior-posterior axis such that more anterior parts of the striatum receive input from more anterior parts of the cortex (Bohanna, et al. 2011a).

Neostriatal shape changes are seen in a number of neurodegenerative and neuropsychiatric disorders which have links to frontostriatal circuits and behavioural disruption. For example, people with bipolar affective disorder show reductions in caudate regions which connect to DLPFC (Ong, et al. 2012) , important for executive control. People with frontotemporal dementia exhibit deficits in oculomotor function, which can be related to alterations in the FEF circuit and the marked posterior atrophy of the caudate in this disorder (Looi, et al. 2011). Shape changes are also seen in chorea-acanthocytosis, which affects the neostriatum and produces choreo-athetoid movements which can be indistinguishable from those seen in HD. Chorea-acanthocytosis patients display major executive function deficits, particularly a greatly increased incidence of obsessive compulsive disorder (OCD), and shape changes are seen in areas of the striatum connected not only to motor circuits but also to all three frontostriatal circuits involved in behaviour (Walterfang, et al. 2011). Similarly, in OCD there are outward shape deformities in the superior, anterior parts of bilateral caudate nucleus,

connected to DLPFC, and in the inferior, lateral portion of the left putamen, connected to limbic areas (Choi, et al. 2007). The eating disorders anorexia nervosa, binge eating disorder and bulimia nervosa, are also all known to have changes in the striatum (Molina-Ruiz, et al. 2020). This collective data suggests that disorders of repetitive thought and movements have significant striatal shape alterations.

Knowledge of the anatomy of this circuitry, and in particular of the topographical nature of striatal organisation, can help to guide treatments. An example is deep brain stimulation, which has widespread utility in Parkinson's disease but is also being used worldwide for psychiatric conditions including Gilles de la Tourette syndrome and OCD. In all three of these disorders the striatum is a major target of deep brain stimulation, and an electrode is placed surgically into this area where targeted currents of electricity modulate the abnormal circuitry and can lead to symptomatic relief (for a recent review see (Horn and Fox 2020)). While deep brain stimulation is a useful treatment for many diseases, it has so far had limited utility in HD, possibly due to the aggressive nature of neurodegeneration (Gonzalez, et al. 2014).

1.3.2 The hippocampus

The hippocampus lies within the medial temporal lobe, bulging in the floor of the inferior horn of the lateral ventricle (Figure 1.5). In gross anatomical terms it can be divided into the hippocampal head, which is the most anterior part, the hippocampal body, and the tail. Based on its cytoarchitecture it is divided into the cornu ammonis subfields CA1-4, the dentate gyrus, and the subiculum (Figure 1.5b). Its main input arrives at the entorhinal cortex from association cortex in the frontal, parieto-occipital, and temporal lobes. These inputs are then processed further in the medial temporal lobe and sent back via subiculum to entorhinal

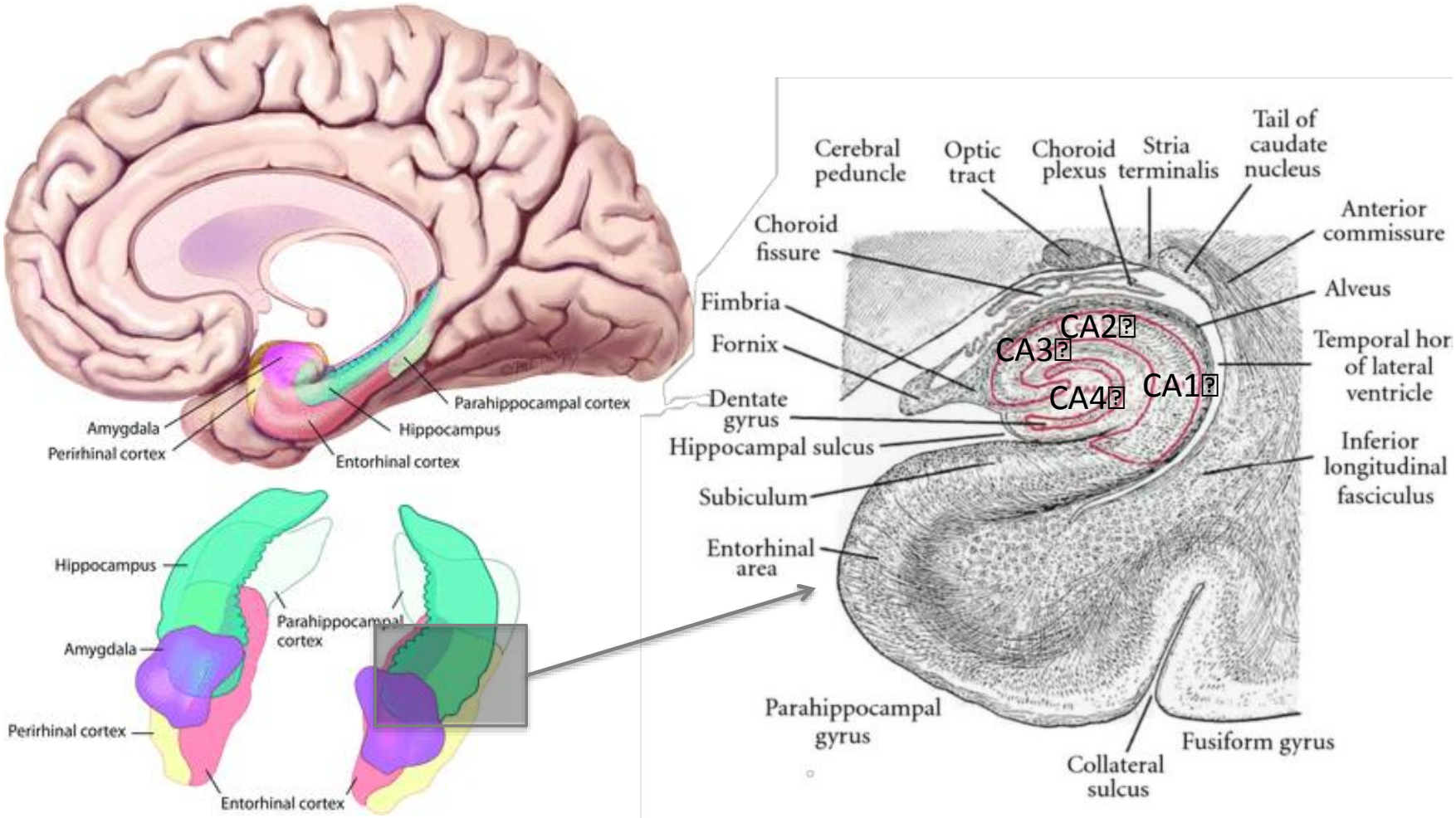

Figure 1.5: The human hippocampus. Schematic view on the sagittal plane (top left) and showing 3-dimensional hippocampi looking from an anterosuperior viewpoint adapted from (Purves 2012) (bottom left), with further emphasis on cytoachitecture (right), shown in the coronal plane and adapted from (Kiernan 2012)

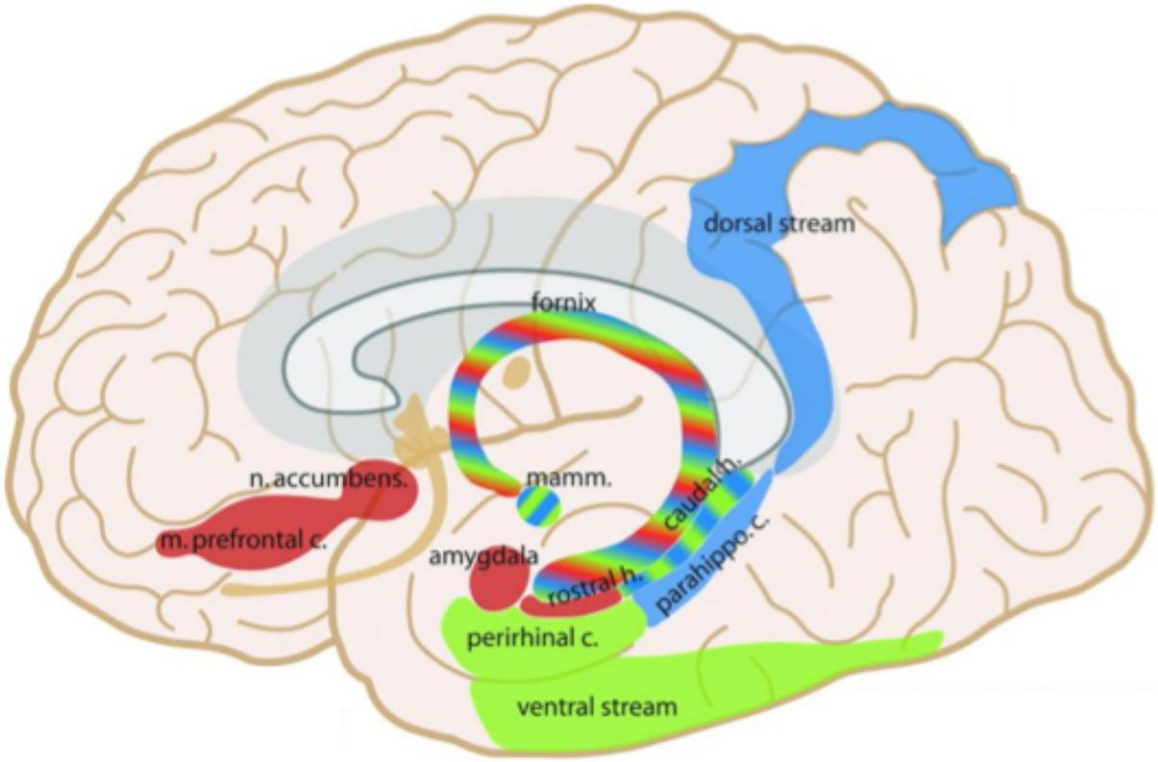

Figure 1.6: Representation of the hippocampus and its main connections (Purves 2012)**.** Anterior (rostral) hippocampus is connected to red areas of the brain above, caudal hippocampus to blue and green areas. The fornix is the major relay of outputs from the hippocampus. n. accumens, nucleus accumbens; m. prefrontal c., medial prefrontal cortex; mamm., mammillary bodies; perirhinal c., perirhinal cortex; rostral h., rostral hippocampus; caudal h., caudal hippocampus; parahippo. c., parahippocampal cortex.

cortex to association cortices for memory storage (Figure 1.6) (Blumenfeld 2010).

There are two major projection pathways from the entorhinal cortex into the hippocampal formation- the perforant pathway and the alvear pathway. The perforant pathway reaches through the subiculum and across the hippocampal sulcus to the granule cell layer of the dentate gyrus. The granule cells then synapse directly on to CA3 pyramidal cells, and via Schaffer collaterals onto CA1 pyramidal cells, both of which then leave the hippocampus via

the fornix. CA1 cells relay through the subiculum to the fornix, as well as back into deeper layers of entorhinal cortex. The alvear pathway projects directly to CA1 and CA3, with outputs similar to the perforant pathway. The fornix carries output to the mammillary bodies of the hypothalamus, the lateral septal nucleus, and the anterior thalamic nucleus. Some inputs reach the hippocampus from the contralateral hippocampus via the hippocampal commissure, and further modulatory inputs arise via the fornix from cholinergic neurons in the medial septal nucleus and the nucleus of the diagonal band (Blumenfeld 2010).

Like the striatum, the hippocampus is also topographically organised. The posterior hippocampus is implicated in memory and spatial navigation whereas anterior hippocampus mediates anxiety related behaviour and learning through its connections to amygdala and hypothalamus (Figure 1.6) (Fanselow and Dong 2010; Moser and Moser 1998; Strange, et al. 2014). The hippocampus receives projections from the cingulate cortex along its long axis. Cingulate areas involved in emotional regulation project to more ventral regions, and cingulate areas involved in spatial processing project to more dorsal regions. Reciprocating projections are similarly organised. There is a gradient of output to the lateral septum and hypothalamus, coming largely from the anterior hippocampus. The hippocampus is connected with the nucleus accumbens and amygdala, with progressively more anterior hippocampal portions projecting to progressively more medial parts of both of these structures. There are different patterns of gene expression in different areas, and in general, neurotransmitter receptor expression varies across the long axis for the majority of transmitter systems (Strange, et al. 2014).

Shape and volume analysis have been applied to the hippocampus in a number of neurodevelopmental and degenerative disorders (Lindberg, et al. 2012; Solowij, et al. 2013;

Wood, et al. 2010). There is considerable interest in hippocampal plasticity, as cognitive training has been shown to increase left hippocampal activation in mild cognitive impairment (Rosen, et al. 2011) and aerobic exercise training has been shown to increase anterior hippocampal size and improve spatial memory (Erickson, et al. 2011). This increase in volume is associated with greater serum levels of BDNF (Erickson, et al. 2011). Limited attention however has been paid to the hippocampus in HD. In those few studies directly addressing hippocampal volume or shape in HD (Majid, et al. 2011; van den Bogaard, et al. 2011b; Younes, et al. 2012), the hippocampus in pre-HD tends to be spared (Majid, et al. 2011; Younes, et al. 2012), although both shape and volume changes do occur later on in disease progression (van den Bogaard, et al. 2011b). Despite known hippocampal plasticity and neurogenesis, no studies have examined longitudinal changes in HD.

1.3.3 Neurogenesis potential near striatum and hippocampus

There are two areas of the adult brain where neurogenesis can occur: the subgranular zone of the dentate gyrus in the hippocampal complex (SGZ), and the subventricular zone (SVZ), which lies just above the caudate (Figure 1.7) (Barani, et al. 2007). Progenitor cells in the SGZ can migrate to the granule cell layer and differentiate into granular neurons which are functionally integrated into the hippocampal circuitry.

Newly generated cells in the SVZ can migrate to affected striatum in a model of HD (Jin, et al. 2005) and in ischaemia, and differentiate into medium spiny neurons (Yamashita, et al. 2006). In HD, increased cell proliferation and neurogenesis have been observed in the SVZ of

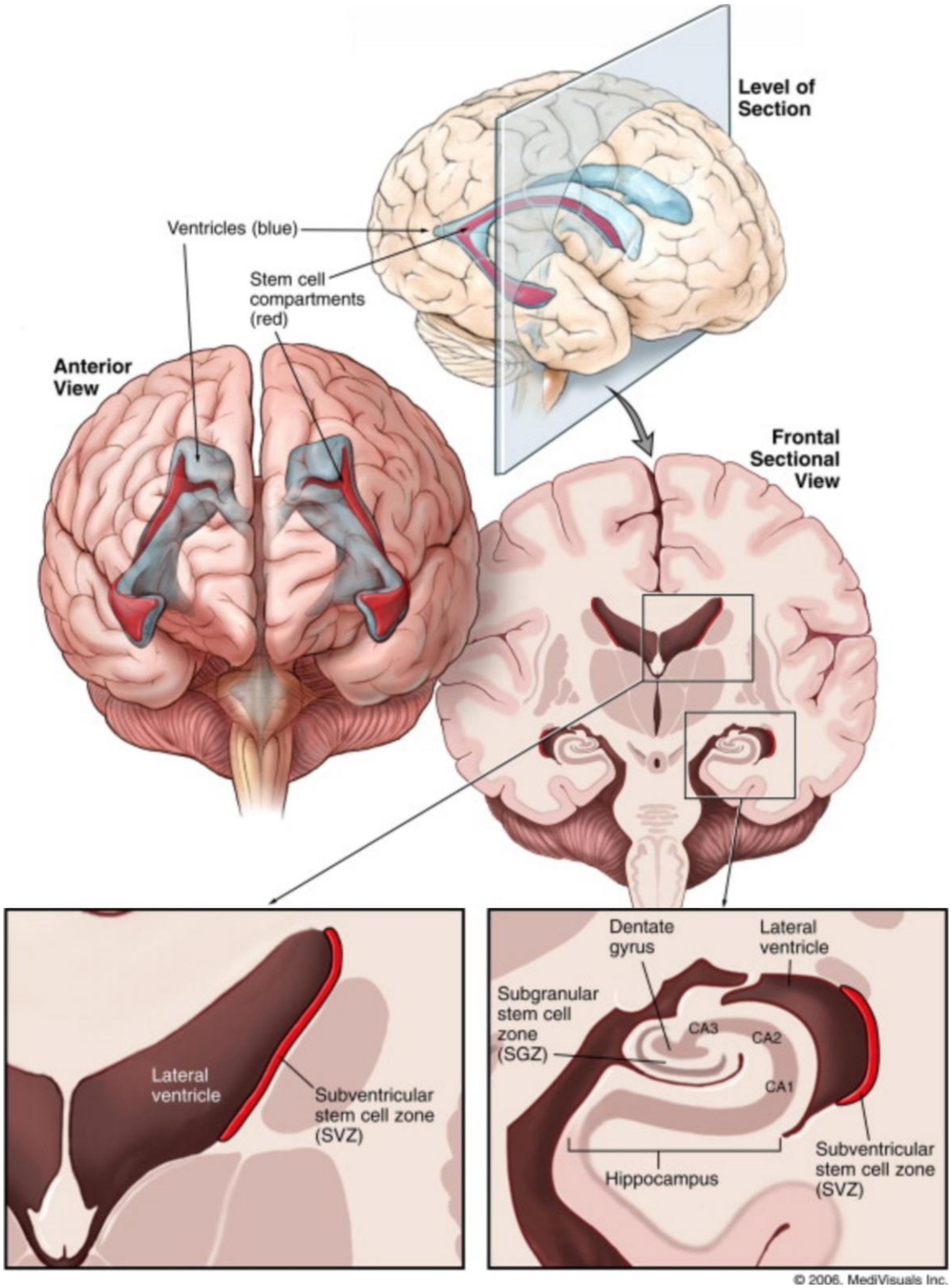

Figure 1.7: Areas of neurogenesis in the adult human brain (Barani, et al. 2007).

the adult human brain (Curtis, et al. 2003), while in the hippocampus *impaired* neurogenesis is observed in humans as well as in murine models (for review see (Curtis, et al. 2012; Gil-Mohapel, et al. 2011; Ransome, et al. 2012)).

Interestingly, treatment with selective serotonin reuptake inhibitors (SSRIs) in transgenic mouse models of HD increases both BDNF levels and neurogenesis in SGZ and SVZ, attenuating the progression of brain atrophy and behavioural abnormalities and increasing survival (Duan, et al. 2008; Grote, et al. 2005; Peng, et al. 2008). Despite this work in animal models and the common use of antidepressants, particularly SSRIs, in HD (Rowe, et al. 2012) there has been surprisingly limited research into the effect of SSRIs on the natural history of human HD progression.

1.3.4 Hippocampal/striatal circuits

The hippocampus and the striatum are involved in parallel memory systems that interact (McDonald and White 1994; White 2009; White and McDonald 2002). Animal studies suggest that the dorsolateral parts of the neostriatum are central to the processing and consolidation of memory for reinforced stimulus-response associations, while the more medial and anterior areas are part of a circuit that includes the hippocampus and mediates relational information and certain forms of working memory (White 2009). Connections between the hippocampus and the ventral striatum, in particular the nucleus accumbens, modulate reward or goal directed behaviour (Fouquet, et al. 2013; Strange, et al. 2014). The caudate is thought to play a critical role in egocentric navigation as opposed to the hippocampus' role in allocentric navigation (McDonald and White 1994; White 2009; White and McDonald 2002), although in some cases in HD the hippocampus can compensate for caudate dysfunction in this memory pathway (Possin, et al. 2017; Voermans, et al. 2004). The

hippocampus and the striatum also interact cooperatively to support episodic memory formation (Sadeh, et al. 2011). Functional MRI (fMRI) studies show that successful memory is associated with greater activity in both the hippocampus and the putamen, with the strength of the correlation predicting memory success (Sadeh, et al. 2011).

1.3.5 The corpus callosum

Further extending our study of subcortical structures in HD, we wished to look at the corpus callosum (CC), as a "spoke" in neural circuitry in addition to the "hubs" discussed above. The CC is the brain's largest white matter bundle and contains most of the commissural fibres connecting the cortices of the two hemispheres (Figure 1.8). The trunk of the callosum is the compact part of the commissure in and near the midline. It is considerably shorter than the hemispheres, which accounts for the enlargements at the ends; these are the genu anteriorly and the splenium posteriorly. The genu tapers into the rostrum of the CC, which is continuous with the lamina terminalis forming the anterior wall of the third ventricle. The ventral surface of the CC forms the roof of the lateral ventricles (Kiernan 2005).

The CC may be used as a proxy for cortical changes and a marker of interhemispheric interconnections and changes in HD. Callosal thickness has previously been shown to be related to thickness in the cortical areas it connects (Hampel, et al. 1998; Teipel, et al. 2002), with connections occurring largely topographically and between hemispheres, but also within certain areas in the same hemisphere (Chao, et al. 2009; Phillips, et al. 2013). This is in contradistinction to the connections which occur through frontostriatal and hippocampal circuitry which do not go through the CC, and thus provides a more comprehensive picture of subcortical changes in HD.

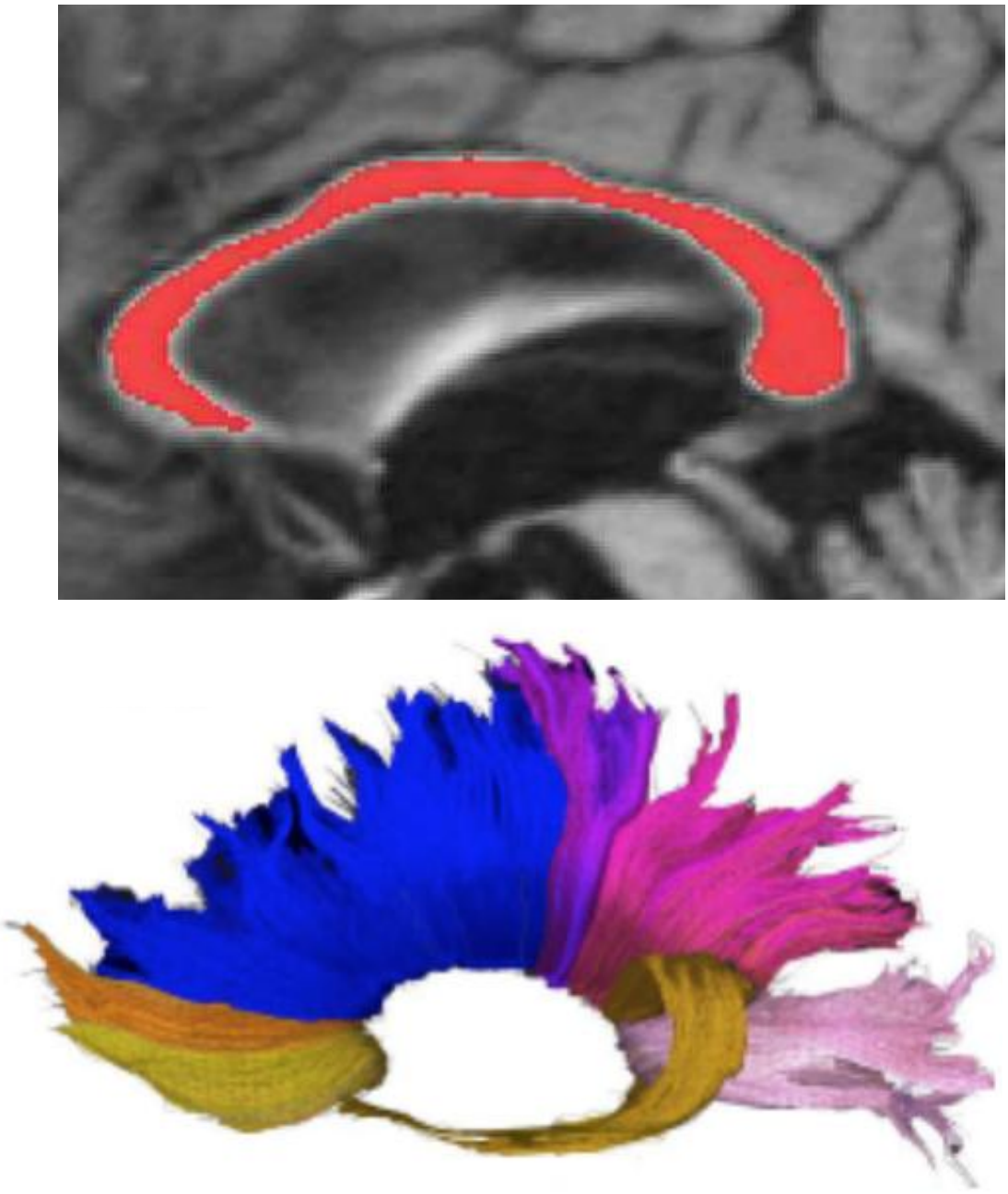

Figure 1.8: Corpus callosum anatomy and connectivity. Reproduced and modified with permission from (Adamson, et al. 2014) (superior image) and (Phillips, et al. 2013) (inferior image). Images are in the sagittal plane, with anterior to the left and posterior to the right. The superior image shows gross anatomy of mid-sagittal corpus callosum, while the inferior image shows tracts within the corpus callosum connecting frontal (yellow), orbitofrontal (orange), superior frontal (blue), superior parietal (purple), posterior parietal (pink), temporal (brown), and occipital (light pink) regions.

In addition to subcortical structures, degeneration of the cerebral cortex is also known to occur in HD (Nopoulos, et al. 2010). Simplifying the analysis of overarching cortical changes, CC morphology has been purported to reflect cortical changes in HD and other neurodegenerative diseases (Rosas, et al. 2010). The CC has specific functional subregions based on connectivity to different parts of the cortex, and changes in these subregions are thought to be the morphological mirror of neuropsychological effects in degenerative disease (Rosas, et al. 2010): changes here may map cortico-cortical circuit abnormalities that underpin neuropsychological change. Diffusion tensor imaging in particular has shown changes in connectivity within the corpus callosum in HD (Bohanna, et al. 2011b; Della Nave, et al. 2010; Dumas, et al. 2012; Rosas, et al. 2006) and certain studies have gone further to show correlations between these changes and motor, oculomotor and cognitive function (Bohanna, et al. 2011b; Dumas, et al. 2012; Rosas, et al. 2006). While diffusivity changes have been seen in the CC as much as a decade prior to disease onset (Rosas, et al. 2010), and have even been correlated with probability of onset within 2-5 years (Dumas, et al. 2012), the picture with callosal shape changes is less clear, and no studies have looked at longitudinal changes.

1.4 The IMAGE-HD study

The IMAGE-HD study is a Melbourne based study which followed a cohort of 36 people with pre-HD, 37 people with symp-HD, and 36 controls, with measures including motor, psychiatric and cognitive tests, 3T MRI brain scans, and other modalities outside the scope of this thesis (diffusion tractography imaging (DTI); fMRI). Participants were recruited in 2008 and 2009 through the HD Predictive Testing Program (Genetic Health Services, Victoria). Healthy controls were matched for age, sex and IQ to the pre-HD individuals. All participants

were right-handed and were free from brain injury, neurological and/or severe diagnosed psychiatric conditions other than HD. The study followed these people over time and took a number of different tests at the start of the study, at 18 months, and at 30 months.

Tests outside of imaging included Unified Huntington Disease Rating Scale (UHDRS) motor assessment (Huntington Study Group 1996); visuo-motor speed and attention (Symbol Digit Modalities Test, SDMT (Smith 1982)), speeded reading (Stroop Word Test, (Stroop 1935)), odour recognition (University of Pennsylvania Smell Identification Test, UPSIT (Doty, et al. 1984)) and motor performance (speeded tapping and self-paced tapping tasks (Stout, et al. 2011)), executive function (Frontal Systems Behaviour Scale, FrSBe (Stout, et al. 2003)) and psychiatric disturbances (Schedule of Compulsions Obsessions and Pathological Impulses, SCOPI (Watson and Wu 2005), Hospital Anxiety and Depression Scale, HADS A and HADS D (Zigmond and Snaith 1983), Beck Depression Inventory score Version II, BDI II (Beck 1996)). All were chosen because of their proven potential in differentiating symp-HD and possibly pre-HD (Stout, et al. 2011; Tabrizi, et al. 2009).

Previous work in the IMAGE-HD study has investigated various different imaging modalities including DTI (Bohanna, et al. 2011a; Dominguez, et al. 2013; Dominguez, et al. 2016; Georgiou-Karistianis, et al. 2013a; Poudel, et al. 2015b; Poudel, et al. 2014b), fMRI (Domínguez, et al. 2017; Georgiou-Karistianis, et al. 2013b; Georgiou-Karistianis, et al. 2014; Gray, et al. 2013; Poudel, et al. 2015a; Poudel, et al. 2014a; Soloveva, et al. 2020), iron studies (Domínguez, et al. 2016), and investigations of other areas including cortex (Shishegar, et al. 2019), thalamus (Furlong, et al. 2020), hypothalamus (Gabery, et al. 2015), and amygdala (Ahveninen, et al. 2018; Alexander, et al. 2020).

My primary PhD supervisor Associate Professor Jeffrey Looi and I (Looi, et al. 2014a) became involved with the IMAGE-HD study after the initial data collection, in order to further investigate morphological change in elements of the subcortical connectome, for reasons described above. I manually traced caudate, putamen and hippocampus and then worked with other collaborators to coordinate and analyse this data in the light of the other clinical information obtained. The CC has a reliable method of analysis which does not require manual tracing and so I coordinated sending this to a further collaborator for computational analysis, before further analysing and interpreting results. Further details of the methods used in the various studies can be found in subsequent sections of this thesis.

Study One of this thesis has been published in the scientific literature (Wilkes, et al. 2019), and will be appended in full to the end of the thesis as well as discussed further within the thesis proper. Work done on this thesis also contributed to another paper published in the literature (Turner, et al. 2016), which found alterations in electroencephalogram (EEG) activity during a motor task in pre-HD even though performance at that stage was not impaired, and correlated changes in EEG with shape abnormalities in the striatum.

1.5 Rationale for thesis

This thesis presents an investigation into subcortical changes in HD and their relationship with clinical, motor, neurocognitive and neuropsychiatric outcomes, with the intention of advancing a biomarker for HD. Investigation focuses on specific "hubs and spokes" within the brain, providing a more comprehensive picture of HD as a whole and the interrelationship between neuroanatomical changes and functional outcomes. Further characterisation of changes in HD increases knowledge of neurodegenerative pathways and the relationship

between quantitative measures of morphology (morphometry) and function *in vivo*, constituting endophenotypes, and aims towards developing biomarkers for prognostication and use in HD treatment trials.

Statistical shape analysis of subcortical structures is emerging as a method to measure highly localised changes in neurodegenerative disease which may be missed by gross volumetric measurement (van den Bogaard, et al. 2011b). In this manner, shape analysis can help to extend knowledge of affected neural pathways (Looi and Walterfang 2012; van den Bogaard, et al. 2011b), as much is known about the topographical organisation of the striatum, hippocampus, and corpus callosum. The topographical organisation of the structures examined in this study lend themselves to shape analysis as they act as homunculi for changes in other parts of the brain, being a more constrained structure to analyse for broader brain patterns.

One particularly interesting question which may be answered by longitudinal shape analysis is whether neurodegeneration in HD occurs by spreading out from the striatum along corticostriatal pathways, or, as has more recently been proposed, whether the picture is more complicated and involves multiple points of co-occuring degeneration, as well as altered neurodevelopment (Younes, et al. 2012). If localised and spreading, there is potential for effective treatment or prevention of HD with a targeted approach, for example injected factors to enhance neuronal survival in the striatum. However if HD is more complex and multifaceted, as seems likely, then more systemic approaches will be needed (Younes, et al. 2012).

Consequently, we have considered the following, namely that: 1) morphological and neuropsychiatric change in HD will provide further knowledge of the link between structure, circuits and function; 2) increased knowledge of structural change in HD will allow biomeasures to be developed towards biomarkers for surrogate endpoints in treatment trials (Georgiou-Karistianis, et al. 2013c); and 3) development of disease-modifying treatments may eventually be informed by an understanding of the progression of subcortical neurodegeneration and how the trajectory of this may be modified by these treatments.

The central questions of this thesis are:

- Is there a difference between subcortical morphology in symp-HD, pre-HD, and controls?
- Do these change over time and progress in a determined pattern?
- Is there a relationship between shape change and motor and neurocognitive outcomes?
- Do these follow the expected relationships with known subcortical circuits in a topographical pattern?
- Can the picture of the above give a better understanding of the pathogenesis of HD and help with the development of a biomarker and endophenotype of HD?

1.6 Scope of thesis

Table 1.2: Scope of thesis. Investigation of the subcortical connectome in HD, with view to development of an endophenotype.

Study	Investigation	Rationale	Endophenotype components
Study One	Baseline analysis of neostriatum and	Key structure in HD and hub in frontostriatal circuitry	Genetics Morphology

	relationship with functional outcomes		Function
Study Two	Longitudinal analysis of neostriatal change	Morphological change over time, investigating potential biomarkers	Genetics Morphology Spatiotemporal signature
Study Three	Baseline analysis of hippocampus and relationship with functional outcomes	Further extension of subcortical connectome in a different but related hub, potential for compensation	Genetics Morphology Function
Study Four	Baseline and longitudinal analysis of the corpus callosum	Major spoke within the connectome, complementary information regarding degeneration	Genetics Morphology Spatiotemporal signature

1.6.1 Study One: Baseline analysis of the neostriatum in Huntington disease, pre-HD, and the relationship between striatal morphology and motor and neurocognitive outcomes

The first chapter of this thesis concerns a baseline shape analysis of the neostriatum in HD and the relationship between striatal morphology and motor and neurocognitive outcomes. The outcomes tested were chosen based on their statistically significant differences between groups. Shape analysis consisted of two separate forms of computational analysis, one the Jacobian shape determinant and one the radial distance between the median line (called thickness for simplicity). Jacobian shape determinant is a more subtle analysis of shape changes from the outer curve, versus the simplicity of looking at distance from a median line, and so analysis differs slightly between these two computational forms.

We hypothesised that quantified measures of neostriatal morphology would significantly differ between controls and individuals with pre-HD and symp-HD. We also hypothesised that neostriatal morphological changes would be associated with cognitive, neuropsychiatric and motor outcomes according to known functional connections.

Chapter 1 has been published in Psychiatry Research: Neuroimaging (Wilkes, et al. 2019).

1.6.2 Study Two: Longitudinal analysis of shape change in the neostriatum in Huntington disease.

We extended the findings from the study in Chapter 1 to look at longitudinal changes in shape in HD. Longitudinal shape analysis in this paper was based on the SPHARM method and manual tracing of the neostriatum, using alterations to manage statistical difficulties in longitudinal analysis and addressing limitations in the current literature. Mixed multiple analysis of variance was used to determine the effect of a number of important areas of interest, namely group membership, versus genetic burden via number of CAG repeats. We hypothesised that we would find similar results to those seen in pathological studies and in the preliminary longitudinal imaging studies, but that we would be able to see these changes in more detail using our advanced method and statistical analysis.

1.6.3 Study Three: Baseline analysis of the hippocampus in Huntington disease and relationship to antidepressant use, implications for neurogenesis.

We extended study of subcortical shape analysis in HD to look at the hippocampus at baseline (via manual tracing and the SPHARM method). We also planned to analyse how any changes

were related to neurocognitive and neuropsychiatric outcomes, in particular whether there was any relationship between size/shape and hippocampal volume. Based on previous work we hypothesised that there would be subtle differences in hippocampal shape between pre-HD and controls, and between symp-HD and controls, but not between pre-HD and symp-HD. We also hypothesised that there would be a relationship between shape and depressive symptoms and that these changes would be attenuated by antidepressant, particularly SSRI use.

1.6.4 Study Four: Analysis of the corpus callosum in Huntington disease as a proxy measure for cortical changes.

Finally, we chose to look at corpus callosum thickness in HD and any longitudinal changes and relationship with motor and neurocognitive outcomes. This analysis used an automated model to determine average callosal thickness based on the mid-sagittal slice, with difference from average thickness determined at all of 100 points along the line of the corpus callosum. This method was developed and implemented by a collaborator in Melbourne and provided a solution to the previous problem of analysing thickness around the genu and the splenium of the callosum. We hypothesised that this more sensitive method of investigation would allow subtle changes to be documented in pre-HD and symp-HD over time, thus revealing more insights about the pattern of neurodegeneration in HD and relationships with clinical and neurocognitive outcomes.

We will begin this thesis by presenting background to the main methods used in all four studies.

2. Methods

This thesis uses data from the IMAGE-HD study to better understand subcortical changes in HD and how they relate to clinical and neurocognitive outcomes. This chapter first explains the IMAGE-HD study, and then provides an overview of the methods used in this thesis.

2.1 The IMAGE-HD Study

2.1.1 Subjects

As part of the IMAGE-HD project (Georgiou-Karistianis, et al. 2013a), in 2008-2009 T1-weighted MRI scans were taken of 36 individuals with pre-HD, 37 with early symp-HD, and 36 healthy matched controls. A range of genetic and neurocognitive assessments were also performed by the IMAGE-HD group. Participants were followed up at 18 and 30 months for further testing. Healthy controls were matched for age, sex and IQ to the pre-HD individuals. All participants were right-handed and were free from brain injury, neurological and/or severe diagnosed psychiatric conditions other than HD.

7 controls, 3 pre-HD and 5 symp-HD dropped out of the study at 18 months, and a further 3 controls, 3 pre-HD and 3 symp-HD dropped out at 30 months, leaving 26 controls, 30 pre-HD, and 29 symp-HD at the end of the study. There are only two missing data points due to MRI scans which were unusable; these are from one control participant and one pre-HD participant at 30 months.

Pre-HD and symp-HD participants underwent gene testing prior to enrolment in the study and had CAG repeat lengths ranging from 39 to 50 (Table 2.1). All were clinically assessed using UHDRS motor subscale (Kieburtz, et al. 1996). HD participants were categorised as pre-HD if they had a UHDRS score of 5 or less (Tabrizi, et al. 2009). Years to onset of diagnostic motor symptoms were estimated via Langbehn's parametric survival model, based on the participant's age and number of CAG repeats (Langbehn, et al. 2004).

Table 2.1: Selected demographic data from IMAGE-HD study

	Mean ± SD		
	Controls (n=36)	Pre-HD (n=36)	Symp-HD (n=37)
Sex (M:F)	12:24	14:22	21:16
Age (years)	42.4±13.4	41.7±9.9	52.1±9.3
CAG repeat number (range)		42±2 (39-46)	43±2 (40-50)
Years to onset (Langbehn method)		15.5±7.0	
Years since diagnosis			2.0±1.6
UHDRS motor score (range)		1 (0-4)	19 (6-60)

The study was approved by the Monash University and Melbourne Health Human Research Ethics Committees and informed written consent was obtained from each participant prior to testing in accord with the Helsinki Declaration. All testing was undertaken at the Royal Children's Hospital, Parkville, Melbourne, Australia.

2.1.2 Imaging

Imaging was performed on a Siemens Magnetom Trio Tim System 3 Tesla scanner with a 32-channel head coil (Siemens AG, Erlangen, Germany) at the Murdoch Children's Research Institute (Royal Children's Hospital, Victoria, Australia). High-resolution T1-weighted images were acquired (192 slices, slice thickness of 0.9 mm, 0.8 mm 0.8 mm in-plane resolution 320 320 field of view, TI=900 ms ,TE=2.59 ms, TR=1900 ms, flip angle=9°).

2.1.3 Motor, neurocognitive and neuropsychiatric assessments

All participants underwent a battery of comprehensive neurocognitive and neuropsychiatric assessments, selected based on their sensitivity in previous large multi-site studies (Stout, et al. 2011; Tabrizi, et al. 2009). This included assessment of premorbid IQ, estimated from the National Adult Reading Test (Nelson and Willison 1991), cognitive function including visuo-motor speed and attention (SDMT (Smith 1982)), speeded reading (Stroop Word Test, (Stroop 1935)), and odour recognition (UPSIT (Doty, et al. 1984)). Participants completed behavioural questionnaires which included executive function (FrSBe (Stout, et al. 2003)) and psychiatric disturbances (SCOPI (Watson and Wu 2005), HADS A and HADS D (Zigmond and Snaith 1983), BDI II (Beck 1996)).

Motor speed and timing were assessed using speeded tapping and paced tapping tasks (Stout, et al. 2011). Variance in inter-trial interval in speeded tapping, ITISTAP, reflected 1/inter-tap interval (ITI) when participants tapped a finger as rapidly as possible during repeated 10 s intervals. Inter-trial interval in participant passed tapping (ITIPTAP) was assessed at two speeds, fast (3Hz) and slow (1.8Hz), where participants were asked to tap along to a paced tone and then to continue tapping after the tone disappeared.

2.1.4 Candidate's involvement in IMAGE-HD study

The candidate planned, designed, coordinated and performed analysis of clinical and neuroimaging data derived from the IMAGE-HD study, specifically:

1) Morphometric structural neuroimaging analysis of caudate, putamen and hippocampus
2) Automated structural neuroimaging analysis of the corpus callosum.

2.2 Structural neuroimaging: manual tracing

This thesis investigates the morphology of key parts of the subcortical connectome using volume, surface-based shape analysis, and thickness measures. A manual segmentation approach was used in this thesis to quantify neuroanatomical changes as this is considered the gold standard in the field, although automated methods are increasingly used in larger datasets due to manual segmentation's labour-intensive nature (Morey, et al. 2009; Power and Looi 2015). Manual segmentation produces volume metrics and binary images that can then be processed further using surface-based shape analysis techniques to give information on subtle localised morphological changes that may not be apparent using volume alone. For the corpus callosum however mid-sagittal thickness is analysed using a semiautomated segmentation technique.

Using the MRI scans above from IMAGE-HD, caudates, putamina, and hippocampi were traced according to previously established protocols described in detail below. For all, ANALYZE 11.0 (Mayo Foundation, Rochester, MI, USA) software is used to create 3D object maps of the structures that can be analysed for changes in volume and surface shape. The caudate and putamen were traced in the axial plane, while the hippocampus was traced

along the coronal plane. All brain MRI scans were analysed by one experienced tracer (FW), blinded to clinical information. Reliability of image analysis was assessed by intraclass correlation (ICC), which was evaluated by repeating right and left sided structural (caudate, putamen, hippocampus) measurements on 10 randomly selected scans (20 comparisons). Intra-rater intra-class correlations were 0.88-0.98.

2.2.1. Manual tracing of the caudate

Manual tracing of the caudate is based on a previously published protocol (Figure 2.1) (Looi, et al. 2008). Tracing occurs in the axial plane and begins at the most inferior slice where the anterior commissure becomes visible as a solid line. At this point the caudate head is distinguishable from the putamen, separated by the internal capsule. The caudate is traced in successive slices moving superiorly. The medial border is the wall of the lateral ventricle and the lateral border is the internal capsule, and tracing continues superiorly until the caudate becomes a thin sliver along the lateral ventricle which then disappears.

2.2.2 Manual tracing of the putamen

Manual tracing of the putamen is based on a previously published protocol (Looi, et al. 2009). Tracing begins on the same axial slice as the caudate, where the anterior commissure is first visible as a solid line and the caudate and putamen are separated by the anterior limb of the internal capsule. The putamen is traced in successive superior slices until it can no longer be seen. For inferior segments of the putamen the medial edge is the lamina separating putamen and globus pallidus, the lateral edge is the external capsule, and the anterior edge is the anterior limb of the internal capsule. As slices progress superiorly the globus pallidus

disappears and the putamen is bordered on its medial side by the anterior and inferior limbs of the internal capsule and on its lateral side by the external capsule.

Images for caudate and putamen are checked in the sagittal plane after tracing is complete in the axial plane and any errors are corrected, then saved for further shape processing described below.

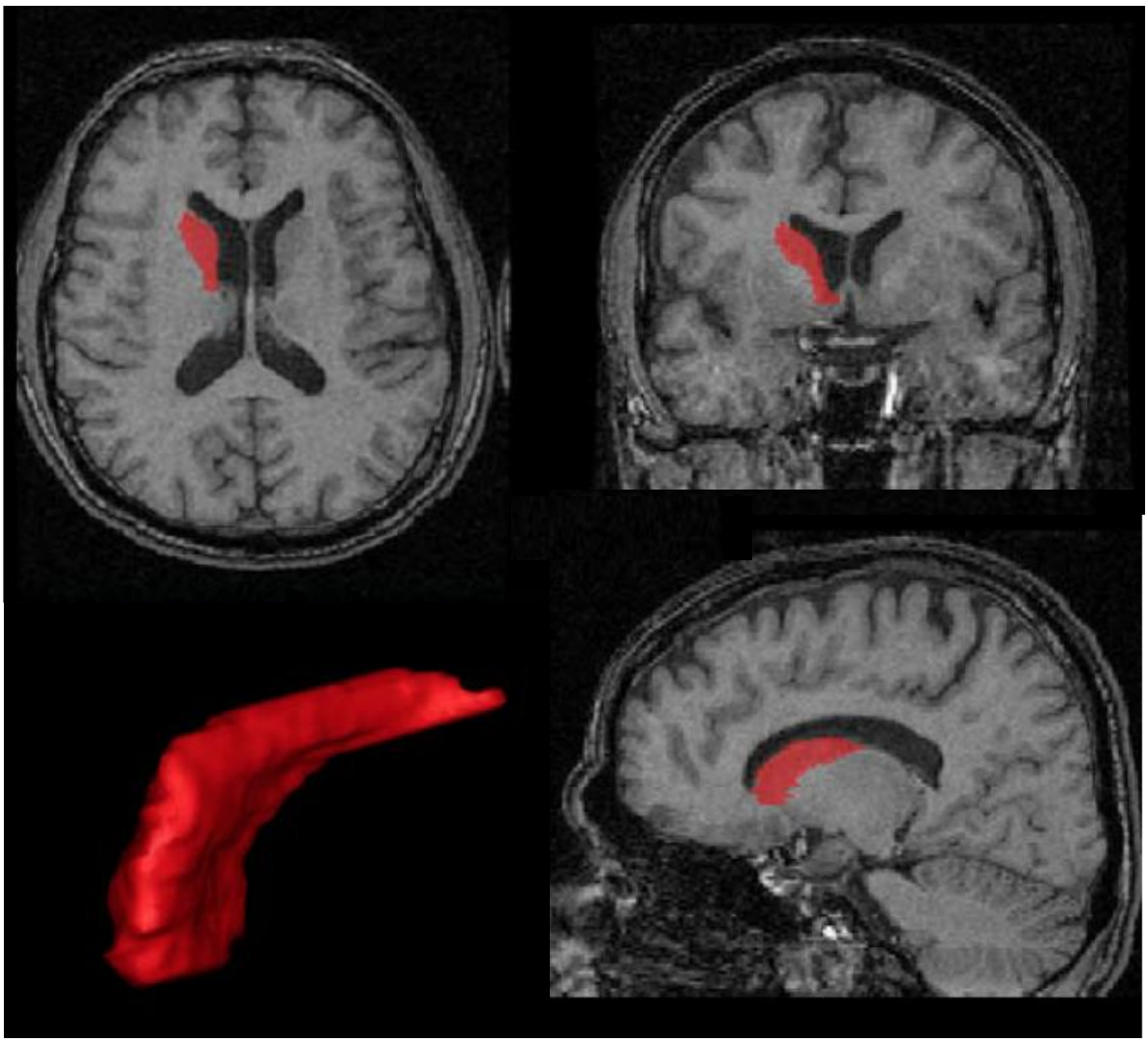

Figure 2.1: Manual tracing of the caudate. Image reproduced and modified from (Looi, et al. 2008) with permission. Caudate shaded in red, with views from all planes, as well as the 3-dimensional image of the same.

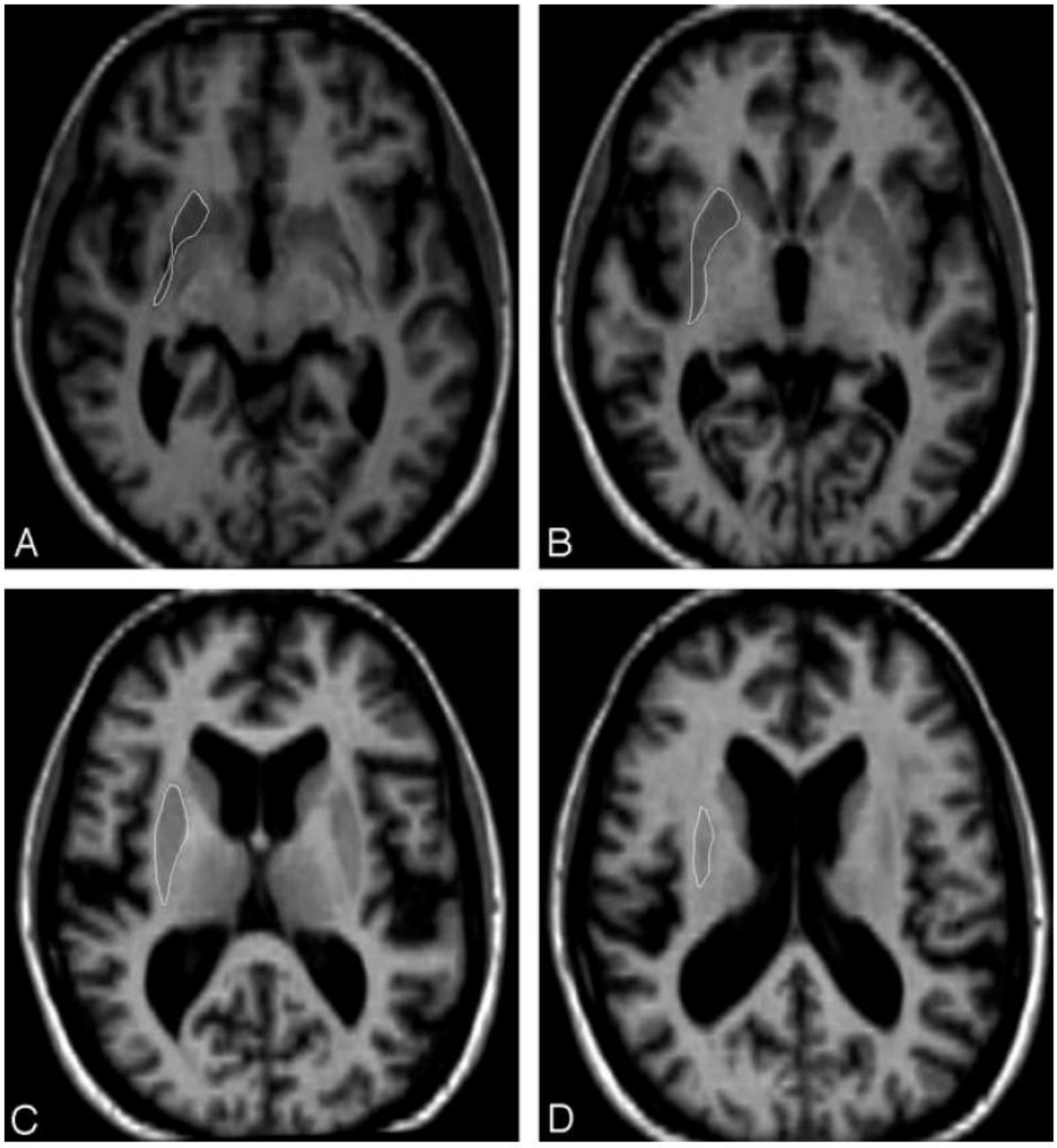

Figure 2.2: Manual tracing of the putamen. Image reproduced and modified from (Looi, et al. 2009) with permission. Putamen outlined in white in the axial plane, from inferior (A) to superior borders (D).

2.2.3 Manual tracing of the hippocampus

Manual tracing of the hippocampus is done according to the Melbourne Brain Centre protocol for extracting hippocampal volume from 3D T1-weighted MRI volumes using the ANALYZE and FSL softwares; this protocol is similarly based on previously published results (Velakoulis, et al. 1999; Watson, et al. 1992). Unlike the caudate and putamen, the hippocampus is traced in the coronal plane from posterior to anterior, starting one slice before the crus of the fornix merges into the thalamus. Slices are then traced anteriorly until the hippocampus disappears and the amygdala appears. To align the images before tracing, all MRI images were aligned along the anterior commissure- posterior commissure (AC-PC) plane in FSL. Tracing was then performed using Analyze software.

Tracing of the hippocampus begins posteriorly just before the crux of the fornix becomes indistinctly separated from the thalamus (Figure 2.3). The inferior border of the hippocampus is the interface between the hippocampal grey matter and the parahippocampal gyrus white matter. The lateral border is the temporal/inferior horn of the lateral ventricle. The superior border includes any white matter superior to the hippocampal grey matter- more posteriorly this is the fornix until it becomes the fimbria and alveus more anteriorly. For the inferior to medial border initially the tracing includes a one-voxel thick line just superior to the white matter of the parahippocampal gyrus, connecting the hippocampal grey matter to the cerebrospinal fluid (CSF) of the quadrigeminal cistern. This line is not included once the CSF of the ambient cistern moves laterally to reach the medial aspect of the fimbria/alveus, as happens more anteriorly in the tracing.

Note that the subiculum is not included in this protocol. The uncus is traced once it appears more anteriorly, as is the hippocampal tail. Once the uncus appears, the medial border of the

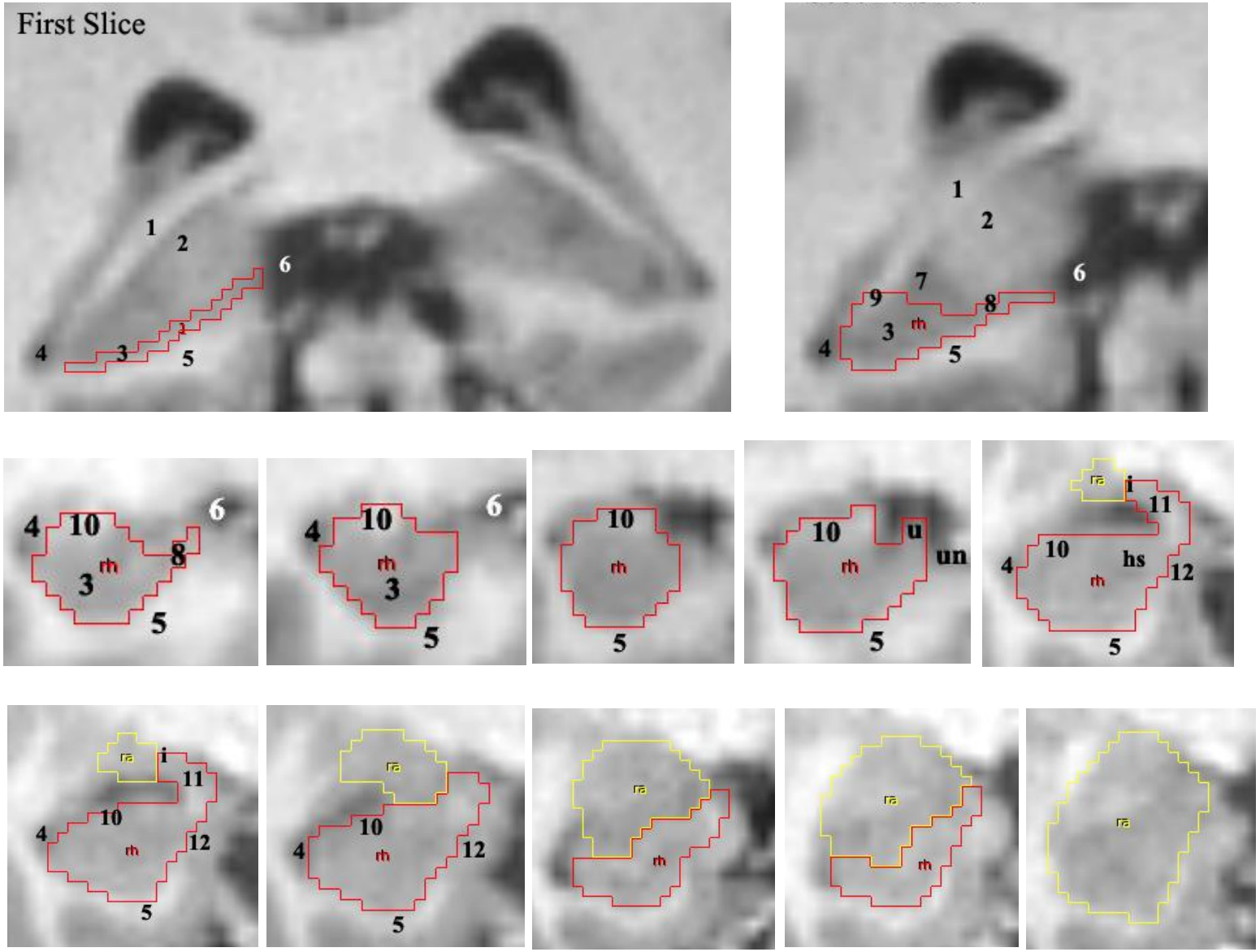
First Slice
1
2
6
4
3
5
1
2
7
6
9
8
rh
3
4
5
4
10
6
8
rh
3
5
4
10
6
rh
3
5
10
rh
5
10
u
un
rh
5
ra
i
11
4
10
hs
12
rh
5
ra
i
11
4
10
12
rh
5
ra
10
12
rh
5
ra
rh
ra

Figure 2.3: Manual tracing of the hippocampus. MRI images from the Melbourne Brain Centre Protocol (Velakoulis, et al. 1999; Watson, et al. 1992). Manual tracing of the hippocampus in the coronal plane, from posterior (top left) to anterior (bottom right). 1. Crus of the fornix; 2. Thalamus; 3. Hippocampal grey matter; 4. Temporal horn of lateral ventricle; 5. Parahippocampal gyrus; 6. Quadrigeminal cistern; 7. CSF in the subarachnoid space of the transverse cerebral fissures/choroidal fissure; 8. One voxel thick tracing of inferior to medial border of hippocampus, from superior to parahippocampal gyrus until reaching the quadrigeminal cistern (not included once quadrigeminal cistern moves laterally to reach the fimbria/alveus); 9. Fornix; 10. Fimbria/alveus; 11. "Seahorse head" of the hippocampus; 12. Inferior/medial border of the hippocampus; i. Isthmus; ra. Amygdala; rh. Hippocampus; u. Uncus; un. Uncal notch

hippocampus becomes the uncal notch. As the amygdala appears anteriorly the hippocampus gains its characteristic "seahorse shape" and starts to shrink while the amygdala increases in size. They are initially connected by an isthmus, then more anteriorly are separated in tracing by a thin strip of white matter between the two structures. When this is not discernible, a straight diagonal line is drawn from the most superior tip of the temporal horn of the lateral ventricle to the semiannicular sulcus. The hippocampus is traced until the temporal horn of the lateral ventricle is not visible, or when the temporal horn moves from a lateral to a completely inferior position.

2.3 Structural neuroimaging: Shape analysis

Methods which assess three-dimensional shape of structures, including those described below, allow analysis of systematic effects and structural-functional correlations of subcortical structures in neurodegenerative disease. They can measure the surface of a

structure precisely, calculate average shapes within groups, and determine differences between groups and correlate with clinically relevant measures (Looi and Walterfang 2012). This forms a clinically useful step between large-scale network studies, which are challenging for multiple reasons (conceptually, computationally and practically), and simple volumetric studies, which yield little detail. They also provide finer anatomical detail than functional studies.

There are a number of potential ways to analyse and compare shapes of structures (Wang, et al. 2011): for simple structures this can be done by computing an intermediate mapping to a canonical space such as a sphere (spherical harmonic point distribution models, SPHARM-PDM, discussed in further detail below) (Styner, et al. 2006), while for more complicated structures large deformation diffeomorphic metric mapping (LDDMM) generates models based on template shapes (Qiu, et al. 2010), and surface tensor-based morphometry uses a tensor based morphometric framework (Chung, et al. 2008). Subcortical surfaces can also be registered to parametric meshes that are imposed on manually traced or automatically segmented boundaries, yielding shape statistics such as radial distance and local area differences (discussed in further detail below) (Gutman, et al. 2015; Gutman, et al. 2012).

Methods discussed below focus on individual structures within the subcortical connectome, with emphasis on the strategic vulnerability of these structures, to develop a map of the connectome in HD and work towards development of an endophenotype (Looi, et al. 2014b). As these methods are specialised and technical, analyses were planned, designed and coordinated with the relevant specialists by the author, with specialist contributions discussed throughout the subsequent studies.

2.3.1 Radial thickness and Jacobian measures

This method uses the manual tracings above to create shape models of the caudate and putamen. A surface-based parametric mapping protocol is used to derive two pointwise shape measures: thickness (radial distance) and the Jacobian determinant (JD- surface dilation ratio) are derived across thousands of points on the surface of the left and right caudate and putamen (Figure 2.4). The protocol is freely available at http://enigma.ini.usc.edu/protocols/imaging-protocols/ and has been published elsewhere (Gutman, et al. 2015; Gutman, et al. 2012).

Thickness, or radial distance, is the local distance measure from medial curve to surface. This directly corresponds to localised volume, where thicker equals more local volume and vice versa. JD is the surface dilation ratio to template structure or local surface area (based on a template structure made from all shapes combined). JD is more reliable as it is made into a smoother measure, whereas Thickness is reportedly easier to interpret. Similarly, JD can capture the stretching/shrinking along the main axis of a region, whereas Thickness only examines radial expansion/contraction. The two measures together therefore provide complementary information that gives more detail than either measure alone (Gutman, et al. 2015; Gutman, et al. 2012). For further discussion, see for example (Tate, et al. 2016; Thompson, et al. 2004; Wang, et al. 2011).

Only shape models that pass visual inspection and that conform to T1-weighted MRI neuroanatomical boundaries using the ENIGMA Shape Analysis Quality Assessment Protocol are used in the analysis. Using the R package *lm* version 3.0.2, a multiple linear regression is fit at each thickness and Jacobian point to test for group differences and associations with clinical features. All analyses are adjusted for age, sex, and intracranial volume. A standard

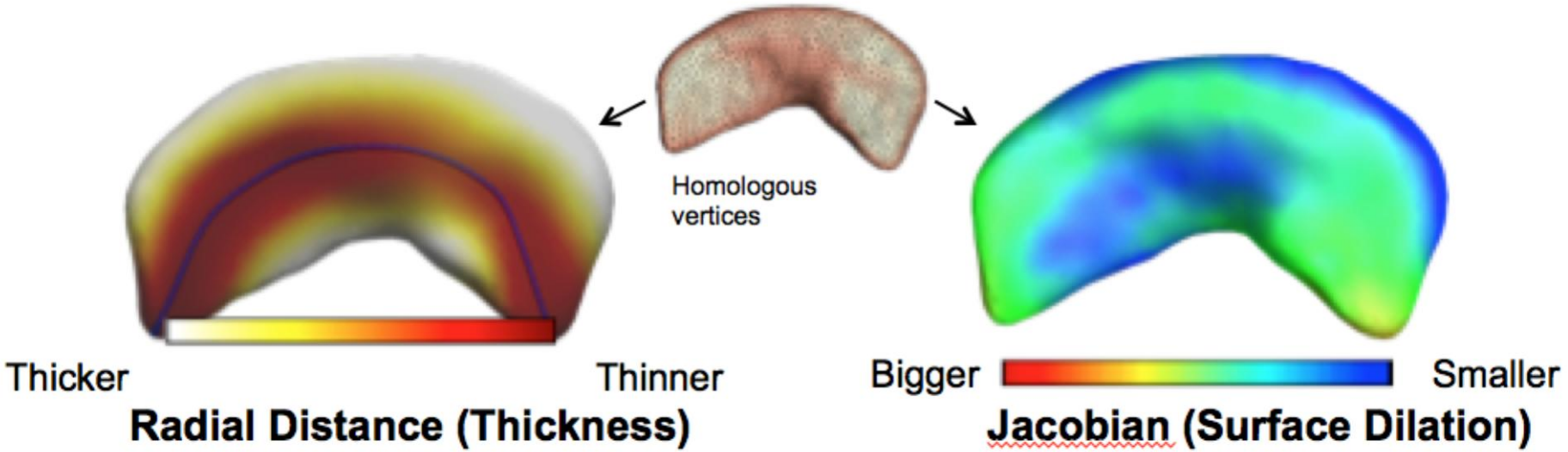

Figure 2.4: Visual representation of radial thickness and Jacobian measures of morphological change. Shape models are created based on manual tracing of caudate and putamen, with two pointwise shape measures (radial thickness and Jacobian surface dilation) derived across thousands of points on the surface.

false discovery rate (FDR) correction is applied at the accepted level of 5% (q=0.05) and implemented in the R function *p.adjusted*.

2.3.2 SPHARM-PDM longitudinal image processing

As there is currently no available method of longitudinal shape analysis using JD or Thickness protocols, the SPHARM-PDM method was modified so as to be able to look at morphological change over time. The SPHARM-PDM approach uses spherical harmonics to map a sphere mesh onto the target segmentation (Figure 2.5). This produces one-to-one mapping of surface vertices and makes possible a comparison of object average surfaces between groups.

Traced structures are processed for shape analysis using the SPHARM-PDM analysis software (https://www.nitrc.org/projects/spharm-pdm/) (Styner, et al. 2006). Segmented 3D binaries are smoothed with a 1mm Gaussian kernel and spherical harmonics are used to generate 1002 corresponding surface points (Levitt, et al. 2009; Styner, et al. 2006). An average shape is created using the control participants at the baseline time, and all structures are aligned to this mean shape using Procrustes alignment. For each participant at each time point, the signed magnitude of displacement along the surface normal from the mean shape is calculated. This displacement vector is used in subsequent shape analysis.

Displacement vector values are used as the dependent variables in all analyses, and thus all analyses are conducted across the 1002 corresponding points for each structure. Linear mixed models are utilised with a random intercept to account for repeated time effects. Predominant interest is in group and time differences. For between group comparisons, effects of group,

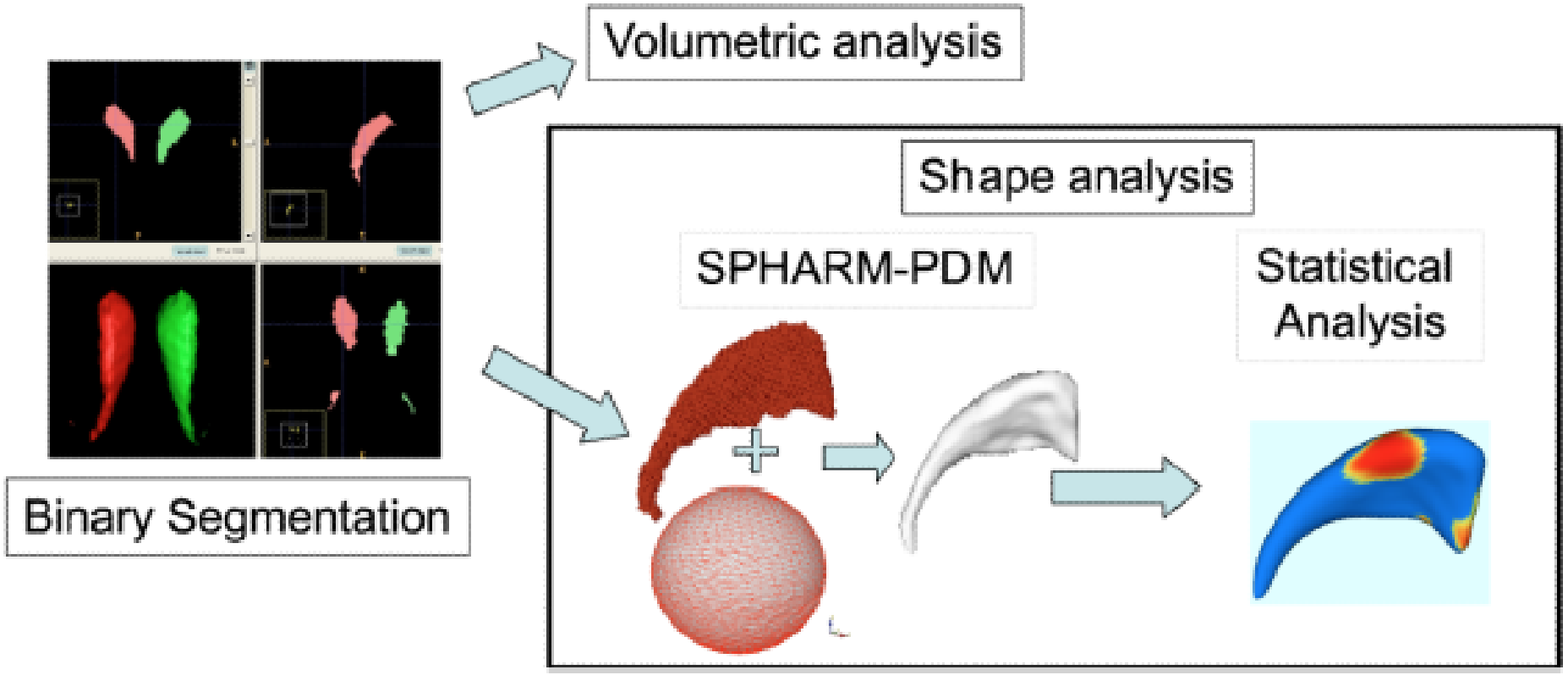

Figure 2.5: Schematic view of SPHARM-PDM pipeline (Styner, et al. 2006). Bilateral caudates are shown, from binary segmentation (red and green), through to SPHARM-PDM and statistical analysis.

time, and the interaction between the two are examined. For covariate analyses (CAG repeats), group by covariate interaction, time by covariate interaction, and three-way group, time and covariate interactions are examined. In all analyses age at baseline scan, sex and ICV at time of scan are used as covariates. P-values across each shape are corrected using FDR with $q < 0.05$.

2.4 Measuring and analysing callosal thickness

Thickness profiles for each midsagittal corpus callosum (CC) were generated from the 3D T1-weighted images using a fully automated pipeline (Adamson, et al. 2014). The thickness of corpus callosum (thickness profile) is determined by segmenting the midsagittal corpus callosum, then computing mid-points running from anterior to posterior so that streamlines can be generated to determine thickness profiles (Adamson, et al. 2014; Adamson, et al. 2011) (Figure 2.6).

Midsagittal plane extraction is performed using alignment to a template. The CC segmentation method consisted of template-based initialisation followed by refinement using a cascade of mathematical morphology operations, then manual editing is performed to correct errors. 100 streamlines are next generated at evenly spaced intervals, running orthogonally along the anterior-posterior trajectory through mid-line from superior to inferior CC. These are non-overlapping nominally parallel lines, the angle of which, running from the superior to inferior borders of the CC, is determined by Laplace's equation (Adamson, et al. 2011). Laplacian methods, previously used to robustly measure cortical thickness in highly curved areas such as sulci and gyri, generate streamlines that do not cross each other and are more representative of true thickness in these structures (Adamson, et al. 2011). From these

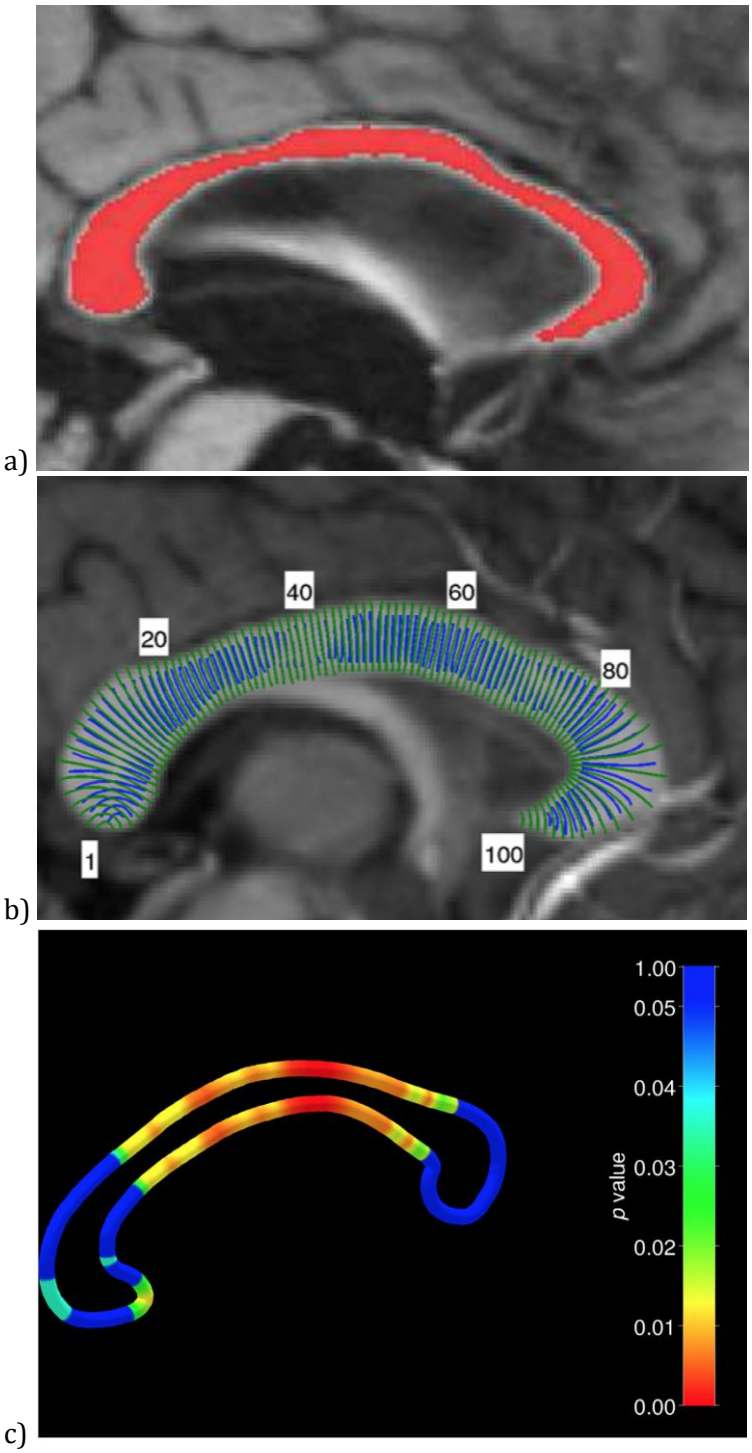

Figure 2.6: Measuring midsagittal callosal thickness. Method and pictures from (Adamson, et al. 2014). a) The corpus callosum is first semi-automatically segmented in the midsagittal plane. b) Thickness streamlines are drawn at 100 nodes along the corpus callosum, using Laplace's equation to determine the angle of the lines. c) Statistical results are displayed on a 3D tube surface that follows an "ideal" CC boundary. Here, example p-values are displayed along the surface.

100 streamlines along the CC, the distances to superior and inferior borders are measured and can be used as markers of regional and overall thickness and compared amongst groups.

Thickness profiles are compared utilising two-sample Welch's T-test, with age and ICV accounted for via regression. As sex differences in CC volume are largely due to variation in brain size, this was controlled for using ICV (Luders, et al. 2014). Multiple comparisons are corrected for via correction for the FDR. Correlations are performed between thickness profiles at each of the nodes with clinical and neurocognitive outcomes, utilising FDR to correct for multiple comparisons. The pipeline for this is available at www.nitrc.org/projects/ccsegthickness.

3. Study One: Baseline striatal morphology in HD

The first study in this thesis investigates the morphology of the striatum in HD and the relationship between morphology and motor and neurocognitive outcomes which are known to be subserved by frontostriatal circuits.

Table 3.1: Study One. Beginning the investigation of the subcortical connectome in HD through a baseline analysis of the neostriatum and its relationship with functional outcomes.

Study	Investigation	Rationale	Endophenotype components
Study One	***Baseline analysis of neostriatum and relationship with functional outcomes***	***Key structure in HD and hub in frontostriatal circuitry***	***Genetics Morphology Function***
Study Two	Longitudinal analysis of neostriatal change	Morphological change over time, investigating potential biomarkers	Genetics Morphology Spatiotemporal signature
Study Three	Baseline analysis of hippocampus and relationship with functional outcomes	Further extension of subcortical connectome in a different but related hub, potential for compensation	Genetics Morphology Function
Study Four	Baseline and longitudinal analysis of the corpus callosum	Major spoke within the connectome, complementary information regarding degeneration	Genetics Morphology Spatiotemporal signature

The following chapter has been published previously. It appears here with small amendments in format to match the overall structure of this thesis, as well as some minor alterations to help with clarity and with fitting in to the broader context of the thesis proper. Publications details are: Striatal morphology and neurocognitive dysfunction in Huntington disease: The IMAGE-HD study. *Psychiatry Research: Neuroimaging*, 291, 1-8 https://doi.org/10.1016/j.pscychresns.2019.07.003, with the full paper also attached as an Appendix to this thesis.

Title:

Striatal morphology and neurocognitive dysfunction in Huntington disease: The IMAGE-HD study.

Authors:

Fiona A. Wilkes[1], Zvart Abaryan[2], Chris R.K. Ching[2], Boris A. Gutman[2,3], Sarah K. Madsen[2], Mark Walterfang[4,5,6], Dennis Velakoulis[4,5], Julie C. Stout[7], Phyllis Chua[8], Gary F. Egan[7,9], Paul M. Thompson[2,10], Jeffrey C.L. Looi[1,4], Nellie Georgiou-Karistianis[7]

Affiliations:

[1] Academic Unit of Psychiatry and Addiction Medicine, the Australian National University Medical School, Canberra Hospital, Yamba Drive, Garran, ACT 2605, Australia
[2] Imaging Genetics Center, Department of Neurology, Stevens Institute for Neuroimaging & Informatics, Keck School of Medicine, University of Southern California, 4676 Admiralty Way, Ste. 200, Health Sciences Campus, Marina del Rey, CA, USA
[3] Department of Biomedical Engineering, Illinois Institute of Technology, 3255 South Dearborn St., Wishnick Hall, Suite 314, Chicago, IL 60616, USA
[4] Melbourne Neuropsychiatry Centre, Royal Melbourne Hospital and University of Melbourne, Level 3 Alan Gilbert Building, 161 Barry St., Calton, VIC 3053, Australia
[5] Neuropsychiatry Unit, Level 2, John Cade Building, Royal Melbourne Hospital, VIC 3050, Australia
[6] Florey Institute of Neuroscience and Mental Health, 30 Royal Parade, Parkville, VIC 3052, Australia

[7] School of Psychological Sciences and Monash Institute of Cognitive and Clinical Neurosciences, 18 Innovation Walk, Clayton Campus, Wellington Road, Monash University, VIC 3800, Australia
[8] Department of Psychiatry, School of Clinical Sciences, Monash University, Monash Medical Centre, Block P, Level 3 246 Clayton Road, Clayton, VIC 3168, Australia
[9] Monash Biomedical Imaging, 770 Blackburn Road, Building 220, Monash University, Clayton, VIC 3800, Australia
[10] Departments of Neurology, Psychiatry, Radiology, Engineering, Pediatrics and Ophthalmology, University of Southern California, CA, USA

Author contributions:

F.A. Wilkes performed the manual segmentation of the neostriatum, coordinated and directed the imaging analysis and wrote the bulk of the manuscript (>80% of total work). Z. Abaryan, C.R.K. Ching and B.A. Gutman performed the imaging analysis under the supervision of P.M. Thompson. J.C. Stout, P.Chua, G.F. Egan, and N. Georgiou-Karistianis were integral to the development and implementation of the overall IMAGE-HD project, of which this study is a sub-project. N. Georgiou-Karistianis is the primary investigator of the IMAGE-HD project and along with M. Walterfang and D. Velakoulis contributed to project design and is a PhD co-supervisor of F.A. Wilkes; J.C.L. Looi contributed to project design and coordination and is F.A. Wilkes' main PhD supervisor. All authors had significant intellectual and practical input into the final manuscript.

3.1 Abstract

We aimed to investigate the relationship between striatal morphology in Huntington disease (HD) and measures of motor and cognitive dysfunction. MRI scans, from the IMAGE-HD study, were obtained from 36 individuals with pre-HD, 37 with early symp-HD, and 36 healthy matched controls. The neostriatum was manually segmented and a surface-based parametric mapping protocol derived two pointwise shape measures: thickness and surface dilation ratio. Significant shape differences were detected between all groups. Negative

associations were detected between lower thickness and surface area shape measure and CAG repeats, disease burden score, and UHDRS total motor score. In symp-HD, UPSIT scores were correlated with higher thickness in left caudate tail and surface dilation ratio in left posterior putamen; Stroop scores were positively correlated with the thickness of left putamen head and body. Self-paced tapping (slow) was correlated with higher thickness and surface dilation ratio in the right caudate in symp-HD and with bilateral putamen in pre-HD. Self-paced tapping (fast) was correlated with higher surface dilation ratio in the right anterior putamen in symp-HD. Shape changes correlated with functional measures subserved by corticostriatal circuits, suggesting that the neostriatum is a potentially useful structural basis for characterisation of endophenotypes of HD.

3.2 Introduction

3.2.1 The role of the striatum in Huntington Disease

Huntington Disease (HD) is caused by a genetic mutation in the *huntingtin* gene, and leads to progressive and currently irreversible motor, psychiatric and cognitive decline (Vonsattel, et al. 1985). Multiple studies are utilising clinical, cognitive, neuropsychiatric, and imaging data to better understand the progression of HD, and to identify biomarkers for use as endpoints in clinical trials (Georgiou-Karistianis, et al. 2013a; Georgiou-Karistianis, et al. 2013c; Paulsen, et al. 2008; Tabrizi, et al. 2009). Atrophy of the neostriatum (caudate nucleus and putamen) has been well established in pre-HD more than a decade prior to disease onset (see (Georgiou-Karistianis, et al. 2013a; Paulsen, et al. 2008; Tabrizi, et al. 2009; van den Bogaard, et al. 2011a)), and becomes more pronounced as individuals approaches clinical diagnosis

(Dominguez, et al. 2013; Dominguez, et al. 2016; Georgiou-Karistianis, et al. 2013a; van den Bogaard, et al. 2011b).

The neostriatum is a crucial hub in corticostriatocortical re-entrant circuits that regulate cognition, emotion, behaviour and motor functions (Figure 3.1) (Draganski, et al. 2008). Structural changes in the striatum may disrupt these corticostriatal pathways (Looi and Walterfang 2012) leading to changes in motor function and related cognitive and neuropsychiatric outcomes in HD (van Duijn, et al. 2007). These circuits are structurally and functionally organised in the striatum in a topographic pattern (Bohanna, et al. 2011a; Haber 2003).

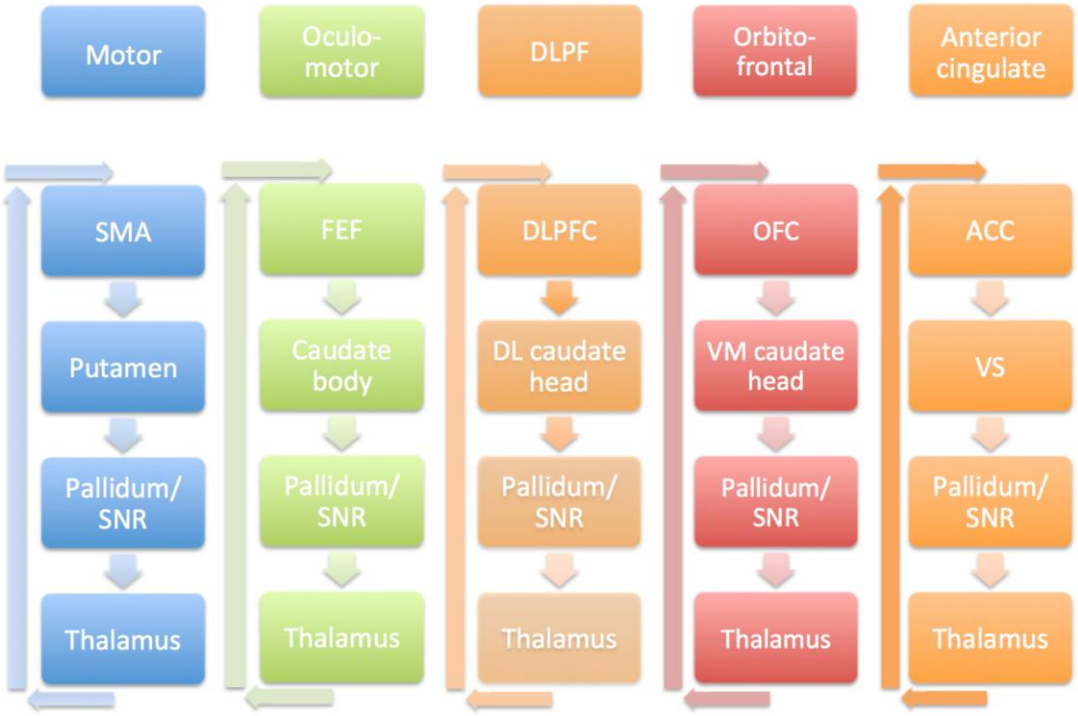

Figure 3.1: Frontostriatal re-entrant circuits. Based on Alexander, 1986 (Alexander, et al. 1986). SMA, supplementary motor area; SNR, substantia nigra pars reticulata; FEF, frontal eye fields; DLPF/C, dorsolateral prefrontal/cortex; DL, dorsolateral; OFC, orbitofrontal cortex; VM, ventromedial; ACC, anterior cingulate cortex; VS, ventral striatum.

HD studies that relate genetic and neuroanatomical measures to clinical outcomes may offer insight into disease mechanisms (Gottesman and Gould 2003). In part, motor dysfunction arises from structural alteration to, or atrophy in, corticostriatal circuit components, including the striatum. Structural atrophy may also be related to the severity of genetic loading as characterised by polyglutamine (CAG) repeat length in the *huntingtin* gene, which has been used in the literature to compute a disease burden score [DBS (CAG length − 35·5) × age] (Georgiou-Karistianis, et al. 2013c). CAG repeat length has long been known to be related to age of onset of disease, with longer repeat length related to earlier onset of motor symptoms of disease (Andrew, et al. 1993; Langbehn, et al. 2004). However, this is thought to account for only around 40-70% of the variance in age of disease onset, with other genes and environmental factors also presumed to play an important role (Ross and Tabrizi 2011; Wexler, et al. 2004).

Changes in striatal morphology have long been observed both in neuropathological and imaging studies of HD (Looi, et al. 2012; Tang, et al. 2019; van den Bogaard, et al. 2011b; Vonsattel, et al. 1985; Younes, et al. 2012). However, to our knowledge, very few studies have investigated the relationship between striatal shape or subregional specific volume changes and measures of dysfunction (Bohanna, et al. 2011a; Kim, et al. 2017; Turner, et al. 2016). Shape analysis is emerging as a potential endophenotype for multiple psychiatric and neurodegenerative diseases, allowing a more nuanced view of the interplay between structure and function (for review, see (Looi, et al. 2014b)). It has the advantage over pure volumetric analysis as it can elucidate subregional structural changes, in multiple disorders, which may not be apparent when looking at volume alone (Berner, et al. 2019; Tang, et al. 2019; Tate, et al. 2019). Further characterisation of these changes will improve knowledge of HD-associated neurodegenerative pathways and provide further insight to relate quantitative measures of

morphology (morphometry) to function. Measures of structural change in HD may also serve as biomarkers or surrogate endpoints for treatment trials (Georgiou-Karistianis, et al. 2013c), and importantly, development of future disease-modifying treatments may be further informed by an understanding of the progression of subcortical neurodegeneration.

3.2.2 Aims and hypotheses

In this investigation we aimed to characterise neostriatal changes in individuals with pre-HD and symp-HD compared to healthy controls, and to correlate changes with measures of clinical, motor, cognitive, and neuropsychiatric function. We hypothesised that quantified measures of neostriatal morphology would significantly differ between controls and individuals with pre-HD and symp-HD. We also hypothesised that neostriatal morphological changes would be associated with cognitive, neuropsychiatric and motor outcomes according to known functional connections.

3.3 Methods

3.3.1 Subjects and measures

Participants for this study, and all measurements, were acquired as part of the IMAGE-HD study (Georgiou-Karistianis, et al. 2013a). Participants included 36 individuals with pre-HD, 37 with early symp-HD, and 36 healthy matched controls. Healthy controls were matched for age, sex, and IQ (Nelson and Willison 1991) to the pre-HD individuals. All participants were right-handed and were free from brain injury, neurological and/or severe diagnosed psychiatric conditions (e.g. bipolar disorder, psychosis) other than HD. All pre-HD and symp-

HD participants underwent a UHDRS motor assessment (Huntington Study Group 1996); inclusion in the pre-HD group required a UHDRS total motor score of ≤ 5. Estimated years to clinical onset was based on the participant's age and the number of CAG repeats on the expanded allele (Langbehn, et al. 2004).

A battery of neurocognitive tests were administered on the day of scanning that were selected based on their sensitivity in detecting differences between groups from previous large scale multi-site studies (Stout, et al. 2011; Tabrizi, et al. 2009). The tests assessed visuo-motor speed and attention (SDMT (Smith 1982)), speeded reading (Stroop Word Test, (Stroop 1935)), odour recognition (UPSIT (Doty, et al. 1984)) and motor performance (speeded tapping and self-paced tapping tasks (Stout, et al. 2011) - inter-trial interval in speeded tapping, ITISTAP; inter-trial interval in participant passed tapping, slow 1.8 Hz, ITIPTAP slow average; and inter-trial interval in participant passed tapping, fast 3 Hz, ITIPTAP fast average). Participants completed behavioural questionnaires which included assessments of behaviours associated with frontal-striatal brain dysfunction, including executive function (FrSBe (Stout, et al. 2003)) and psychiatric disturbances (SCOPI (Watson and Wu 2005), HADS A and HADS D (Zigmond and Snaith 1983), BDI II (Beck 1996)).

The IMAGE-HD study was approved by the Monash University and Melbourne Health Human Research Ethics Committees; informed written consent was obtained from each participant prior to testing in accord with the Helsinki Declaration. All testing was undertaken at the Royal Children's Hospital, Parkville, Melbourne, Australia. Ethics approval for this sub-project was obtained from Monash University and the Australian National University.

3.3.2 Imaging

Imaging was performed on a Siemens Magnetom Trio Tim System 3 Tesla scanner with a 32-channel head coil (Siemens AG, Erlangen, Germany) at the Murdoch Children's Research Institute (Royal Children's Hospital, Victoria, Australia). High-resolution T1-weighted images were acquired (192 slices, slice thickness of 0.9 mm, 0.8 mm x 0.8 mm in-plane resolution, 320 x 320 mm field of view, TI=900 ms, TE=2.59 ms, TR=1900 ms, flip angle=9°). No participants were excluded on the basis of poor quality scans or missing data.

3.3.3 Volumetric analysis

Neostriatal volumes for each scan were measured by a single trained researcher (FW) using manual segmentation according to a validated protocol (intra-rater intraclass correlation 0.88-0.98) (Looi, et al. 2008; Looi, et al. 2009) and ANALYZE 11.0 (Mayo Foundation, Rochester, MI, USA) software. Details of the protocol have been published previously (Looi, et al. 2008; Looi, et al. 2009)- briefly, these are performed in native space and trace both the caudate and putamen separately in the axial plane from a starting point at the level of the anterior commissure, then every slice superiorly until their upper boundaries (Figure 3.2, 3.3). This method misses the nucleus accumbens/more limbic areas, and traces only the neostriatum proper.

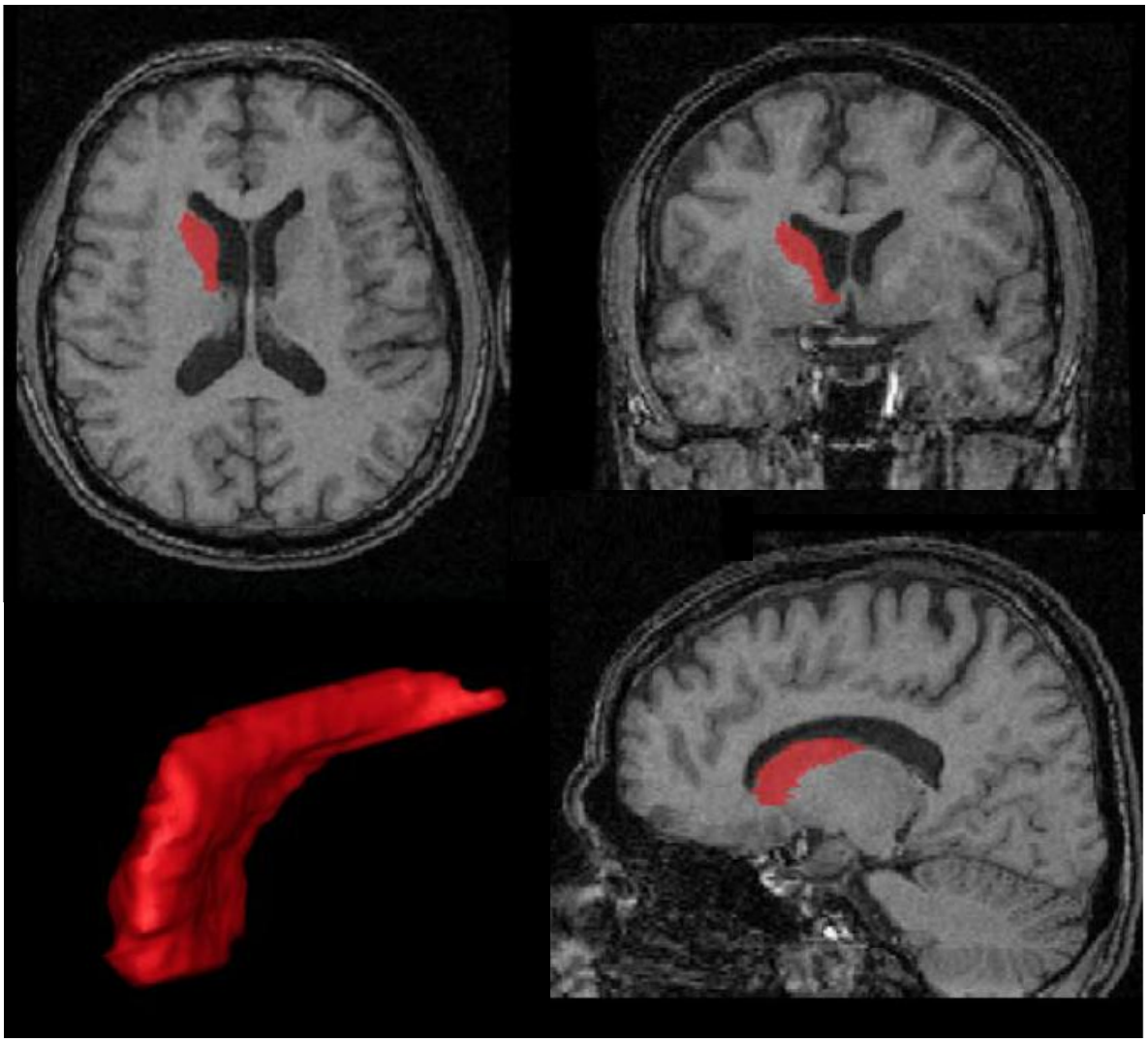

Figure 3.1: Manual tracing of the caudate. Image reproduced and modified from (Looi, et al. 2008) with permission. Caudate shaded in red, with views from all planes, as well as the 3-dimensional image of the same.

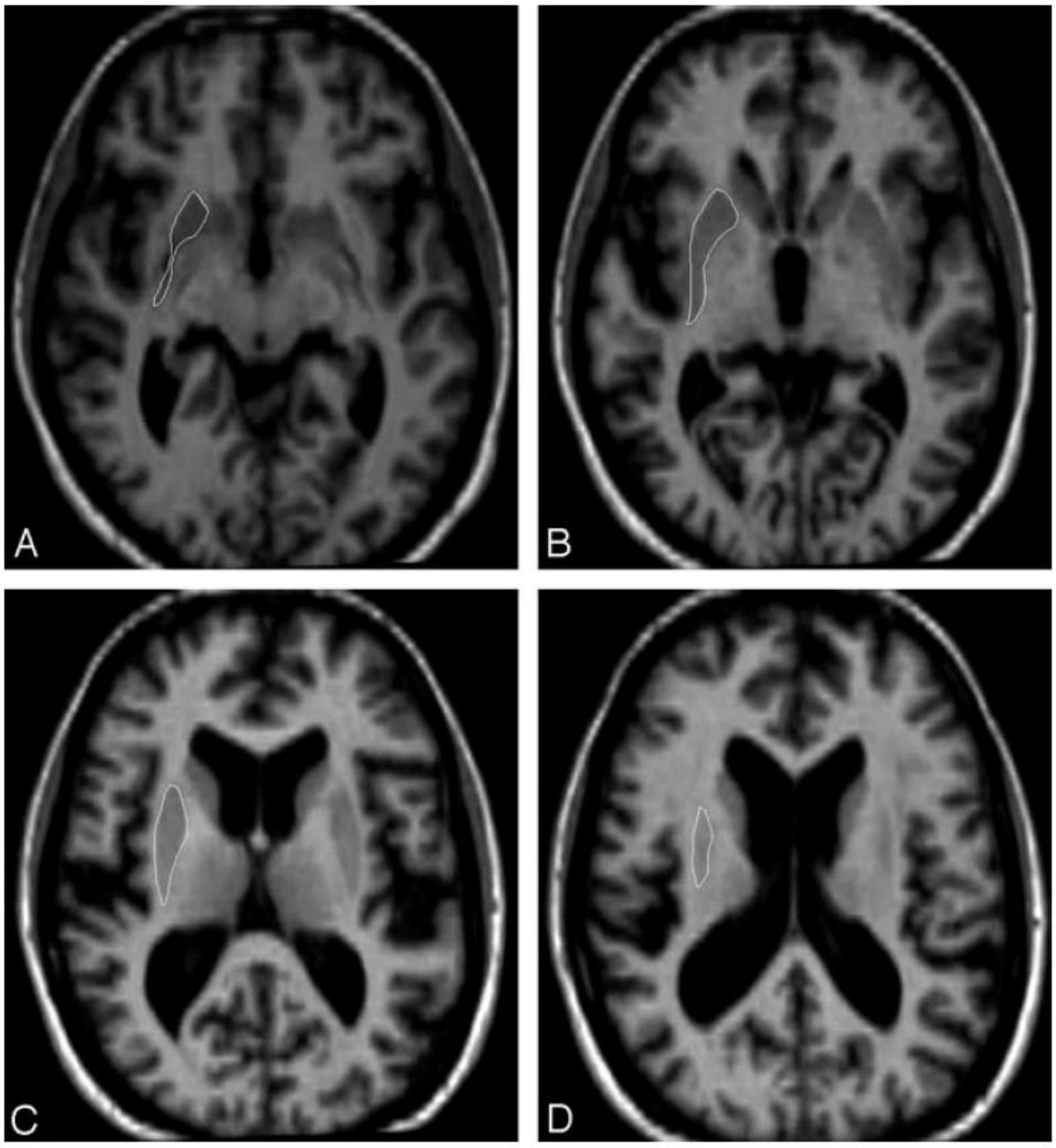

Figure 3.3: Manual tracing of the putamen. Image reproduced and modified from (Looi, et al. 2009) with permission. Putamen outlined in white in the axial plane, from inferior to superior borders.

Statistical analysis of volume and other baseline data was performed using SPSS 20.0 (Chicago, Ill., USA) and significance was set at $P<0.05$. Multivariate analysis of covariance (MANCOVA) was used to test statistical significance between the subject groups with age, sex and intracranial volume (ICV) as covariates (Table 3.2). ICV was calculated from outputs from FMRIB's Software Library FSL 4.1.6 1, for more details see (Georgiou-Karistianis, et al. 2013a). Preliminary checks were conducted to ensure there was no violation of assumptions of normality, homogeneity of variances, and reliable measurement of the covariate.

3.3.4 Shape analysis

A surface-based parametric mapping protocol derived two pointwise shape measures from the manual tracing above: thickness (radial distance) and the Jacobian determinant (surface dilation ratio) were derived across 2502 points on the surface of each of the left and right caudate and putamen. The protocol is freely available at http://enigma.ini.usc.edu/protocols/imaging-protocols/ (Figure 3.4) (Gutman, et al. 2015; Gutman, et al. 2012).

Striatal shape atlases were created from the manual segmentations first, and then the ENIGMA shape pipeline was modified to use these instead of free-surfer based atlases. Briefly, thickness, or radial distance, is a local distance measure from the medial curve to the surface. The Jacobian determinant is the surface dilation ratio relative to template structure, or a measure of the local surface area (relative to a template structure made from all manually traced shapes combined). For clarity in results/discussion, radial distance will be referred to as "thickness" and the Jacobian determinant will be referred to as surface expansion/contraction.

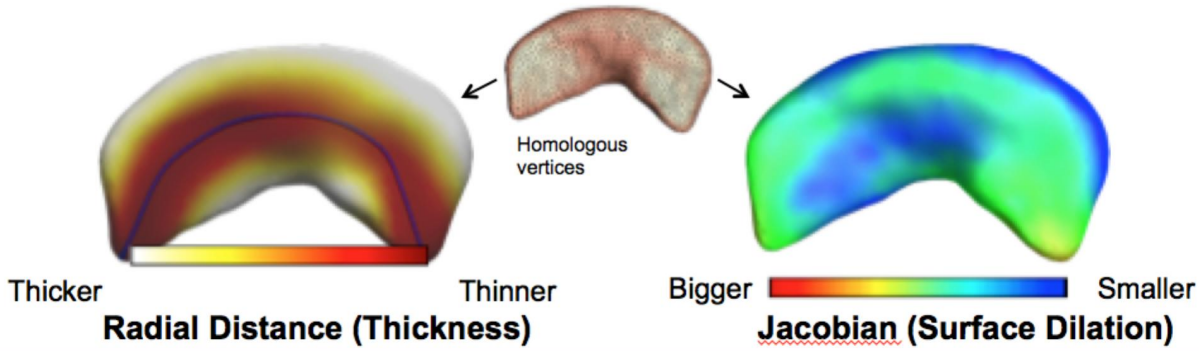

Figure 3.4: Visual representation of radial thickness and Jacobian measures of morphological change. Shape models are created based on manual tracing of caudate and putamen, with two pointwise shape measures (radial thickness and Jacobian surface dilation) derived across thousands of points on the surface.

Only shape models that passed visual inspection and that conformed to T1-weighted MRI neuroanatomical boundaries using the ENIGMA Shape Analysis Quality Assessment Protocol were used (http://enigma.ini.usc.edu/protocols/imaging-protocols/). Using the R package *lm* version 3.0.2, a multiple linear regression was fit at each thickness and Jacobian point to test for group differences and associations with clinical features. All analyses were adjusted for age, sex, and intracranial volume. A standard FDR correction was applied at the accepted level of 5% (q=0.05), as implemented in the R function *p.adjusted*.

3.4 Results

3.4.1 Demographics and clinical details

Group differences were assessed with non-parametric tests (Table 3.2). There were significant differences between groups in measures of self-paced tapping (1.8 Hz and 3 Hz), SDMT,

speeded tapping, UPSIT and Stroop ($p < 0.001$) and BDI-II ($p < 0.05$), but not in ICV, verbal IQ, SCOPI total OCD, FRSBE, or HADS anxiety or depression. Mann-Whitney U tests revealed significant differences between all three groups in all motor tests and in SDMT ($p \leq 0.017$). There were also significant differences between symp-HD and both controls and pre-HD in UPSIT and in Stroop ($p \leq 0.017$), and a significant difference between symp-HD and controls on the BDI-II ($p \leq 0.017$).

Table 3.2: Demographic and selected data across groups.[†]

	Mean ± SD		
	Controls (n=36)	Pre-HD (n=36)	Symp-HD (n=37)
Covariates and clinical information:			
Sex (M:F)	12:24	14:22	21:16
Age (years)	42.4±13.4	41.7±9.9	52.1±9.3
ICV (cm^3)	1456.4±143.5	1414.7±156.8	1400.8±155.7
CAG repeat number		42±2 (range 39-46)	43±2 (range 40-50)
Disease Burden Score (DBS)		269.4±52.7	378.5±67.8
Years to onset		15.5±7.0	
Years since diagnosis			2.0±1.6
UHDRS motor score (range)		1 (0-4)	19 (6-60)
Significant differences: All 3 groups[a]			
Putaminal volume	5969±797	5065±1089	3449±775
Caudate volume	7385±1162	6052±1574	4392±981

Speeded tapping (ms)	219.9±38.1	243.7±45.0	364.5±162.2
Self-paced tapping (1/SD ITI) 333ms	29.1±8.3	23.8±8.7	11.4±5.7
Self-paced tapping (1/SD ITI) 550ms	23.8±7.7	19.6±7.4	10.5±4.1
SDMT	56.3±10.1	51.5±8.6	36.0±11.7
Two comparisons[b]			
UPSIT	34.0±3.1	32.7±5.0	26.2±7.1
Stroop	109.8±16.6	104.4±17.5	82.5±22.0

ICV: Intracranial volume; DBS: (CAG-35.5)*age; YtO: approximate years to onset, modified Langbehn method (Langbehn, et al. 2004); YSD: Years since diagnosis; ITI: Inter-tap interval; SDMT: Symbol Digit Modalities Test; Age , sex and ICV were used as covariates in all analyses.

†For a full list see (Georgiou-Karistianis, et al. 2013a), although note that more subjects have been included in the symp-HD group since this initial publication.

a Symp-HD versus pre-HD, symp-HD versus controls, and pre-HD versus controls all $p \leq 0.017$

b Symp-HD versus pre-HD and symp-HD versus controls, $p \leq 0.017$

3.4.2 Volume and shape

There were significant differences in striatal volume between all three groups with control volumes larger than pre-HD, which were significantly larger than symp-HD (Table 3.2). Significant striatal shape differences were also detected between all groups (Figure 3.5), with controls showing larger shape metrics (increased thickness and surface expansion) than pre-HD, and pre-HD larger than symp-HD. These shape differences mapped across large areas of the striatum, with more extensive differences detected using the Jacobian shape metric (local

surface area expansion/contraction). The greatest shape differences were between controls and symp-HD, but there were also widespread shape differences between pre-HD and symp-HD and between pre-HD and controls. The greatest differences were in surface contraction and decreased thickness in the right putamen in pre-HD compared to controls and left putamen in symp-HD compared to pre-HD.

3.4.3 Correlations- shape

Significant negative associations were detected between striatal thickness and surface expansion/contraction measure and the number of CAG repeats, DBS, and UHDRS total motor score in pre-HD, symp-HD, or both (Figure 3.6). Again, greater areas of association were seen with the Jacobian surface contraction/expansion measures than with the thickness metric. In pre-HD, there were widespread significant negative associations between lower thickness and surface contraction in caudate and putamen and both CAG repeat number and DBS. These associations were detected to a much lesser extent in symp-HD, with only small areas of association between lower surface area shape measures and increasing DBS in patches of bilateral caudate, as well as left anterior putamen. Increasing CAG repeat number was only associated with lower surface area shape measures in left caudate head and anterior tail in symp-HD. Changes were similar but much less extensive when measuring thickness.

Figure 3.5: Shape differences between groups (next page). Top panel: Significant differences based on Jacobian determinant, indicating surface dilation due to subregional volume change. Bottom panel: Significant differences based on radial distance ("thickness"), or distance of the vertex from the medial curve of the structure. Beta value = regression coefficient, or "slope".

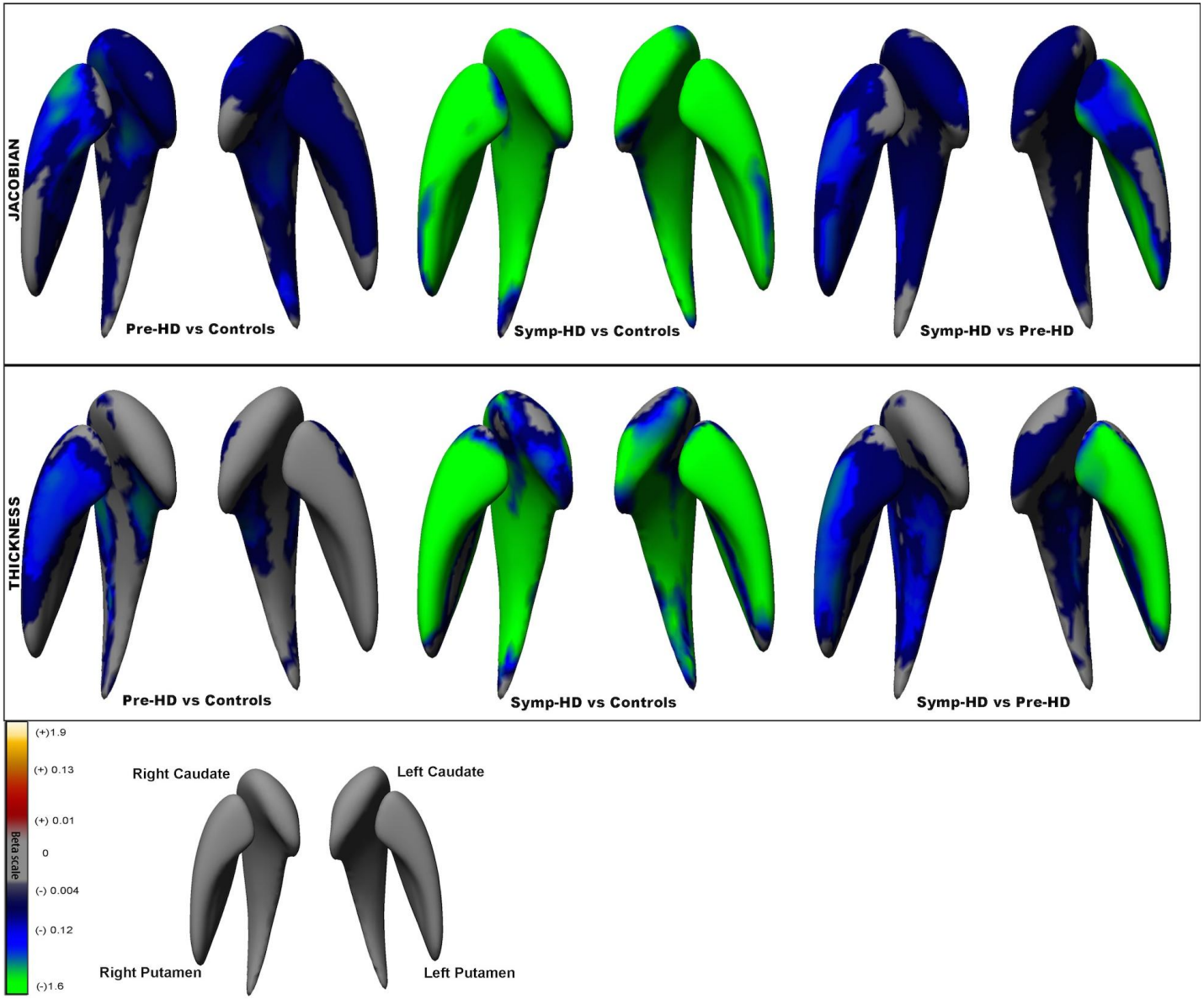
JACOBIAN
Pre-HD vs Controls
Symp-HD vs Controls
Symp-HD vs Pre-HD
THICKNESS
Pre-HD vs Controls
Symp-HD vs Controls
Symp-HD vs Pre-HD
(+)1.9
(+) 0.13
(+) 0.01
0
(-) 0.004
(-) 0.12
(-)1.6
Beta scale
Right Caudate
Left Caudate
Right Putamen
Left Putamen

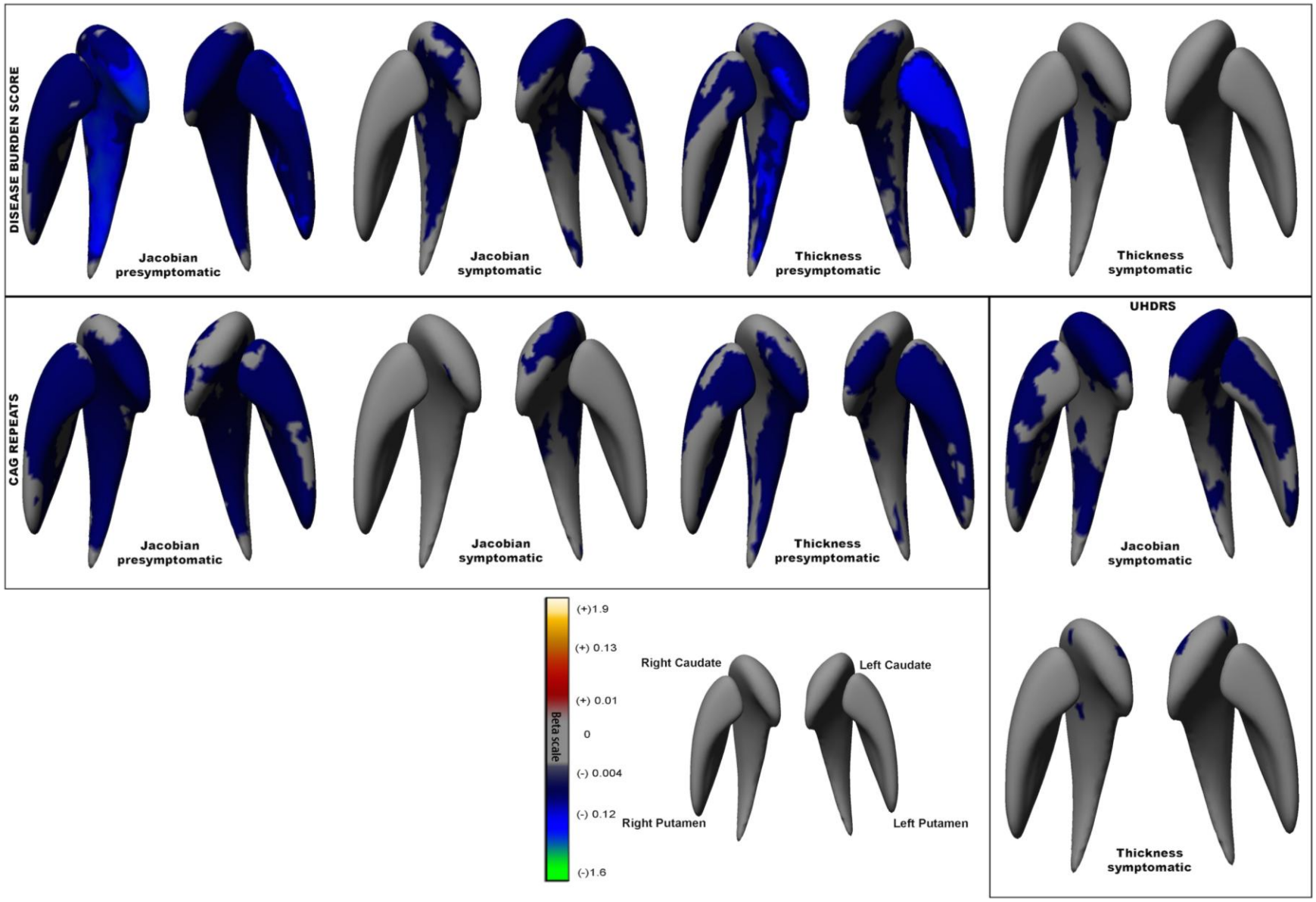
DISEASE BURDEN SCORE
Jacobian presymptomatic
Jacobian symptomatic
Thickness presymptomatic
Thickness symptomatic
CAG REPEATS
Jacobian presymptomatic
Jacobian symptomatic
Thickness presymptomatic
UHDRS
Jacobian symptomatic
Thickness symptomatic
(+)1.9
(+) 0.13
(+) 0.01
0
(-) 0.004
(-) 0.12
(-)1.6
Beta scale
Right Caudate
Left Caudate
Right Putamen
Left Putamen

Figure 3.6: Correlations between neostriatal shape and measures of disease burden. Panels indicate all significant correlations within each measure of disease burden: DBS, CAG repeats, and UHDRS motor scores. Jacobian = correlation based on surface dilation due to subregional volume change. Thickness = correlation based on radial distance, or distance of the vertex from the medial curve of the structure. Beta value = regression coefficient, or "slope".

Of the other motor and neurocognitive measures tested against shape changes in neostriatum, only UPSIT, Stroop, and self-paced tapping (slow and fast) showed significant correlations (Figure 3.7). There were significant associations between surface contraction in bilateral caudate and putamen in symp-HD and increasing UHDRS (motor) scores. These were limited to only patches of bilateral caudate head when thickness was tested.

In symp-HD, UPSIT scores were correlated with thickness of left caudate body and surface expansion in left posterior putamen, both in very limited regions. Stroop scores were positively correlated with the thickness of left putamen head and body. The regions of volume change are also very limited in these associations.

Self-paced tapping (slow) was correlated with surface expansion of the right caudate in symp-HD and with bilateral putamen in pre-HD, although when thickness was tested these correlations were confined to only anterior right caudate in symp-HD and right putamen in pre-HD. Self-paced tapping (fast) was correlated with right anterior putaminal higher surface expansion in symp-HD only.

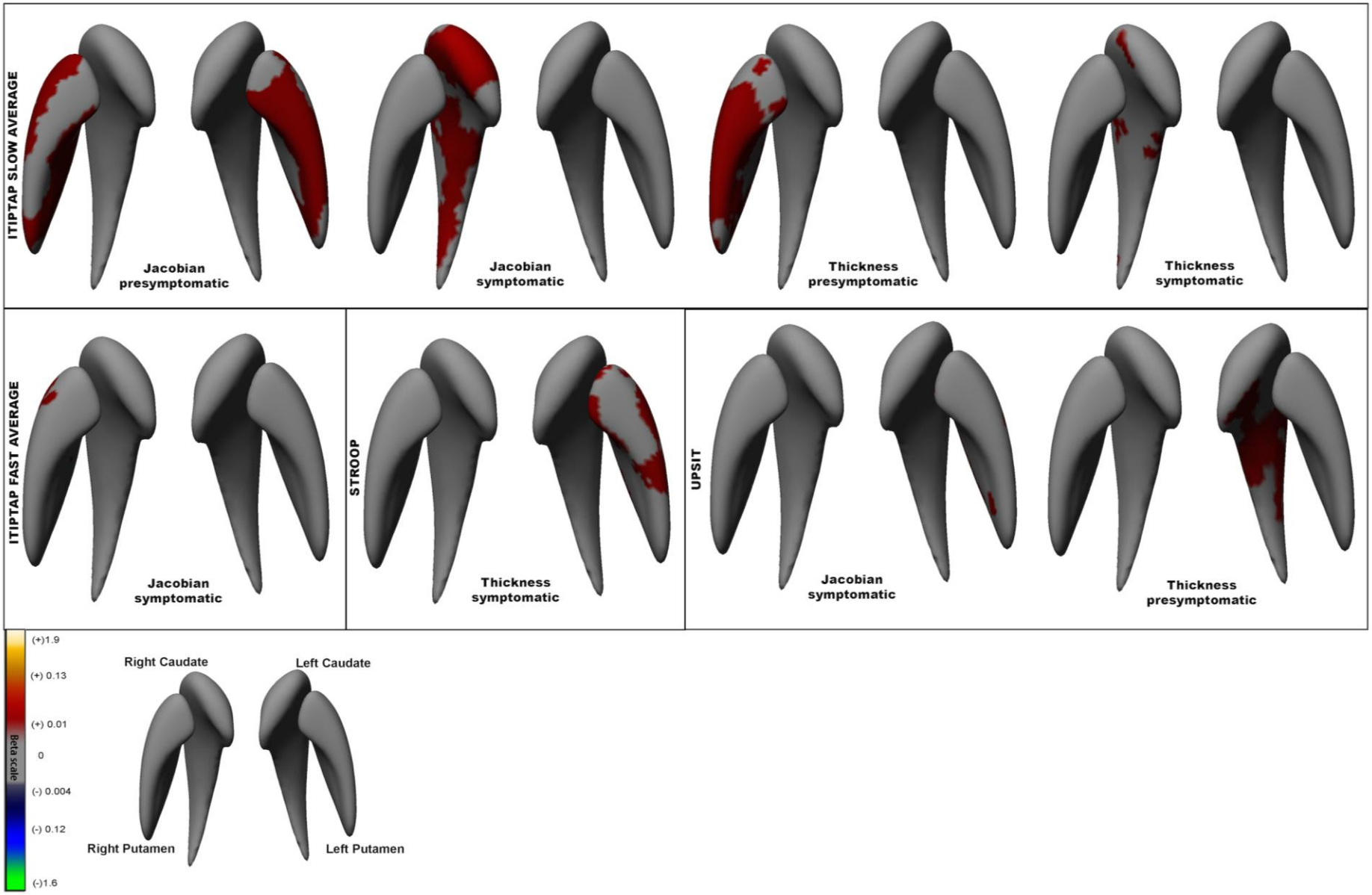
ITIPTAP SLOW AVERAGE
Jacobian presymptomatic
Jacobian symptomatic
Thickness presymptomatic
Thickness symptomatic
ITIPTAP FAST AVERAGE
Jacobian symptomatic
STROOP
Thickness symptomatic
UPSIT
Jacobian symptomatic
Thickness presymptomatic
(+)1.9
(+) 0.13
(+) 0.01
0
(-) 0.004
(-) 0.12
(-)1.6
Beta scale
Right Caudate
Left Caudate
Right Putamen
Left Putamen

Figure 3.7: Neostriatal shape correlations with motor and cognitive test scores. Panels indicate all significant correlations within each measure with significant results: ITIPTAP slow average (inter-trial interval in participant passed tapping, slow 1.8Hz), ITIPTAP fast average (inter-trial interval in participant passed tapping, fast 3Hz), Stroop, and UPSIT. Jacobian = correlation based on surface dilation due to subregional volume change. Thickness = correlation based on radial distance, or distance of the vertex from the medial curve of the structure. Beta value = regression coefficient, or "slope".

3.5 Discussion

This study has confirmed significant differences between controls, pre-HD and symp-HD in neostriatal volume and shape metrics that quantify morphologic structural brain change. The regions of change in this area, while using different methods and investigating both pre-HD and symp-HD, confirm similar patterns of striatal atrophy (Faria, et al. 2016; Kim, et al. 2017; Tang, et al. 2019; van den Bogaard, et al. 2011b; Younes, et al. 2012). It extends current research by finding that these morphologic changes correlate with CAG repeat number and DBS and that morphologic changes in specific areas in pre-HD and symp-HD are associated with motor and cognitive differences, which may provide insight into how subcortical morphometric changes relate to disease pathogenesis.

Interestingly, of the two measures used to identify shape changes, the Jacobian measurement of shape change showed more extensive and stronger correlations than the radial thickness measure. As the Jacobian measurement incorporates more dimensions of the data than the simple scalar value of thickness, it may be better suited to discriminate relevant shape changes (Gutman, et al. 2015; Gutman, et al. 2012). However, both measures remain useful in subcortical shape analysis (Tate, et al. 2019): radial thickness directly corresponds to localised volume, whereas the Jacobian determinant can capture the stretching/shrinking along the main axis of a region, making them different but complementary measures.

3.5.1 CAG repeat length correlations with shape

Increasing number of CAG repeats correlated with surface contraction and decreased thickness throughout the neostriatum in pre-HD. In contrast, in symp-HD, the number of CAG repeats was only associated with surface contraction in left anterior caudate. This may be a statistical artefact due to the destructive nature of HD - by the time of clinical diagnosis, there is already marked neurodegeneration, particularly in the striatum, whereas there is much more variation in size of the striatum in pre-HD. However, there is also evidence that the factors that determine age of disease onset in pre-HD (largely but not exclusively CAG) do not explain all of the disease progression once it has become manifest (Aziz, et al. 2018). In this study, reduced areas of shape correlation with CAG repeat length in symp-HD, but widespread correlations between shape and UHDRS throughout caudate and putamen, may also provide indirect evidence for the idea that CAG repeat length has less of an influence on disease progression. Similarly, there were also significant negative associations between neostriatal surface area shape measures and DBS. These correlations were greatest in pre-HD and less apparent in symp-HD.

3.5.2 Shape correlations with motor measures

Overall neostriatal volumes have been correlated with motor and cognitive outcomes in a number of studies in HD (Aylward, et al. 2012; Bechtel, et al. 2010; Delmaire, et al. 2012; Misiura, et al. 2017) but to our knowledge only two studies have examined striatal subregional morphology and motor outcomes in HD (Bohanna, et al. 2011a; Turner, et al. 2016). Both studies investigated the IMAGE-HD cohort or a subset.

Bohanna and colleagues have previously found the greatest differences in volume and diffusion tensor imaging measures in dorsal areas of the striatum that have connections to primary motor and somatosensory cortices; subregion-specific volume was also strongly correlated with the UHDRS motor score (Bohanna, et al. 2011a).

Using a subset of the IMAGE-HD cohort, Turner and colleagues (Turner, et al. 2016) measured EEG components of sensorimotor integration in 12 individuals with pre-HD and 7 with symp-HD and correlated these with shape changes in the striatum. All results occurred in the context of abnormal processing but normal task execution. Unregulated premotor activation was correlated with shape deflation of the dorsal putamen bilaterally, as well as deflation in anterior inferior putamen (left > right). This was thought to reflect the ability to recruit compensatory network from frontal motor projection areas. In contrast, delayed timing of neural premotor activation was significantly correlated with shape deflation in the right caudate (anterolateral and dorsomedial areas only). Here, caudate shape deflation was thought to impair motor planning and execution (Turner, et al. 2016).

Self-paced finger tapping has been previously shown to be impaired in both pre-HD and symp-HD individuals (Bechtel, et al. 2010; Georgiou-Karistianis, et al. 2013a; Stout, et al. 2011). This task requires participants to listen to a tone presented at a certain rate (1.8 or 3.0 Hz), to tap along with this tone, and then to continue tapping at the same rate after cessation of the tone (Stout, et al. 2011). "ITIPTAP slow average" measures the variance in self-paced tapping to a slow beat. In pre-HD, worsening accuracy in this measure was correlated with shape contraction throughout bilateral putamen (and reduced thickness in right putamen). Interestingly, in symp-HD this correlation was lost and instead worsening accuracy in self-paced tapping scores were correlated with right caudate shape contraction, throughout the

entire caudate. This is consistent with the results found by Turner and colleagues above (Turner, et al. 2016), suggesting that initially the bilateral putamen is able to recruit compensatory networks to help in motor tasks, but eventually this fails and consequently, right caudate atrophy impairs motor planning and execution, leading to worsening outcomes without any remaining compensatory measures. The regions of shape and volume change in these associations implicate the surface mapping of afferents from a wide range of circuits, including but not limited to the rostral premotor (to a lesser degree) and caudal motor corticostriatal circuits that converge on the striatum (Draganski, et al. 2008; Haber 2003). Fast self-paced tapping is thought to be more difficult, requiring greater involvement of the frontal cortex rather than the striatum (Delmaire, et al. 2012), which may explain why there are fewer significant correlations seen between self-paced tapping (fast) and striatal shape in our study, apart from in the anterior right putamen in a region that has connections to frontal cortex.

3.5.3 Shape correlations with neurocognitive measures

Of the neurocognitive measures tested, UPSIT and Stroop, but not SDMT, showed correlations with striatal shape metrics in symp-HD. There were no significant correlations detected between neostriatal shape and any cognitive measures in pre-HD or in controls. To our knowledge only one previous study has investigated the correlation between neostriatal shape change and neurocognitive measures; Kim and colleagues manually segmented the caudates of individuals with pre-HD and correlated shape changes here with composite measures of executive function and working memory. They found that scores in these domains mapped to anteromedial caudate (Kim, et al. 2017).

The UPSIT is a complex task involving integration from a number of areas. Scores in UPSIT have been associated with diffusion tensor MRI mean diffusivity in the parietal lobe, medial temporal lobes, cingulum and insula, as well as caudate nucleus and anterior putamen (Delmaire, et al. 2012). Here, we have found that in symp-HD, better scores in UPSIT are related to increased thickness of left mid-caudate and surface expansion in left posterior putamen. The regions of both shape and volume difference are very limited in these associations, and implicate the surface mapping of afferents from the orbitofrontal and dorsolateral-prefrontal corticostriatal circuits that converge on the left caudate, as well as known areas of connections with temporal lobe in left putamen (Draganski, et al. 2008; Haber 2003).

Similarly, the Stroop Word Test requires executive control (MacLeod and MacDonald 2000). In this study Stroop scores were positively correlated with left anterior putaminal thickness in symp-HD, in regions mapping to orbitofrontal and dorsolateral-prefrontal corticostriatal circuits (Draganski, et al. 2008; Haber 2003). Of note, correlations with both Stroop and UPSIT were in the left neostriatum only- the dominant hemisphere for all subjects. Integrity of tracts between the putamen and prefrontal areas are thought to be critical for executive function (Liston, et al. 2006). Damage to these tracts and others, as reflected in the shape abnormalities here, can affect not only the more obvious motor symptoms of HD but also subtler circuitry controlling executive function. The small regions of associations here compared to the larger areas of association in Kim et al.'s study (Kim, et al. 2017) likely reflect the composite nature of their measures. Our study however remains an important addition to the current body of work because it adds precise anatomical detail to this knowledge of circuitry, and extends into further measures of caudate and putamen, as well as motor, cognitive and clinical measures.

3.6 Limitations

We focused on the morphology of the striatum as a sentinel measure of structural change within corticostriatal circuits, which we believe is more easily quantified than the entirety of the corticostriatal pathways. Inferences regarding the effect of shape differences on known underlying subfields are limited by our shape analysis technique. Some inferences may be made based on neuroanatomical sources (Draganski, et al. 2008; Haber 2003), but ongoing work involves the challenging task of mapping known neuroanatomical subfields to the surface of our subcortical shape models. Future studies may provide additional insights into the underlying subfield effects detected by this powerful shape analysis technique.

3.7 Conclusions/clinical implications

We have replicated and extended on previous work showing that quantified measures of neostriatal morphology differ significantly across controls, pre-HD and symp-HD. We found the thickness and surface expansion/dilation measures correspond to the surface mapping of afferents from corticostriatal circuits in HD. Furthermore, neostriatal shape correlated with motor, neurocognitive and clinical measures subserved by such circuits, suggesting that the neostriatum is a potentially useful structural basis for characterisation of endophenotypes of HD. Future work in HD should investigate the spatiotemporal progression of striatal atrophy and its genetic and clinical correlates: to assess the usefulness of such quantifiable endophenotypes (striatal structure and frontostriatal function) to understand the pathophysiology of the disorder, monitor disease progression and ultimately, assess response to clinical interventions (Looi and Santillo 2017).

4. Study Two: Longitudinal striatal morphology in HD

Building from the information gained in Study One regarding the role of the neostriatum in HD and its relationship to motor and neurocognitive outcomes, Study Two moves on to investigate longitudinal changes in morphology and work towards a biomarker for future tests of treatments in HD. Until recently longitudinal shape change has been difficult to investigate due to methodological and statistical issues. A member of our extended research group has developed a method which solves these issues, leading to increased opportunities to investigate and develop an endophenotype and biomarkers of HD.

Table 4.1: Study Two. Continuing the investigation of the subcortical connectome in HD through longitudinal analysis of the neostriatum: working towards a biomarker.

Study	Investigation	Rationale	Endophenotype components
Study One	Baseline analysis of neostriatum and relationship with functional outcomes	Key structure in HD and hub in frontostriatal circuitry	Genetics Morphology Function
Study Two	***Longitudinal analysis of neostriatal change***	***Morphological change over time, investigating potential biomarkers***	***Genetics Morphology Spatiotemporal signature***
Study Three	Baseline analysis of hippocampus and relationship with functional outcomes	Further extension of subcortical connectome in a different but related hub, potential for compensation	Genetics Morphology Function

Study Four	Baseline and longitudinal analysis of the corpus callosum	Major spoke within the connectome, complementary information regarding degeneration	Genetics Morphology Spatiotemporal signature

Title:

The shape of things to come. Mapping spatiotemporal progression of striatal morphology in Huntington disease: The IMAGE-HD study.

Authors:

F.A. Wilkes[1], D. Jakabek[2], M. Walterfang[3,4], D. Velakoulis[3,4], J.C. Stout[5], P. Chua[6], G.F. Egan[5], J.C.L. Looi[1,3], N. Georgiou-Karistianis[5]

Affiliations:

[1] Research Centre for the Neurosciences of Ageing, Academic Unit of Psychiatry and Addiction Medicine, Australian National University Medical School, Canberra Hospital, Canberra, Australia
[2] Graduate School of Medicine, University of Wollongong, Wollongong, Australia
[3] Neuropsychiatry Unit, Royal Melbourne Hospital, Melbourne Neuropsychiatry Centre, University of Melbourne and Northwestern Mental Health, Melbourne, Australia
[4] Florey Institute of Neuroscience and Mental Health, University of Melbourne, Melbourne, Australia
[5] School of Psychological Sciences and the Turner Institute of Brain and Mental Health, Monash University, Melbourne, Australia
[6] Department of Psychiatry, School of Clinical Sciences, Monash University, Monash Medical Centre, Melbourne, Australia

Author contributions:

F.A. Wilkes performed the manual segmentation of the neostriatum, coordinated and directed the imaging analysis and wrote the bulk of the manuscript (>80% of total work). D. Jakabek developed and performed the longitudinal statistical shape analysis. J.C. Stout, P.Chua, G.F. Egan, and N. Georgiou-Karistianis were integral to the development and implementation of the overall IMAGE-HD project, of which this study is a sub-project. N. Georgiou-Karistianis is the primary investigator of the IMAGE-HD project and along with M. Walterfang and D. Velakoulis contributed to project design and is a PhD co-supervisor of F.A. Wilkes; J.C.L. Looi contributed to project design and coordination and is F.A. Wilkes' main PhD supervisor. All authors had significant intellectual and practical input into the final manuscript.

4.1 Abstract

Mapping the spatiotemporal progression of neuroanatomical change in HD is fundamental to developing potential clinical biomeasures suitable for prognostication. Statistical shape analysis to measure the striatum, a key structure of interest, has been performed in HD. However, there have been few longitudinal studies, primarily due to the complexity in modelling shape change across progressive time points.

To address the limitations of the current literature, we utilised the Spherical Harmonic Point Distribution Method (SPHARM-PDM) to generate point distribution models of shapes for individuals, and used linear mixed models to test for localised shape change over time. We performed this method on T1-weighted brain MRI scans from the IMAGE-HD study from 36

individuals with pre-HD, 37 with early symp-HD, and 36 healthy matched controls, with scans repeated at 18 and 30 months.

We found significant differences in shape of the striatum between groups. Significant group-by-time interaction was observed for the putamen bilaterally, but not for caudate, with a differential rate of shape change between groups over time and deflation more pronounced in the symp-HD group. The main effect of CAG repeats on shape in pre-HD and symp-HD occurred for the entire bilateral striatum. Later time points demonstrated increased deflation with increased CAG repeat number in the left caudate head and tail, and right caudate medial body.

This is the first time that such robust statistical analysis of shape change in HD has been able to be performed and has profound implications for the development of a morphological biomarker in HD.

4.2 Introduction

In HD, atrophy of the neostriatum, caused by a trinucleotide repeat expansion in the *huntingtin* gene, leads to progressive motor, psychiatric and cognitive disturbances (Vonsattel, et al. 1985). Neostriatal volume begins to reduce more than 10.8 years before predicted onset of motor symptoms (van den Bogaard, et al. 2011a), with more pronounced atrophy the closer an individual is to predicted onset (van den Bogaard, et al. 2011b). Mapping the spatiotemporal progression of neuroanatomical change in HD, such as in the striatum, is fundamental to developing endophenotypes (intermediate phenotypes such as

cognitive, motor and behavioural changes (Gottesman and Gould 2003) which may lead to development of clinically relevant biomeasures suitable for staging disease and monitoring treatment response. Based on prior work (Looi and Walterfang 2012), we explore the role of the striatum as a spatiotemporal structural basis (Looi and Santillo 2017) for endophenotypes of HD.

4.2.1 Striatal shape in HD

Morphological changes in the striatum in HD were initially observed in post-mortem studies (Vonsattel, et al. 1985; Vonsattel and DiFiglia 1998), with atrophy beginning in the dorsal medial head of the caudate and putamen, as well as early loss in the tail of the caudate (Douaud, et al. 2006; Kassubek, et al. 2004; Roos, et al. 1985; Vonsattel, et al. 1985; Vonsattel and DiFiglia 1998), a finding which has been largely confirmed using more recent imaging modalities (Looi, et al. 2012; van den Bogaard, et al. 2011b; Younes, et al. 2012). Statistical shape analysis of the striatum has been performed in premanifest as well as manifest HD (Looi, et al. 2012; van den Bogaard, et al. 2011b; Younes, et al. 2012): small areas of shape displacement occur in people with premanifest HD 11.6y from predicted disease onset (van den Bogaard, et al. 2011b), with more pronounced changes occurring in the medial caudate nucleus and putamen in those closer than 10.8y to predicted onset (van den Bogaard, et al. 2011b). Using an index of degree of exposure to the toxic polyglutamine repeats (a so-called “CAP-score”, based on CAG repeat length and age) significant shape differences can be seen in caudate and putamen in people with premanifest HD with high CAP scores, and in left putamen in the mid CAP scores group (Younes, et al. 2012).

4.2.2 Mapping spatiotemporal progression of striatal atrophy in HD: the current state of play

There have been few longitudinal studies of striatal shape change in HD, primarily due to the complexity in modelling shape change across progressive timepoints, though linear mixed effects models show promise (Gerig, et al. 2016). Studies have utilised tensor-based morphometry, Large Deformation Diffeomorphic Metric Mapping (LDDMM) (Muralidharan, et al. 2014; Muralidharan, et al. 2016), and the *BrainPrint* package which combines complex shape descriptors with linear mixed models analysis (Wachinger, et al. 2016). Each of these methodologies has their own limitations. Tensor-based methods have thus far relied on subtraction between baseline and follow-up to quantify changes, which becomes limited when multiple time points are involved.

To date, only four studies have investigated longitudinal striatal shape change in HD (Hong, et al. 2017; Muralidharan, et al. 2014; Muralidharan, et al. 2016; Ramirez-Garcia, et al. 2020). Using data from the PREDICT-HD study, Muralidharan and colleagues utilised diffeomorphic trajectories to compare caudate (Muralidharan, et al. 2014) and right putamen (Muralidharan, et al. 2016) shapes in pre-HD, with observed contraction in the head and tail and expansion in the medial body of the caudate, and deflation of the anterior and posterior aspects of the right putamen, with again some medial inflation increasing with higher CAP scores. In these studies, the significance of local shape change was not tested, nor did the authors examine for shape change association with CAG repeats. Hong and colleagues (Hong, et al. 2017) have tried to address some of these issues in a feasibility study comparing intrinsic shape properties of a subject specific shape trajectory in comparison to a normalised 4D shape atlas representing normal ageing. However, this has not yet overcome the issue of statistically testing for localised shape changes (Hong, et al. 2017). Most recently, Ramirez-Garcia and colleagues (Ramirez-Garcia, et al. 2020) performed longitudinal surface based

analysis on 17 people with HD and 17 controls, with two scans over a 16 month period: this used the FMRIB Integrated Registration and Segmentation Tool (FIRST) software of FSL version 6.0 to identify shape-deformation pattern in a vertex-wise fashion. This does provide localised changes, but assesses changes with t-tests only and there was no ability to account for variables such as age, ICV, or CAG repeat number.

4.2.3 A method to measure spatiotemporal progression

To address the limitations of the current literature (and those of longitudinal shape analysis more broadly), we propose to utilise the Spherical Harmonic Point Distribution Method (SPHARM-PDM) (Styner, et al. 2006) to generate point distribution models of shapes for individuals, and use linear mixed models to test for localised shape change over time. We sought to conduct shape analysis using SPHARM-PDM as distinct from LDDMM to determine if longitudinal changes in striatal morphology are measurable using different methodology and hold true across methods. As such, we hypothesised that we would find similar results to those seen in pathological studies and in the preliminary longitudinal imaging studies, but that we would be able to see these changes in more detail using our advanced method and statistical analysis. It is hoped that further characterisation of changes in HD will increase knowledge of neurodegenerative pathways and the relationship between quantitative measures of morphology (morphometry) and function *in vivo*, constituting endophenotypes, and aimed towards developing biomeasures that may yield single or composite biomarkers for prognostication and use in HD treatment trials.

4.3 Methods

4.3.1 Subjects and measures

As part of the IMAGE-HD project (Georgiou-Karistianis, et al. 2013a), T1-weighted brain MRI scans were obtained from 36 individuals with pre-HD, 37 with early symp-HD, and 36 healthy matched controls. These scans were repeated 18 months after the initial scan and again 12 months afterwards. Healthy controls were matched for age, sex and IQ to the pre-HD individuals. All participants were right-handed (Georgiou-Karistianis, et al. 2013a). The IMAGE-HD study was approved by the Monash University and Melbourne Health Human Research Ethics Committees and informed written consent was obtained from each participant prior to testing in accord with the Helsinki Declaration. All testing was undertaken at the Royal Children's Hospital, Parkville, Melbourne, Australia. Ethics approval for this neuroimaging sub-project has also been obtained from both Monash University and from the Australian National University.

Imaging was performed on a Siemens Magnetom Trio Tim System 3 Tesla scanner with a 32-channel head coil (Siemens AG, Erlangen, Germany) at the Murdoch Children's Research Institute (Royal Children's Hospital, Victoria, Australia). High-resolution T1-weighted images were acquired (192 slices, slice thickness of 0.9 mm, 0.8 mm 0.8 mm in-plane resolution 320 320 field of view, TI=900 ms ,TE=2.59 ms, TR=1900 ms, flip angle=9°).

4.3.2 Shape analysis

A single trained researcher (FW) manually segmented the neostriatum on MRI scans of subjects using a validated protocol (intra-rater intraclass correlation 0.88-0.98) (Looi, et al. 2008; Looi, et al. 2009) and ANALYZE 11.0 (Mayo Foundation, Rochester, MI, USA) software.

Traced structures were processed for shape analysis using the SPHARM-PDM analysis software (https://www.nitrc.org/projects/spharm-pdm/) (Figure 4.1) (Styner, et al. 2006). Segmented 3D binaries were smoothed with a 1mm Gaussian kernel and spherical harmonics were used to generate 1002 corresponding surface points (Levitt, et al. 2009; Styner, et al. 2006). An average shape was created using the control participants at the baseline time, and all structures were aligned to this mean shape using Procrustes alignment. For each participant at each time point, we calculated the signed magnitude of displacement along the surface normal from the mean shape. This displacement vector was used in subsequent shape analysis.

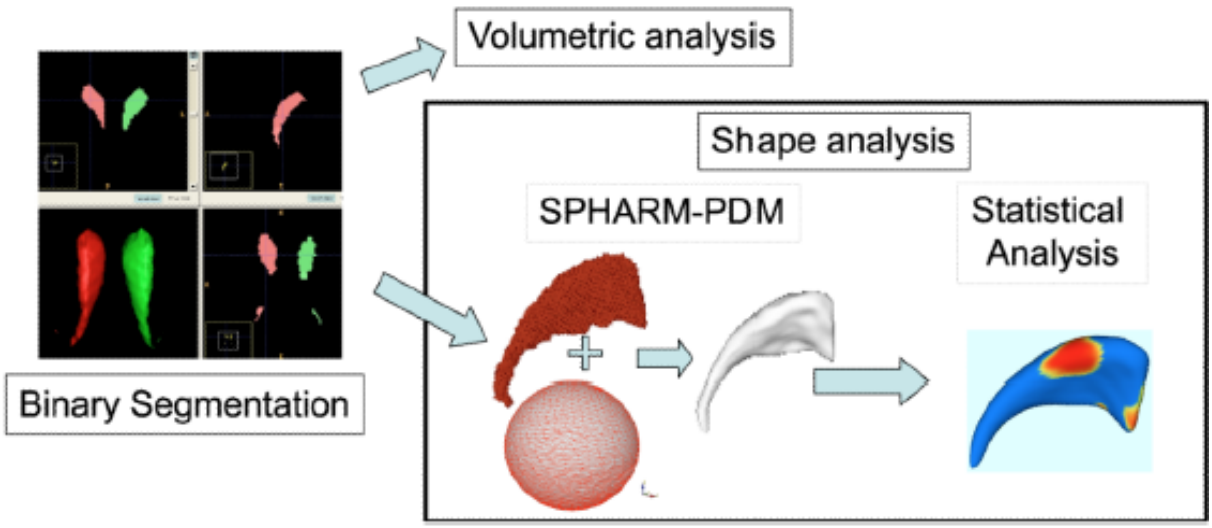

Figure 4.1: Schematic view of SPHARM-PDM pipeline (Styner, et al. 2006)

Displacement vector values were used as the dependent variables in all analyses, and thus all analyses were conducted across the 1002 corresponding points for each structure. We utilised linear mixed models with a random intercept to account for repeated time effects. Predominant interest was in group and time differences. (a) For between group comparisons, we examined effects of group, time, and the interaction between the two. (b) For covariate analyses (CAG repeats), we were interested in the group by covariate interaction, time by covariate interaction, and three-way group, time and covariate interaction. In all analyses age at baseline scan, sex and intracranial volume at time of scan were used as covariates. P-values across each shape were corrected using a FDR with $p < 0.05$. For the purposes of results and discussion, significant differences were only considered at the FDR corrected level.

4.4 Results

Basic demographic data as well as neostriatal volumes can be seen in Table 4.2. There were significant differences in putamen and caudate volumes between all three groups at each time point. There were also significant decreases in putamen volume between the initial scan and follow up scans at 18 and 30 months in both pre-HD and symp-HD, as well as between the initial scan and final 30 month scan in controls. There were no significant differences in overall caudate volume over time in any group.

Table 4.2: Demographic and volume data across groups.

	Mean ± SD		
	Controls	Pre-HD	Symp-HD
N (sample sizes)	36	36	37
Age	42 ± 13	42 ± 10	52 ± 9
Total ICV (cm^3)	1457 ± 144	1415 ± 157	1401 ± 156
CAG repeats		42 ± 2	43 ± 2
Estimated YtO		16 ± 7	
Duration of illness (years)			2 ± 2
Bilateral caudate volume (mm^3)			
N	29	33	32
Time 1***	7385 ± 1162	6052 ± 1574	4392 ± 981
18 months***	7647 ± 1092	6179 ± 1604	4480 ± 1014
30 months***	7434 ± 1087	5993 ± 1577	4171 ± 985
Bilateral putamen volume (mm^3)			
N	26	30	29
Time 1***	5969 ± 797	5065 ± 1090	3449 ± 775
18 months***	5793 ± 826	4377 ± 1065^{+++}	2846 ± 764^{+++}
30 months***	5605 ± 830^{++}	4564 ± 1117^{+++}	2781 ± 824^{+++}

SD, standard deviation; ICV, intracranial volume; YtO, estimated years to disease onset; Between groups, controlling for age and ICV: *$p \leq 0.05$; ** $p \leq 0.01$; *** $p \leq 0.001$. Within groups over time (compared to Time 1, controlling for age and ICV): $^{+}p \leq 0.05$; $^{++}p \leq 0.01$; $^{+++}p \leq 0.001$. There were no significant changes in gross bilateral volume between 18 months and 30 months.

4.4.1 Group effects- shape

There was a significant main effect for group type, controlling for different time points (Figure 4.2). Widespread deflation was observed over the surface of all structures, with a small amount of inflation in the inferomedial caudate body, indicating that there were significant differences in shape of the striatum between the groups (controls, pre-HD and symp-HD) at all time points, while controlling for time.

Significant group by time interaction was observed for the putamen bilaterally (Figure 4.3), but not for caudate, indicating that there was a differential rate of shape change between groups (controls, pre-HD and symp-HD) over time in putamen only. Shape deflation was observed across the anterior and posterior lateral aspects of the right putamen, middle of the lateral aspect of the left putamen, and medial aspects of the putamen bilaterally. Examination of regression slopes indicates that such deflation was more pronounced in the symp-HD group.

4.4.2 CAG repeats- shape

The main effect of CAG repeats on shape in the HD group (across all groups and time points) occurred for the entire bilateral striatum (Figure 4.4). For the putamen, it was across most of the surface, whilst for the caudate, deflation was more prominent in the head and tail, with shape in the medial body largely unrelated to CAG expansion. This association did not differ between groups (controls, pre-HD and symp-HD), i.e., there was no significant group-by-CAG-repeat interaction effect.

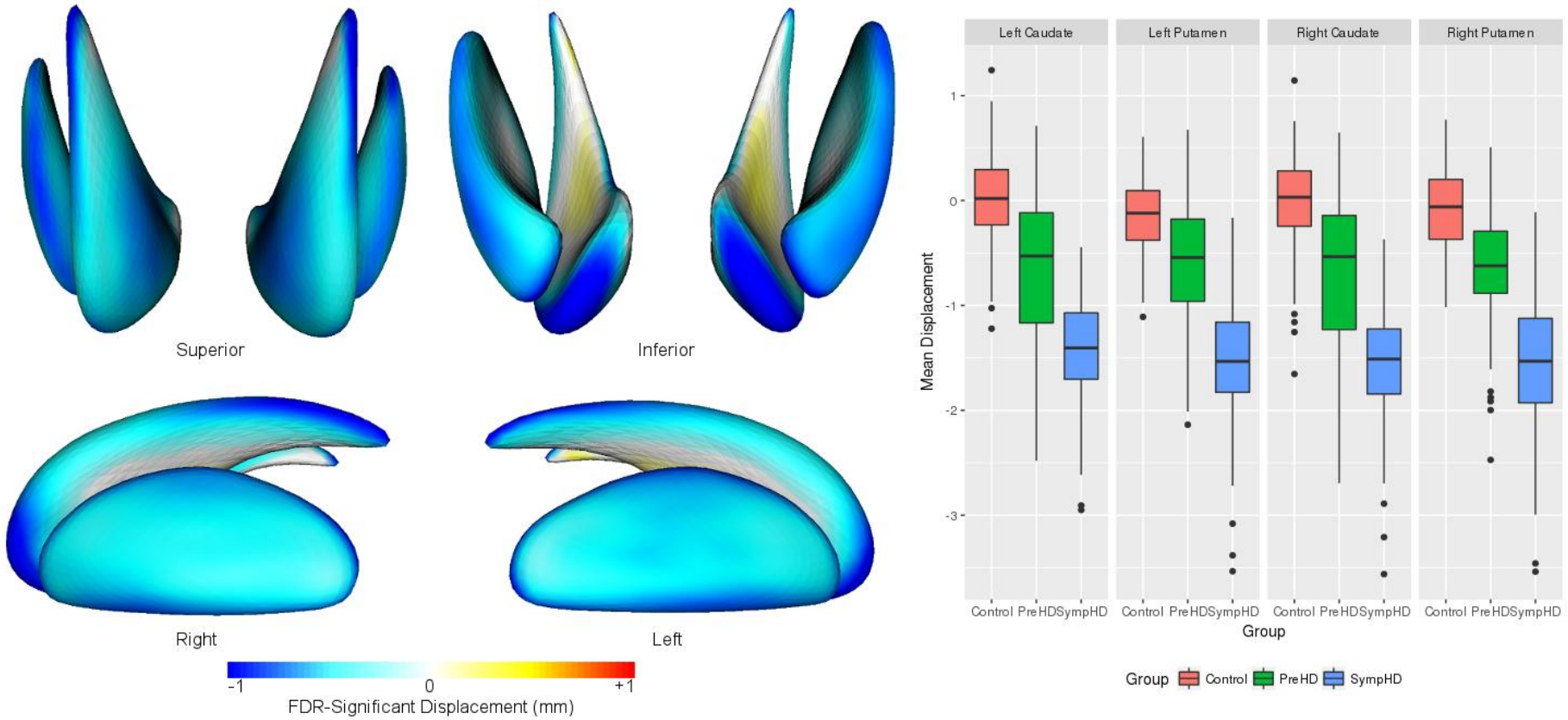

Figure 4.2: Main effect of group type, controlling for different time points. Left panels display regions of FDR-significant shape change (in mm) of the striatum from different views. Superior view is in neurological convention, such that left-hand structures are to the left of the view. Inferior view is in radiological convention, such that left-hand images are on the right of the view. Cooler colours indicate shape deflation, warmer colours indicate inflation, and white indicates no significant shape change. The graph on the right plots the mean shape change for significant regions for each participant across groups and structures.

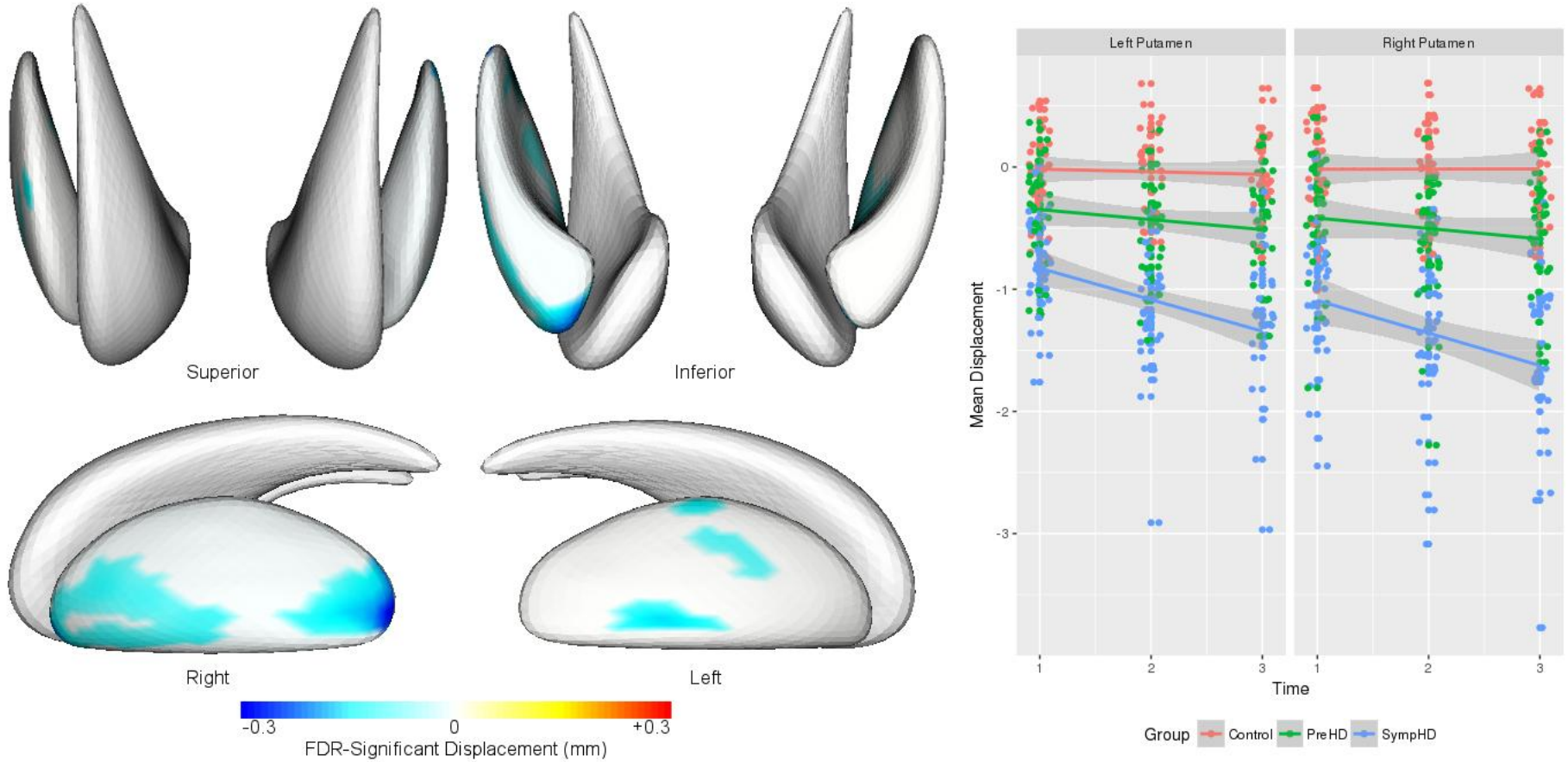

Figure 4.3: Group by time interaction. Left panels display regions of FDR-significant shape change (in mm) of the striatum from different views. Superior view is in neurological convention, such that left-hand structures are to the left of the view. Inferior view is in radiological convention, such that left-hand images are on the right of the view. Cooler colours indicate shape deflation, warmer colours indicate inflation, and white indicates no significant shape change. The graph on the right plots the mean shape change for significant regions for each participant across time, groups and structures. Shaded areas represent 95% confidence intervals.

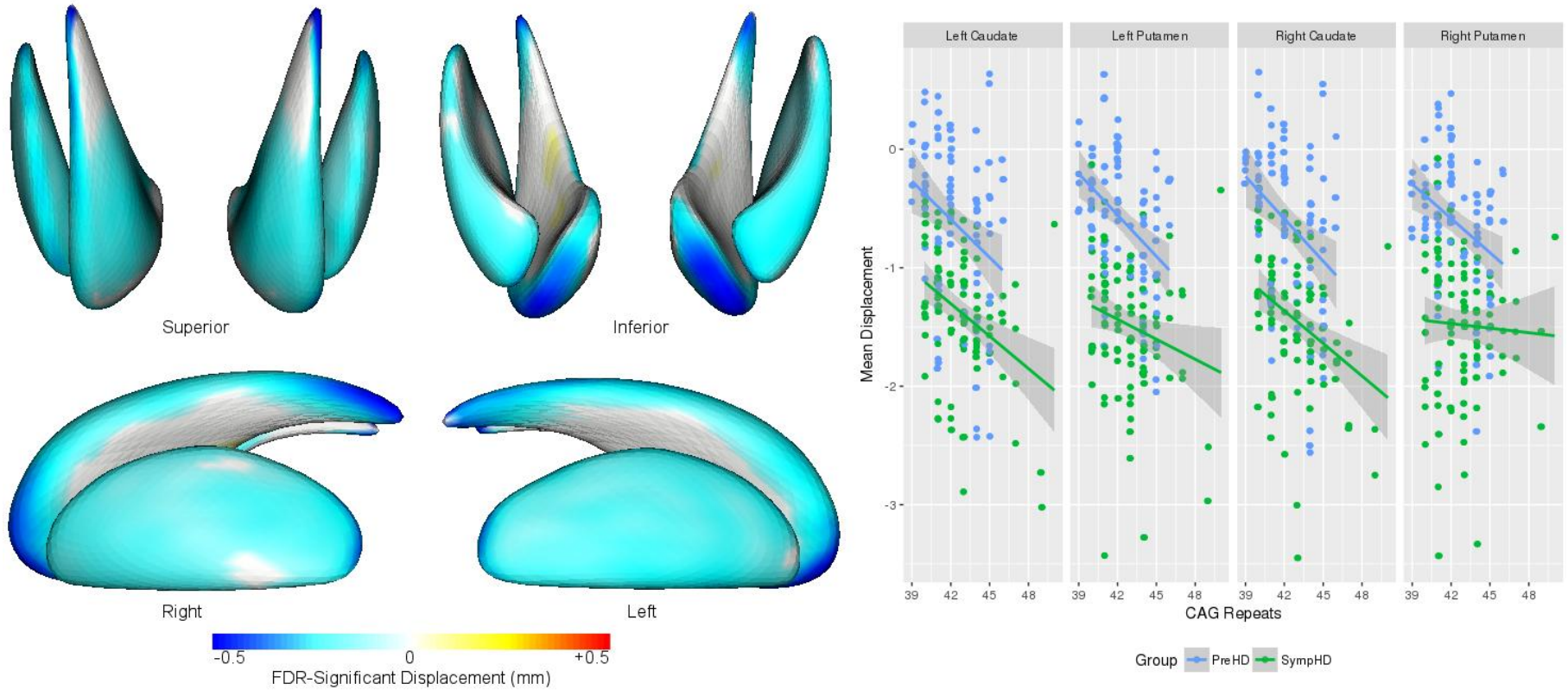

Figure 4.4: Main effect of CAG repeats on shape. Left panels display regions of FDR-significant shape change (in mm) of the striatum from different views. Superior view is in neurological convention, such that left-hand structures are to the left of the view. Inferior view is in radiological convention, such that left-hand images are on the right of the view. Cooler colours indicate shape deflation, warmer colours indicate inflation, and white indicates no significant shape change. The graph on the right plots the association between mean shape change and CAG repeats for significant regions for each participant across groups and structures.

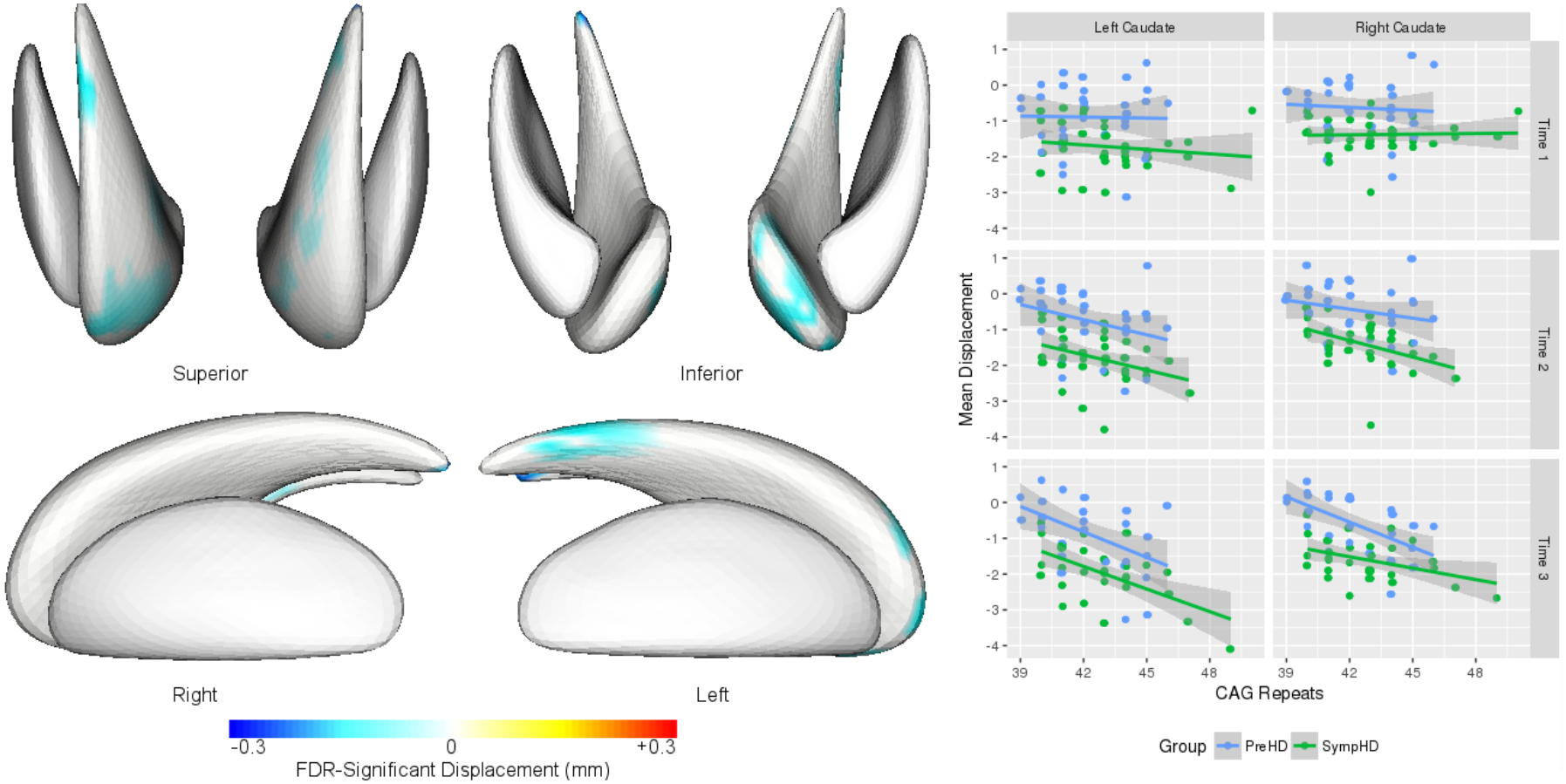

Figure 4.5: Time by CAG interaction effect. Left panels display regions of FDR-significant shape change (in mm) of the striatum from different views. Superior view is in neurological convention, such that left-hand structures are to the left of the view. Inferior view is in radiological convention, such that left-hand images are on the right of the view. Cooler colours indicate shape deflation, warmer colours indicate inflation, and white indicates no significant shape change. The graph on the right plots the mean shape change for significant regions for each participant across groups and structures.

In contrast to the lack of group-by-CAG-repeat interaction effect, there was a significant time-by-CAG-repeat interaction effect (Figure 4.5). Later time points demonstrated an association between increased CAG repeats and increased deflation in the left caudate head and tail, and right caudate medial body. There were no statistically significant differences between pre-HD and symp-HD in relation to time-by-CAG-repeat effect.

4.5 Discussion

Using a novel shape analysis method and a linear mixed methods model from previous research, we have been able to visualise and quantify longitudinal shape change in the neostriatum in HD, thus confirming local longitudinal shape changes in the neostriatum (Hong, et al. 2017; Muralidharan, et al. 2014; Muralidharan, et al. 2016) with sequential MRI scans. Additionally, we have demonstrated that the putamen, but not the caudate, experiences greater rates of shape change over 30 months. This accelerated shape change is predominantly in the posterior of the right putamen, the anterior right putamen, and lateral left putamen. Regional patterns of striatal atrophy are consistent with previous longitudinal HD work (Muralidharan, et al. 2014; Muralidharan, et al. 2016; Wijeratne, et al. 2018) indicating robust findings confirmed via a new methodology.

We demonstrated a significant association between shape deflation and increasing CAG repeats across the neostriatum. We also found a significant effect of time on the deflation by CAG repeat effect, with increased atrophy in the left caudate head and tail, and the right caudate body. This suggests that these regions of the caudate are particularly vulnerable to atrophy over time in those with higher CAG repeats, regardless of their clinical pre-HD or symp-HD classification. This is consistent with previous cross-sectional volumetric measures

of striatal structures which demonstrated a greater rate of atrophy for higher CAG repeat lengths (Aylward, et al. 2011a).

4.5.1 Shape changes in relationship to frontostriatal circuits

Group by time interactions indicating shape deflation in the bilateral putamen implicate a variety of frontostriatal circuits, including motor circuitry as well as re-entrant circuits involving orbitofrontal and dorsolateral prefrontal cortex (impulse control and executive function respectively) (Draganski, et al. 2008), and fit with the known deterioration in motor, cognitive, and psychiatric symptoms as HD progresses (Ross and Tabrizi 2011). Changes in the integrity of these tracts are also seen in cross-sectional studies of pre-HD and symp-HD (Bohanna, et al. 2011a; Hong, et al. 2018; Kloppel, et al. 2008; Marrakchi-Kacem, et al. 2013), although importantly there is some ability to compensate for deficits at early stages (Kloppel, et al. 2009; Turner, et al. 2016).

4.5.2 Implications for pathophysiology

While CAG repeat length plays a dominant role in HD phenotype and contributes to roughly 56% of the variation in age of onset of disease (Gusella, et al. 2014), other genetic and environmental factors are also thought to play a role (Wexler, et al. 2004) and there is less consensus of the role of CAG repeat number in disease progression (Aylward, et al. 2011b; Hobbs, et al. 2010; Langbehn, et al. 2019; Rosas, et al. 2011; Ruocco, et al. 2008; Sun, et al. 2017). For striatal volume, longitudinal studies have found an association between CAG repeat number and higher atrophy rates in some brain structures but not necessarily the striatum (Hobbs, et al. 2010; Rosas, et al. 2011; Ruocco, et al. 2008), whereas cross-sectional studies do show an association between CAG repeat number and striatal volume (Aylward, et

al. 2011b; Rosas, et al. 2011). More recently, Langbehn and colleagues (Langbehn, et al. 2019) have shown early changes in basal ganglia volume which are related to CAG repeat lengths, with linear decreases in volume over time and minimal acceleration with ageing. This is in contrast with overall white matter and ventricular changes which are related to CAG repeat length and continue to accelerate with ageing, and with other overall grey matter volumes which show a far weaker dependence on CAG repeat length and accelerate slightly with age (Langbehn, et al. 2019). These previous studies concord with our finding of a CAG-by-time interaction effect being limited to only the very anterior and posterior caudate regardless of group status (pre-HD or symp-HD). Previous research is also consistent with our finding of a group-by-time interaction involving only the putamen; that is, change in putamen shape over time in symp-HD appears to be somewhat independent of CAG repeat length.

4.5.3 Towards an endophenotype of HD

Increased shape deflation in the putamen with time is consistent with some previous volumetric work (Tabrizi, et al. 2009; Wijeratne, et al. 2018), although of note a recent analysis combining brain volumes from the PREDICT-HD, TRACK-HD and IMAGE-HD studies showed that caudate volume was the best (volumetric) imaging marker for pre-HD (Wijeratne, et al. 2020). However, using caudate volume as a biomarker for potential treatment trials would still require 661 participants in a study to achieve power of >80% assuming a 20% treatment effect. This study pooled data from the three studies, with significant differences amongst groups in DBS and total motor score, which may explain some of the differences in results (Wijeratne, et al. 2020). Shape was also not investigated and may be a more sensitive biomarker and provide better opportunity to test potential treatments. The complexity of changes in HD, found in our study and increasingly highlighted in the

literature, indicate the usefulness of composite structural morphology measures, including shape analysis, to construct an endophenotype of HD.

Methodologically, we believe that this is the first example of integrating the SPHARM-PDM method of shape description with a linear mixed model analysis strategy. Our analysis provides statistical tests across points, allowing us to empirically examine regional shape change over time, which is a significant methodological advancement. Additionally, we are able to map the trajectory of gene-structural correlations, such as the relationship between CAG repeat number and shape changes over time.

4.6 Limitations

Despite this advantage over previous work, the limitation of this methodology is that it only captures shape change along the surface normal. Thus, significant lateral displacement or shearing is not captured, reducing the sensitivity of the analysis. This study also used manual tracing of the putamen and caudate over three time periods as the basis for longitudinal shape analysis. This labour-intensive method is limited by the need to have an experienced tracer and the increased amount of time necessary for manual tracing. Nonetheless, we believe that manual tracing is currently superior to automated methods of segmentation (Looi, et al. 2008; Looi, et al. 2009).

4.7 Conclusions/clinical implications

We have mapped longitudinal shape change in the neostriatum in HD extending the findings of previous linear mixed model shape analysis. To our knowledge this is the first time that such robust statistical analysis of shape change in HD has been performed. Such shape analysis mixed model methods have profound implications for the development of a morphological biomarker in HD, and allows spatiotemporal signatures to be derived for the progression of atrophy of the striatum in HD. These spatiotemporal signatures may assist in understanding pathophysiology towards prognostication and analysing the effectiveness of disease-modifying treatments. Further characterisation of these changes increases knowledge of neurodegenerative pathways and the relationship between neostriatal shape and function *in vivo*, constituting an endophenotype, and a potential biomarker for prognostication and use in HD treatment trials.

5. Study Three: Hippocampal morphology and neurocognitive dysfunction in HD.

Study Three extends investigation from the striatum to other areas of the subcortical connectome with the aim of developing an endophenotype of HD.

Table 5.1: Study Three. Continuing the investigation of the subcortical connectome in HD through analysis of the hippocampus and its relationship with functional outcomes.

Study	Investigation	Rationale	Endophenotype components
Study One	Baseline analysis of neostriatum and relationship with functional outcomes	Key structure in HD and hub in frontostriatal circuitry	Genetics Morphology Function
Study Two	Longitudinal analysis of neostriatal change	Morphological change over time, investigating potential biomarkers	Genetics Morphology Spatiotemporal signature
Study Three	***Baseline analysis of hippocampus and relationship with functional outcomes***	***Further extension of subcortical connectome in a different but related hub, potential for compensation***	***Genetics Morphology Function***
Study Four	Baseline and longitudinal analysis of the corpus callosum	Major spoke within the connectome, complementary information regarding degeneration	Genetics Morphology Spatiotemporal signature

The hippocampus is known to be altered in HD, and this has implications for the cognitive and neuropsychiatric changes which go along with the disease. The hippocampus has connections to the striatum- most specifically but not limited to the nucleus accumbens- and connects the limbic-motor circuit. Furthermore, both areas have connections to, or contain,

areas of neurogenesis in the adult brain, and are implicated in increased neurogenesis in pathological conditions. We hypothesised differences in hippocampal shape related to known areas of neurogenesis as well as connections to striatum.

Title:

Hippocampal morphology in Huntington disease, implications for plasticity and pathogenesis: The IMAGE-HD study.

Authors:

F.A. Wilkes[1], D. Jakabek[2], M. Walterfang[3,4], D. Velakoulis[3,4], J.C. Stout[5], P. Chua[6], G.F. Egan[5], J.C.L. Looi[1,3], N. Georgiou-Karistianis[5]

Affiliations:

[1] Research Centre for the Neurosciences of Ageing, Academic Unit of Psychiatry and Addiction Medicine, Australian National University Medical School, Canberra Hospital, Canberra, Australia
[2] Graduate School of Medicine, University of Wollongong, Wollongong, Australia
[3] Neuropsychiatry Unit, Royal Melbourne Hospital, Melbourne Neuropsychiatry Centre, University of Melbourne and Northwestern Mental Health, Melbourne, Australia
[4] Florey Institute of Neuroscience and Mental Health, University of Melbourne, Melbourne, Australia
[5] School of Psychological Sciences and the Turner Institute of Brain and Mental Health, Monash University, Melbourne, Australia
[6] Department of Psychiatry, School of Clinical Sciences, Monash University, Monash Medical Centre, Melbourne, Australia

Author contributions:

F.A. Wilkes performed the manual segmentation of the hippocampus, coordinated and directed the imaging analysis and wrote the bulk of the manuscript (>80% of total work). D.

Jakabek performed the shape analysis. J.C. Stout, P.Chua, G.F. Egan, and N. Georgiou-Karistianis were integral to the development and implementation of the overall IMAGE-HD project, of which this study is a sub-project. N. Georgiou-Karistianis is the primary investigator of the IMAGE-HD project and along with M. Walterfang and D. Velakoulis contributed to project design and is a PhD co-supervisor of F.A. Wilkes; J.C.L. Looi contributed to project design and coordination and is F.A. Wilkes' main PhD supervisor. All authors had significant intellectual and practical input into the final manuscript.

5.1 Abstract

We extended the investigation of HD from the neostriatum to the hippocampus, another key neuronal hub. Hippocampal shapes were analysed with SPHARM in 36 individuals with pre-HD, 37 with early symp-HD, and 36 healthy matched controls.

There were no significant differences in hippocampal volume between groups after controlling for age and intracranial volume. Unexpectedly, a significant difference in both right and left hippocampal volume was found in people with symp-HD who took SSRIs, despite there being no significant differences between anxiety or depressive symptoms or motor incapacity. Significant shape deflation was seen in the right hippocampal head in symp-HD.

Volume and shape differences broadly corresponded with previous findings in HD, with several important new findings which shed light on the pathogenesis of HD, as well as pointing towards new areas of investigation.

5.2 Introduction

HD is a neurodegenerative condition which is known to start early in the neostriatum before progressing to more marked degeneration in both the neostriatum and other areas of the brain and is related to motor, cognitive, and neuropsychiatric decline (Vonsattel, et al. 1985). Depression, anxiety, irritability, apathy, obsessions and compulsions, perseveration and psychosis have all been reported in HD (Paulsen, et al. 2001; Thompson, et al. 2012; van Duijn, et al. 2014; van Duijn, et al. 2007). Depression and anxiety are common in people with HD, with 60% of people experiencing low mood and 71% experiencing anxiety over the course of some longitudinal studies (Thompson, et al. 2012), but also in pre-HD (Julien, et al. 2007). Part of the clinical progression later in HD can be the development of psychosis as well as dementia, and a number of people with HD are on antidepressants as well as antipsychotics (used for both chorea and psychiatric symptoms) (Begeti, et al. 2016; Stahl and Feigin 2020). Currently available agents for symptomatic control in HD are minimal, and there is no current cure despite intensive research (Stahl and Feigin 2020). In this study, we wanted to extend the investigation of HD from the neostriatum to other key neuronal hubs which also have relationships with clinical symptoms seen in HD, in particular cognitive decline and psychiatric issues such as depression and anxiety.

5.2.1 The hippocampus

The hippocampus is crucial for learning and memory (Tulving 2002), in particular for combining spatial and non-spatial memories into “what happened where”, based on processing information from diverse areas of the brain (Knierim, et al. 2014). Hippocampal atrophy occurs in Alzheimer disease along with impaired memory (Zeng, et al. 2021), whereas increased spatial memory occurs alongside increased hippocampal size in London

cab drivers (Maguire, et al. 2000). Of note, the hippocampus and the striatum are involved in parallel memory systems which can interact (McDonald and White 1994; White 2009; White and McDonald 2002). The caudate is thought to play a critical role in egocentric navigation as opposed to the hippocampus' role in allocentric navigation (McDonald and White 1994; White 2009; White and McDonald 2002), although in some cases in HD the hippocampus can compensate for caudate dysfunction in this memory pathway (Possin, et al. 2017; Voermans, et al. 2004).

In gross anatomical terms the hippocampus can be divided into the hippocampal head, which is the most anterior part, the hippocampal body, and the tail. Based on its cytoarchitecture it can also be divided into the cornu ammonis subfields CA1-4, the dentate gyrus, and the subiculum (Figure 5.1) (Blumenfeld 2010). Posterior hippocampus is implicated in memory and spatial navigation whereas anterior hippocampus mediates anxiety related behaviour and learning through its connections to amygdala and hypothalamus (Fanselow and Dong 2010; Moser and Moser 1998; Strange, et al. 2014). Both inputs and outputs to and from hippocampus are topographically organised (Strange, et al. 2014). The hippocampus is also connected with the nucleus accumbens and amygdala, with progressively more anterior hippocampal portions projecting to progressively more medial parts of both of these structures (Strange, et al. 2014).

There are two areas of the adult brain where neurogenesis can occur: the subgranular zone of the dentate gyrus in the hippocampal complex (SGZ), and the subventricular zone (SVZ), which lies just above the caudate (Barani, et al. 2007). Progenitor cells in the SGZ can migrate to the granule cell layer and differentiate into granular neurons which are functionally

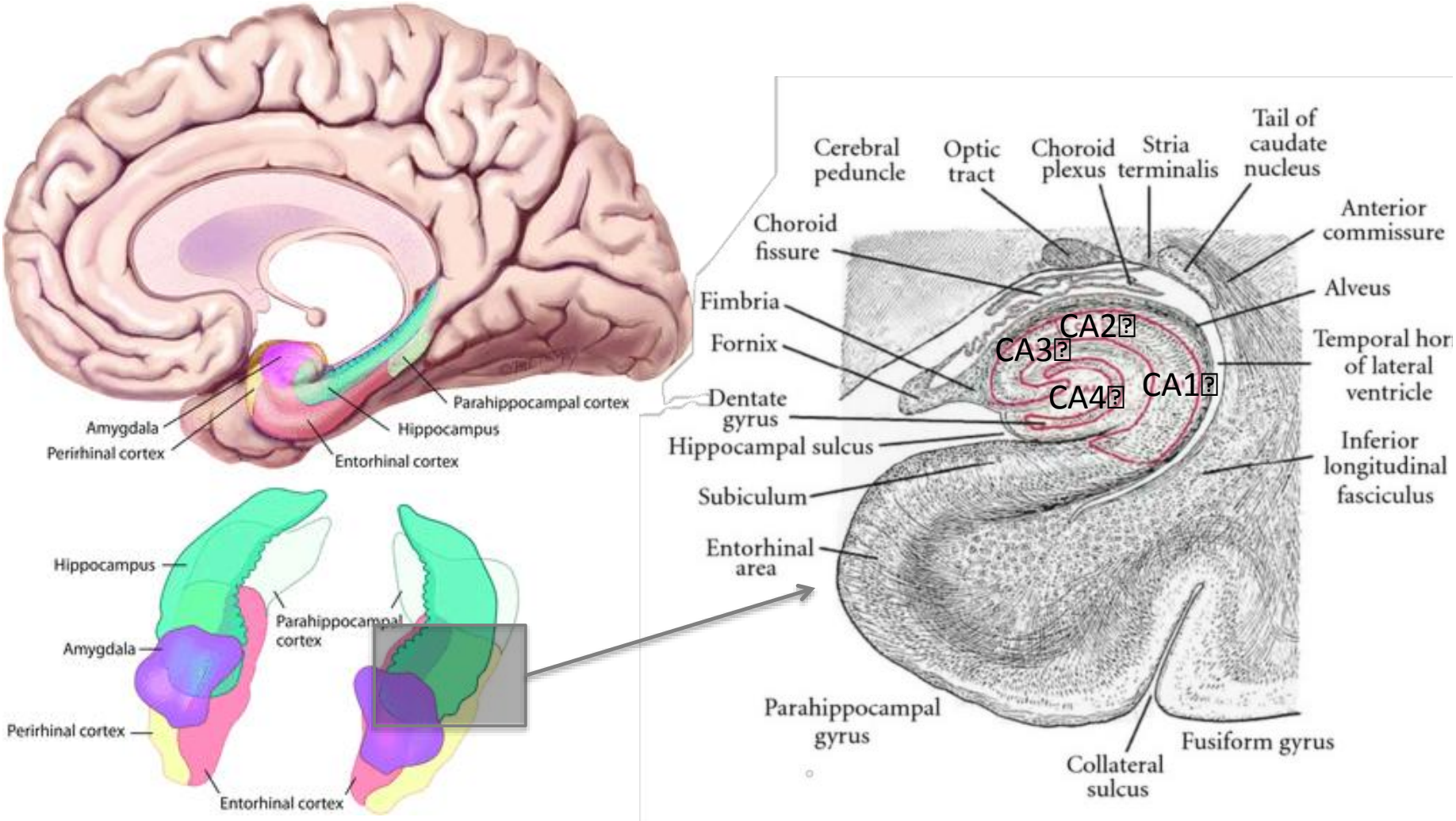
Parahippocampal cortex
Amygdala
Hippocampus
Perirhinal cortex
Entorhinal cortex
Hippocampus
Parahippocampal cortex
Amygdala
Perirhinal cortex
Entorhinal cortex
Cerebral peduncle
Optic tract
Choroid plexus
Stria terminalis
Tail of caudate nucleus
Choroid fissure
Anterior commissure
Fimbria
Alveus
Fornix
CA2
CA3
CA4
CA1
Temporal horn of lateral ventricle
Dentate gyrus
Hippocampal sulcus
Inferior longitudinal fasciculus
Subiculum
Entorhinal area
Parahippocampal gyrus
Fusiform gyrus
Collateral sulcus

Figure 5.1: The human hippocampus. Schematic view on the sagittal plane (top left) and showing 3-dimensional hippocampi looking from an anterosuperior viewpoint (bottom left) adapted from (Purves 2012), with further emphasis on cytoachitecture, shown in the coronal plane (right) and adapted from (Kiernan 2012).

integrated into the hippocampal circuitry. Treatment with selective serotonin reuptake inhibitors (SSRIs) in transgenic mouse models of HD increases both BDNF levels and neurogenesis in SGZ and SVZ, attenuating the progression of brain atrophy and behavioural abnormalities and increasing survival (Duan, et al. 2008; Grote, et al. 2005; Peng, et al. 2008). Despite this work in animal models and the common use of antidepressants, especially SSRIs, in HD (Rowe, et al. 2012) there has been limited research into the effect of SSRIs on the natural history of human HD progression.

Shape and volume analysis have been applied to the hippocampus in a number of neurodevelopmental and degenerative disorders (Lindberg, et al. 2012; Solowij, et al. 2013; Wood, et al. 2010), and there is considerable interest in hippocampal plasticity, as cognitive training has been shown to increase left hippocampal activation in mild cognitive impairment (Rosen, et al. 2011) and aerobic exercise training to increase anterior hippocampal size and improve spatial memory (Erickson, et al. 2011). Notably, this increase in volume is associated with greater serum levels of BDNF (Erickson, et al. 2011). Antidepressant use and recovery from depression also cause increases in neurogenesis and alters BDNF in the hippocampus (Boldrini, et al. 2009; McKinnon, et al. 2009; Nogovitsyn, et al. 2020; Phillips, et al. 2015).

5.2.2 Volume and shape of the hippocampus in HD

Several studies have addressed hippocampal volume and a few have addressed hippocampal shape in HD. In pre-HD, some studies have found no significant volume change at baseline or over one or more years (Aylward, et al. 2013; Majid, et al. 2011; Tang, et al. 2019), nor shape change in hippocampus at baseline (Younes, et al. 2012). In symp-HD baseline differences in volume have been seen (Coppen, et al. 2018; van den Bogaard, et al. 2011b), but no longitudinal changes in hippocampal volume over a period of up to 6 years (Ramirez-Garcia, et al. 2020; Wijeratne, et al. 2018). Other studies have found a significant decrease in left hippocampus volume only in pre-HD versus controls, compared to significant decreases bilaterally in symp-HD (van den Bogaard, et al. 2011b). This was also reflected in small areas of bilateral shape deflation in hippocampal head and tail in symp-HD only in this study (van den Bogaard, et al. 2011b). In other studies where people with pre-HD are stratified according to genetic load and age, small amounts of bilateral shape change have been seen in posterior hippocampus in those people with pre-HD with highest load (Faria, et al. 2016). In a different study of pre-HD, when the hippocampus is split into subregions (CA1, CA2, CA3/dentate gyrus [DG] and subiculum) small but significant surface differences were seen in the left hemisphere across all three stratified pre-HD groups, whereas in the right hemisphere significant differences were seen only in the middle and high load groups (Tang, et al. 2019). In the lowest load groups, differences were mostly in CA2, while by higher loads these differences mostly affected CA3/DG bilaterally, with the next most affected areas being CA2 in the left hemisphere and CA1 in the right (Tang, et al. 2019).

Several studies have further investigated the correlation between imaging differences in hippocampus in HD and functional outcomes. Negative correlations have been found between

UPSIT scores and mean diffusivity (MD) in the hippocampus bilaterally (Delmaire, et al. 2012), as well as volume of the superior right hippocampus (Scahill, et al. 2013).

5.2.3 Hypotheses

While HD has its most marked effects on the neostriatum, it also has more subtle effects on other subcortical areas. We wanted to investigate any potential differences in the hippocampus and in particular to investigate possible relationships with related psychiatric and neurocognitive outcomes.

We hypothesised that there would be subtle hippocampal shape differences between pre-HD and controls, and between HD and controls, that these differences would be related to depressive symptoms and attenuated by use of SSRI antidepressant medication, and that hippocampal shape would also be related to UPSIT scores, but not to scores on other cognitive tests not directly involving the mesial temporal lobe (Delmaire, et al. 2012).

5.3 Method

5.3.1 Subjects

Subjects in this study were 36 individuals with pre-HD, 37 with early symp-HD, and 36 healthy matched controls. Healthy controls were matched for age, sex and IQ to the pre-HD individuals. All participants were right-handed and were free from brain injury, neurological and/or severe diagnosed psychiatric conditions other than HD.

5.3.2 Measures

A number of tests were taken by all of the individuals involved in the study. These included motor measures: UHDRS (Kieburtz, et al. 1996), self-paced tapping (1.8 Hz and 3 Hz) and speeded tapping (Stout, et al. 2011); cognitive measures: verbal IQ, SDMT (Smith 1982), UPSIT (Doty, et al. 1984) and Stroop (Stroop 1935); and psychiatric measures: BDI-II (Beck 1996), SCOPI total OCD (Watson and Wu 2005), FrSBe (Stout, et al. 2003), and HADS anxiety and depression (Zigmond and Snaith 1983). Medications and medication doses for general and psychiatric health were also recorded. Demographic data as well as use of SSRIs can be seen in Table 5.2. MRI scans were taken of all subjects on a 3T scanner in the Royal Melbourne Children's Hospital at three time points: baseline, 18 months and 30 months. For this study we chose to look at UHDRS as a measure of motor incapacity from disease, as well as UPSIT, BDI-II, HADS anxiety, and HADS depression, due to their links with the hippocampus as described in other sections of this chapter.

The IMAGE-HD study was approved by the Monash University and Melbourne Health Human Research Ethics Committees and informed written consent was obtained from each participant prior to testing in accord with the Helsinki Declaration. All testing was undertaken at the Royal Children's Hospital, Parkville, Melbourne, Australia. Ethics approval for this neuroimaging sub-project was also obtained from both Monash University and from the Australian National University.

5.3.3 Manual tracing

Hippocampi were manually traced by a single trained researcher (FW) according to a previously published protocol (Figure 5.2) (Velakoulis, et al. 1999; Watson, et al. 1992).

Briefly, all MRI images were aligned along the AC-PC (anterior commissure- posterior commissure) plane in FSL. Tracing was then performed using Analyze software using a protocol modified from Watson and colleagues (Watson, et al. 1992) and explained in more detail in Chapter 2.2.3. In brief, tracing occurs in the coronal plane from posterior to anterior, from the head of the hippocampus just before the crux of the fornix becomes indistinctly separated from the thalamus. The inferior border is the interface between the hippocampal grey matter and the parahippocampal gyrus white matter. The lateral border is the temporal/inferior horn of the lateral ventricle. The superior border includes any white matter superior to the hippocampal grey matter- more posteriorly this is the fornix and then becomes the fimbria and alveus more anteriorly. The subiculum is not included in this protocol. The uncus is traced once it appears more anteriorly, as is the hippocampal tail. As tracing continues the amygdala appears anteriorly and the hippocampus shrinks and eventually disappears.

Figure 2.3: Manual tracing of the hippocampus (next page)**.** MRI images from the Melbourne Brain Centre Protocol (Velakoulis, et al. 1999; Watson, et al. 1992). Manual tracing of the hippocampus in the coronal plane, from posterior (top left) to anterior (bottom right). 1. Crus of the fornix; 2. Thalamus; 3. Hippocampal grey matter; 4. Temporal horn of lateral ventricle; 5. Parahippocampal gyrus; 6. Quadrigeminal cistern; 7. CSF in the subarachnoid space of the transverse cerebral fissures/choroidal fissure; 8. One voxel thick tracing of inferior to medial border of hippocampus, from superior to parahippocampal gyrus until reaching the quadrigeminal cistern (not included once quadrigeminal cistern moves laterally to reach the fimbria/alveus); 9. Fornix; 10. Fimbria/alveus; 11. "Seahorse head" of the hippocampus; 12. Inferior/medial border of the hippocampus; i. Isthmus; ra. Amygdala; rh. Hippocampus; u. Uncus; un. Uncal notch

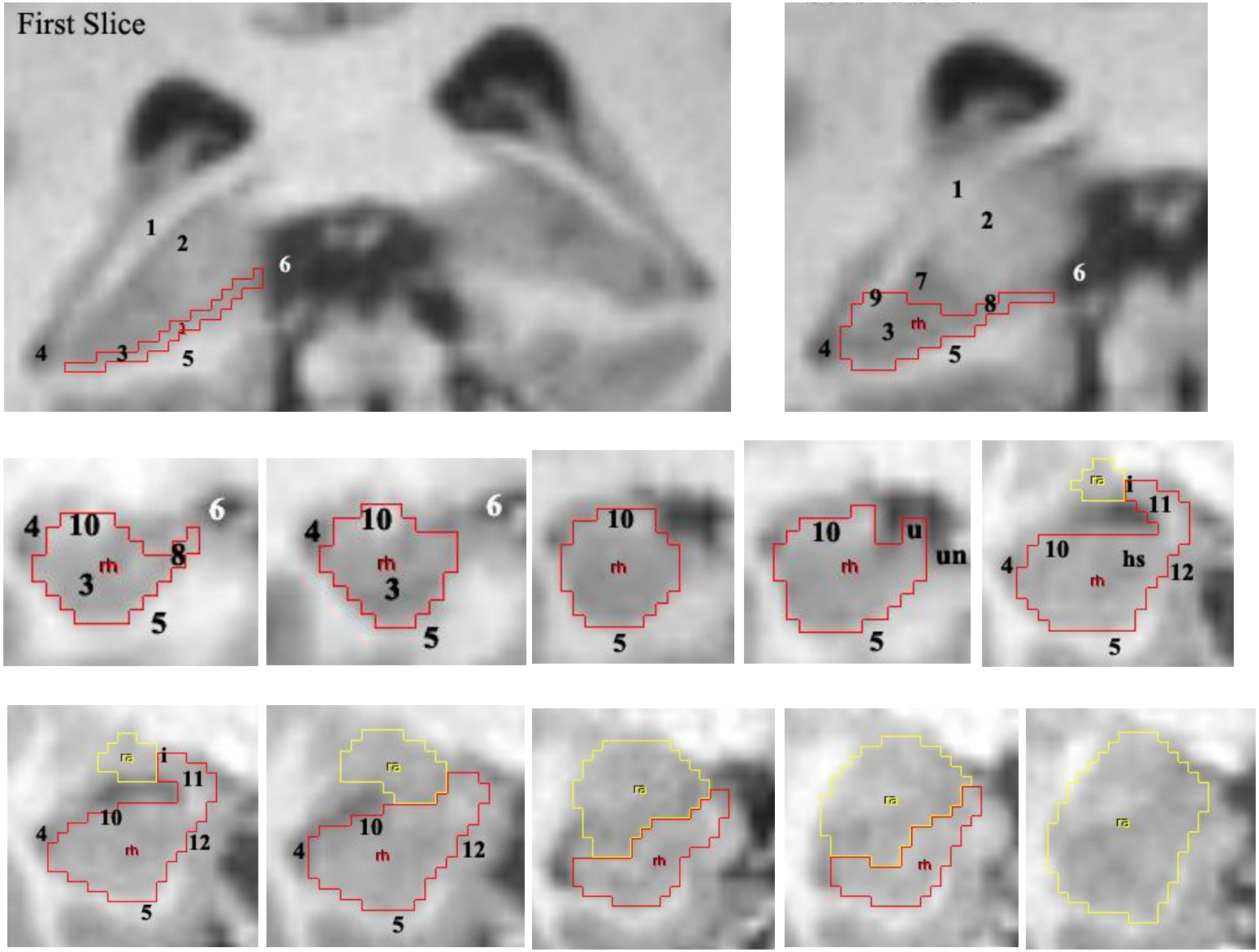
First Slice
1
2
6
4
3
5
1
2
7
6
9
8
3
rh
4
5
4
10
6
8
rh
3
5
4
10
6
rh
3
5
10
rh
5
10
u
un
rh
5
ra
i
11
4
10
hs
12
rh
5
ra
i
11
4
10
rh
12
5
4
10
ra
12
rh
5
ra
rh
ra
rh
ra

5.3.4 Volumetric analysis

Statistical analysis of volume and other baseline data was performed using SPSS 20.0 (Chicago, Ill., USA) and significance was set at $P<0.05$. Multivariate analysis of covariance (MANCOVA) was used to test statistical significance between the subject groups with age, sex and ICV as covariates (Table 5.2, Table 5.3). Preliminary checks were conducted to ensure there was no violation of assumptions of normality, homogeneity of variances, and reliable measurement of the covariate. Bonferroni corrections for multiple comparisons were used where appropriate.

5.3.5 SPHARM shape analysis

Traced structures were processed for baseline shape analysis using the SPHARM-PDM analysis software (https://www.nitrc.org/projects/spharm-pdm/) (Styner, et al. 2006). For each participant the signed magnitude of displacement was calculated along the surface normal from the mean shape. This displacement vector was used in subsequent shape analysis. Displacement vector values were used as the dependent variables in all analyses, and thus all analyses were conducted across the 1002 corresponding points for each structure. In all analyses age, sex and intracranial volume were used as covariates. Pearson's correlation analyses were performed with the independent variable calculated as the magnitude of displacement between surface normals at each vertex from the mean shape. Covariates and correction for multiple comparisons were performed as for the group comparisons. P-values across each shape were corrected using a FDR with $p < 0.05$. For the purposes of results and discussion, significant differences were only considered at the FDR corrected level.

5.4 Results

5.4.1 Baseline volumetric data

Demographic and selected data across groups can be seen in Table 5.2 below. There were significant differences in UPSIT scores between groups as well as SSRI use, with 35% of participants in the symp-HD group using an SSRI in the period of the initial study, as opposed to 3% of controls (1 person). 4 people (11%) used SSRIs in pre-HD. After controlling for age and ICV there were no significant differences in hippocampal volume between groups.

Table 5.2: Demographic and selected data across groups.

	Mean ± SD		
	Controls (n=36)	Pre-HD (n=36)	Symp-HD (n=37)
Sex (M:F)	12:24	14:22	21:16
Age (years)	42.4±13.4	41.7±9.9	52.1±9.3
ICV (cm^3)	1456.4±143.5	1414.7±156.8	1400.8±155.7
UHDRS motor score (range)		1 (0-4)	19 (6-60)
UPSIT[a]	34.0±3.1	32.7±5.0	26.2±7.1
BDI-II	4.0±4.1	8.7±9.8	8.2±7.2
HADS-A	5.0±2.8	6.6±3.5	5.5±3.4
HADS-D	2.6±3.1	2.7±3.0	2.8±2.4
SSRI use	3%	11%	35%
Right hipp. vol. (mm^3)	3188.2±396.7	3197.4±414.7	3118.8±492.0
Left hipp. vol. (mm^3)	3100.6±343.0	3016.8±453.9	2884.6±475.0

ICV: Intracranial volume; UHDRS: Unified Huntington Disease Rating Scale; UPSIT: University of Pennsylvania Smell Identification test; BDI-II: Beck depression inventory mark II; HADS-A: Hospital anxiety and depression scale- anxiety; HADS-D: Hospital anxiety and depression scale- depression; SSRI: selective serotonin reuptake inhibitors; hipp. vol.: hippocampal volume.

[a]Significant differences between groups, $p \leq 0.01$. Note that Levene's test for homogeneity is violated for UPSIT, however results remain significant at more stringent alphas.

When controlling for age and group status, there were no significant partial correlations between hippocampal volume (right or left) and scores on any of UPSIT, BDI-II, HADS-A or HADS-D. Given the low numbers for SSRI use in controls and in pre-HD, the relationship between SSRI use and outcomes (psychiatric measures and hippocampal volumes) was only assessed in symp-HD. When stratifying into SSRI users versus non-users, a significant difference in both right and left hippocampal volume was found, despite there being no significant differences between anxiety or depressive symptoms or motor incapacity as measured by the UHDRS total motor score (Table 5.3).

5.4.2 Baseline shape differences

Baseline shape differences can be seen in Figure 5.3. There were no significant differences between groups in left hippocampal shape. In the right hippocampus there was a significant shape deflation in the anterior hippocampal head, in an area corresponding to CA3. There were no significant correlations between SSRI use and hippocampal shape in symp-HD.

Table 5.3: SSRI use and relationship with psychiatric symptoms, hippocampal volume, and motor incapacity in symp-HD (±SD)

	SSRI users (n=13) 7 male, 6 female	SSRI non-users (n=22) 13 male, 9 female
Demographic data		
Sex (M:F)	7:6	13:9
Years since diagnosis	2.5±1.4	1.7±1.6
Age (y)	54.1±10.6	50.9±8.7
ICV (cm^3)	1352.1±138.3	1407.3±152.3
Dependent variables		
UHDRS motor score	22.5±12.9	17.9±12.3
BDI-II	4.0±4.1	8.7±9.8
HADS-A	6.2±3.9	5.1±3.2
HADS-D	3.2±2.7	2.7±2.2
Right hipp. vol. (mm^3)[a]	2818.7±318.1	3246.7±489.1
Left hipp. vol. (mm^3)[a]	2596.6±330.8	3001.2±470.7

UHDRS: Unified Huntington Disease Rating Scale; UPSIT: University of Pennsylvania Smell Identification test; BDI-II: Beck depression inventory mark II; HADS-A: Hospital anxiety and depression scale- anxiety; HADS-D: Hospital anxiety and depression scale- depression; SSRI: selective serotonin reuptake inhibitors; hipp. vol.: hippocampal volume.

[a]Significant differences between groups, $p<0.05$.

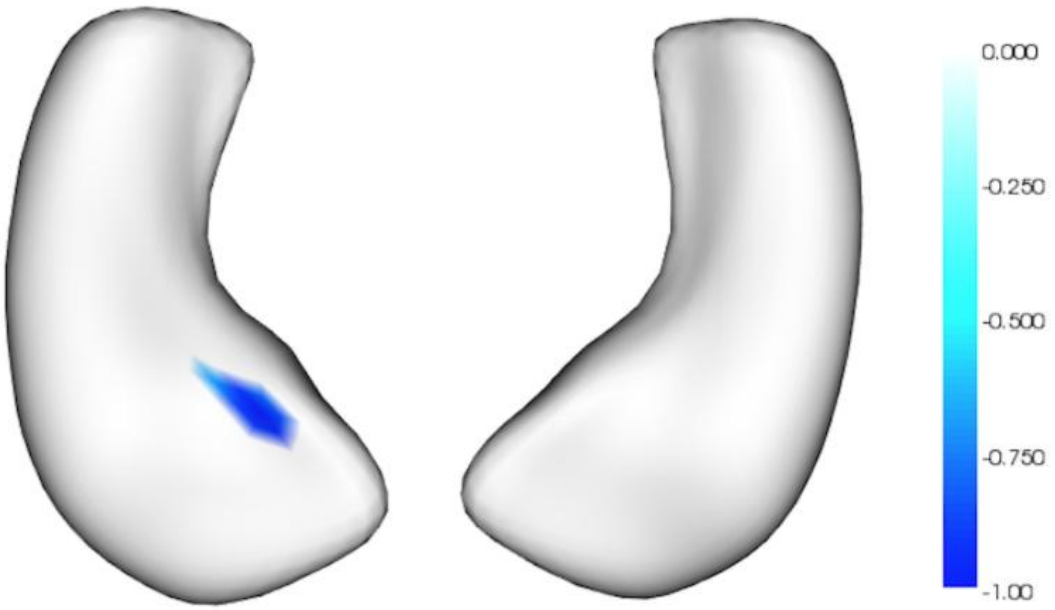

Figure 5.3: Significant differences in baseline hippocampal shape in symp-HD compared to controls. Picture is aligned as if the viewer is looking from the forehead through to the back of the head, so left-sided images here are right hippocampus, and vice versa. Blue = shape contraction, scale is in mm.

5.5 Discussion

We used manual tracing of the hippocampus to investigate hippocampal shape and volume in HD and the relationship with neuropsychiatric symptoms as part of a broader investigation of the subcortical connectome in HD. We found no differences in hippocampal volume between controls and pre-HD or symp-HD, but interestingly did find a decrease in hippocampal volume in people with symp-HD who were on SSRI antidepressants, a counterintuitive finding which will be discussed in further detail below. We also found a shape deflation in the right hippocampal head in an area corresponding to CA3, but no correlation with SSRI use.

5.5.1 Volumetric differences in hippocampus

After controlling for age and ICV we found no significant differences in hippocampal volume between groups. Previous studies show mixed results in this regard, with some finding unilateral or bilateral changes in pre-HD close to disease onset, and/or bilateral changes in symp-HD (Ciarochi, et al. 2016; Coppen, et al. 2018; van den Bogaard, et al. 2011b). Other studies however find no such differences (Aylward, et al. 2013; Majid, et al. 2011; Ramirez-Garcia, et al. 2020; Wijeratne, et al. 2018). It is possible that the lower number of cases in this study has driven our results, or that participants here are in the early stages of symp-HD rather than more advanced stages.

5.5.2 Clinical correlations

We did not find any significant associations between hippocampal size and depression or anxiety symptoms in this dataset (BDI-II, HADS-A or HADS-D). This is likely also due to the exclusion of participants with major mental illness, meaning that average scores on all measures in all groups fell under the cut off for depression or anxiety (Smarr and Keefer 2011). Despite this lack of association there was a significant difference in hippocampal volume in symp-HD SSRI users versus non-users. Decreased bilateral hippocampal volume was found in people with symp-HD who took SSRIs, although there was no difference between groups in depressive or anxious symptoms or in motor symptoms, nor in the sex distribution of both groups.

Our results appear to conflict with previous studies in humans with depression and in mouse models of HD. Human studies have suggested that there is a smaller hippocampal volume in

humans with depression after disease onset (McKinnon, et al. 2009; Nolan, et al. 2020), and in particular that hippocampal tail volumes are decreased in participants with depression, while those who achieved early sustained remission on antidepressants had significantly greater hippocampal tail volumes than those who didn't (Nogovitsyn, et al. 2020). Similarly, in mouse models of HD, treatment with SSRIs increases neurogenesis in the SGZ and attenuates brain atrophy (Duan, et al. 2008; Grote, et al. 2005; Peng, et al. 2008). Here, we have found a volume decrease in people with symp-HD who are on SSRI antidepressants, which is not related to time since diagnosis, sex, motor incapacity, or anxious or depressive symptoms. This is a significant new finding and requires further exploration. It must be noted again here that significant psychiatric disease was an exclusion criterion for participation in IMAGE-HD. Therefore, everyone in the study who is on an antidepressant no longer has significant depressive symptoms (Table 5.3. The cut off score for depression in HADS-D is 8 (Zigmond and Snaith 1983), while for BDI-II the minimum score for moderate depression is 20 and severe depression requires a score of 29 or higher (Beck 1996)). This may also have had an effect of results, for example by masking partial treatment of depression and related lower hippocampal volumes, which have not been modified by SSRI treatment. Unfortunately, possibly due to the low numbers in this study, there were no significant shape correlations with SSRI use, and replication with larger numbers is required.

We had expected to see a correlation between scores on UPSIT and hippocampal size/shape, given both its relationship with DTI changes in HD (Scahill, et al. 2013) and its known involvement with the medial temporal lobe (Delmaire, et al. 2012). Unexpectedly, this was not found in our data. UPSIT scores were significantly worse in people with symp-HD compared to pre-HD and controls, which did not differ significantly between each other. UPSIT is a score out of 40, counting the number identified correctly of 40 different smells.

Controls scored an average of 34 correct, pre-HD scored 33, and symp-HD only 26. Of note, "normal" scores in the UK are defined as 34-40 for males and 35-40 for females, "mild microsmia" as 30-33 (males) and 31-34 (females), "microsmia" as 26-29 in both sexes, "severe microsmia" as 19-25 in both sexes, and "anosmia" as anything less than 19 (Muirhead, et al. 2013). The clustering of scores in the less disabled range for all groups including symp-HD may have meant that there was less variation for a correlation with hippocampal shape to be seen. Interestingly, UPSIT scores vary by culture, and are known to be lower in Australian subjects than in UK or North American subjects (Mackay-Sim 2001).

5.5.3 Hippocampal shape analysis

When looking at shape analysis, we found significant deflation in the right hippocampal head in symp-HD compared to controls, but no longitudinal shape changes. This is perhaps unsurprising as there have been no longitudinal changes noted in hippocampal volume in other studies (Ramirez-Garcia, et al. 2020; Wijeratne, et al. 2018). With regards to baseline differences, previous studies have variously found small bilateral areas of deflation in hippocampal head and tail in symp-HD (van den Bogaard, et al. 2011b), or when looking only at larger numbers of pre-HD participants, have found significant bilateral decreases in hippocampal tail in those closer to disease onset (Faria, et al. 2016; Tang, et al. 2019), with smaller changes in the hippocampal body in those further away from disease onset, beginning in the left hemisphere (Tang, et al. 2019).

Areas of shape change correspond roughly to shape deflation in CA3 of the hippocampal head (noting that the subiculum is not included in this method of tracing hippocampus). This is in contrast to a previous study which found shape decreases in CA2 initially in pre-HD further from disease onset, then decreases in CA3/dentate gyrus closer to disease onset (Tang, et al.

2019). Hippocampal shape changes in HD may help to shed light on whether neuronal degeneration in HD occurs in a pattern that spreads out from the striatum (Poudel, et al. 2019) or begins from multiple foci of cell autonomous neurodegeneration (Tang, et al. 2019). If network spread were the case, we would hypothesise a) that it would be the areas of the hippocampus that have connections to the striatum which degenerate first in pre-HD and symp-HD, and b) that those regions of decrease corresponded to areas of the hippocampus that receive inputs (dentate gyrus/CA3, CA1) rather than perform other roles. Our results favour network spread, as degeneration occurs in anterior hippocampus, which is topographically connected to striatum, and in CA3 which receives neuronal inputs from the rest of the brain.

5.6 Limitations

The use of manual versus automated techniques is labour-intensive and subspecialised, yet we believe that the use of a rigorously anatomical basis for tracing and description of the hippocampal borders means that further detail can be gleaned using this method than from the more broad strokes of automation. However, the intensive nature of manual segmentation of the hippocampus in particular meant that this was only feasible for the baseline but not follow up scans. For the baseline analysis we used the manual tracings rather than automated segmentations as this remains more anatomically accurate, particularly when there are distortions of normal anatomy (Fung, et al. 2019; Germeyan, et al. 2014).

5.7 Conclusions

We confirmed and extended findings of hippocampal change in HD by showing shape deflation in an input region of the right hippocampal head in symp-HD, suggesting shape change following degeneration from the striatum. We also found a significant decrease in hippocampal volume in people with symp-HD who were medicated with SSRIs compared to those who were not, an intriguing finding which warrants further investigation and may have implications for further symptomatic treatment in HD. These results add further information about the pathogenesis of HD and point towards new areas of investigation. They also highlight the importance of shape analysis to look at regional change, as subtlety is missed in blunt volume analysis, and provide important insights into network changes in neurodegenerative disease.

6. Study Four: Callosal thickness in HD

The neostriatum and the hippocampus provide complementary information about neuropathological changes in HD and are interrelated, as discussed in previous Chapters. Both give snapshots of structural change in different pathways and how these are related to behavioural outcomes. This Chapter extends this information by looking at the corpus callosum as a "spoke" rather than a "hub" within neuronal networks, and as a proxy measure for more widespread degeneration (and compensation) across the cortex in pre-HD and symp-HD.

Table 6.1: Study Four. Extending the analysis of the subcortical connectome in HD by analysis of the corpus callosum, the major spoke within the larger network, to provide a broader overview of neuroanatomical changes in HD.

Study	Investigation	Rationale	Endophenotype components
Study One	Baseline analysis of neostriatum and relationship with functional outcomes	Key structure in HD and hub in frontostriatal circuitry	Genetics Morphology Function
Study Two	Longitudinal analysis of neostriatal change	Morphological change over time, investigating potential biomarkers	Genetics Morphology Spatiotemporal signature
Study Three	Baseline analysis of hippocampus and relationship with functional outcomes	Further extension of subcortical connectome in a different but related hub, potential for compensation	Genetics Morphology Function
Study Four	***Baseline and longitudinal analysis of the corpus***	***Major spoke within the connectome, complementary***	***Genetics Morphology***

callosum	*information regarding degeneration*	*Spatiotemporal signature*

Title:

Callosal thickness progressively changes in Huntington disease: 30 month IMAGE-HD data.

Authors:

F.A. Wilkes[1], M. Walterfang[2,3], C. Adamson[4], M.L. Seal[4], D. Velakoulis[2,3], G.R. Poudel[5], J.C. Stout[6], P. Chua[7], G.F. Egan[6], J.C.L. Looi[1,2], N. Georgiou-Karistianis[6]

Affiliations:

[1] Research Centre for the Neurosciences of Ageing, Academic Unit of Psychiatry and Addiction Medicine, Australian National University Medical School, Canberra Hospital, Canberra, Australia
[2] Neuropsychiatry Unit, Royal Melbourne Hospital, Melbourne Neuropsychiatry Centre, University of Melbourne and Northwestern Mental Health, Melbourne, Australia
[3] Florey Institute of Neuroscience and Mental Health, University of Melbourne, Melbourne, Australia
[4] Murdoch Children's Research Institute, Melbourne, Australia
[5] Mary Mackillop Institute for Health Research, Australian Catholic University, Melbourne, Australia
[6] School of Psychological Sciences and the Turner Institute of Brain and Mental Health, Monash University, Melbourne, Australia
[7] Department of Psychiatry, School of Clinical Sciences, Monash University, Monash Medical Centre, Melbourne, Australia

Author contributions:

F.A. Wilkes coordinated and directed the imaging analysis and wrote the bulk of the manuscript (>80% of total work). C. Adamson performed the thickness profile analysis, using a technique developed in conjunction with M. Walterfang and M.L. Seal. J.C. Stout, P.Chua,

G.F. Egan, and N. Georgiou-Karistianis were integral to the development and implementation of the overall IMAGE-HD project, of which this study is a sub-project. N. Georgiou-Karistianis is the primary investigator of the IMAGE-HD project and along with M. Walterfang and D. Velakoulis contributed to project design and is a PhD co-supervisor of F.A. Wilkes; J.C.L. Looi contributed to project design and coordination, and is F.A. Wilkes' main PhD supervisor. All authors had significant intellectual and practical input into the final manuscript.

6.1 Abstract

The corpus callosum (CC) provides a unique opportunity to investigate a proxy marker of widespread neurodegeneration in HD. In this study we investigated callosal thickness across different stages of HD using a novel method of estimating mid-sagittal thickness profiles, and correlated these changes with functional outcomes. 36 pre-HD participants, 37 symp-HD and 36 healthy controls were examined at three time points over 30 months as part of the IMAGE-HD study. A fully automated pipeline was used to generate a thickness profile for each mid-sagittal corpus callosum for each participant, which were compared between groups and longitudinally at 100 nodes along the length of the callosum. Correlations were performed with clinical and neurocognitive outcomes. Participants with symp-HD showed significant reductions in callosal thickness and, for the first time in this level of detail, significant decreases were seen in callosal thickness over time. There were no significant correlations between regional callosal thickness and clinical or neurocognitive outcomes within either the pre-symptomatic or symptomatic HD groups. While corpus callosum thickness is not impacted early in the disease process, it becomes affected after symptom onset, reflecting the spread of neurodegeneration to other structures.

6.2 Introduction

HD is an autosomal dominant neurodegenerative disease causing progressive motor, cognitive and psychiatric disturbances (Kirkwood, et al. 2001). Although the most noticeable neuroanatomical change in HD is gross atrophy of the neostriatum (caudate and putamen), cortical regions and white matter tracts are also affected (Della Nave, et al. 2010; Di Paola, et al. 2012; Dumas, et al. 2012; Hobbs, et al. 2012; Kloppel, et al. 2008; Phillips, et al. 2013; Poudel, et al. 2014b; Rosas, et al. 2010; Rosas, et al. 2006; Sritharan, et al. 2010; Vonsattel, et al. 1985; Weaver, et al. 2009). As the major interhemispheric commissure, the corpus callosum (CC) is the largest spoke in the "hubs and spokes" of neuronal circuitry (Looi, et al. 2014b). Further investigation of the CC in HD may provide a unique opportunity to strategically investigate more widespread neurodegeneration, providing a further opportunity to develop more efficient and clinically translatable biomarkers of disease (Adamson, et al. 2018).

Previous research in symp-HD has shown decreased volume and thickness of the CC (Crawford, et al. 2013; Della Nave, et al. 2010; Di Paola, et al. 2012; Hobbs, et al. 2012; Rosas, et al. 2010), with progressive deterioration over time (Crawford, et al. 2013). Changes during the pre-HD stages are less extensive, but become more pronounced as individuals approach disease onset (Crawford, et al. 2013; Rosas, et al. 2010). However, many previous studies have used either total CC area or regional areas based on gross subdivision schemes (Crawford, et al. 2013; Della Nave, et al. 2010; Hobbs, et al. 2012), which may not be sensitive to subtle shape changes. The availability of increased computational processing power has facilitated the development of new, sophisticated semi-automated shape analysis pipelines for the CC that show increased sensitivity for the detection of change in disorders

such as HD, where volume changes are small but nonetheless significant (Adamson, et al. 2014; Adamson, et al. 2011).

The CC can be divided into functional subregions based on its homotopic cortico-cortical connections (Chao, et al. 2009; Hofer and Frahm 2006) (Figure 6.1). As such, regional changes in CC may be reflected in cognitive, emotional or motor functional outcomes related to neural circuits subserved by those regions (Della Nave, et al. 2010; Di Paola, et al. 2012; Dumas, et al. 2012; Phillips, et al. 2013; Rosas, et al. 2010; Rosas, et al. 2006). Briefly, the anterior one-third, including the genu, connects frontal regions; the middle one-third connects pre-motor and supplementary motor cortices; and smaller subregions in the posterior third connect motor cortex, sensory cortex, and parietal, temporal and occipital cortices, although there are also a small number of heterotopic connections between different cortical regions (Chao, et al. 2009). While a number of studies have examined correlations between DTI changes and functional outcomes (Dumas, et al. 2012; Gregory, et al. 2015; Phillips, et al. 2013; Poudel, et al. 2014b; Rosas, et al. 2010; Rosas, et al. 2006), few have found correlations between macroscopic changes. One study found correlations in symp-HD between decreased white matter volume in the genu and motor connections of the CC with cognitive outcomes (Della Nave, et al. 2010), while another found smaller baseline volumes in early HD were associated with impaired Circle Tracing (Crawford, et al. 2013).

In this study, we extended the macrostructural investigations of CC across different stages of HD using a novel method of estimating mid-sagittal thickness profiles that is robust longitudinally, allowing assessment of spatiotemporal change (Adamson, et al. 2014). This is relevant given the growing interest in discovering imaging markers in HD (that may extend to regions outside the striatum), and analytic methods that can best track disease progression

Figure 6.1: Corpus callosum connectivity. Reproduced and modified with permission from (Phillips, et al. 2013) (left image) and (McColgan, et al. 2018) (right image). Left image is in the sagittal plane, with anterior to the left and posterior to the right, and shows tracts within the corpus callosum connecting anterior frontal (yellow), orbitofrontal (orange), superior frontal (blue), superior parietal (purple), posterior parietal (pink), temporal (brown), and occipital (light pink) regions. Right image is in the axial plane and shows interhemispheric connections.

with concomitant functional relevance (Bohanna, et al. 2008; Georgiou-Karistianis, et al. 2013c). We hypothesised that this more sensitive method of investigation would allow subtle changes to be documented in pre-HD and symp-HD over time, thus revealing more insights about the pattern of neurodegeneration in HD and relationships with clinical and neurocognitive outcomes.

6.3 Methods

6.3.1 Participants

Thirty-six pre-HD, 37 symp-HD, and 36 healthy control volunteers were included in this investigation, all recruited as part of the IMAGE-HD study (Georgiou-Karistianis, et al. 2013a). Controls were matched for age, sex and premorbid IQ (National Adult Reading Test (Nelson and Willison 1991)) to the pre-HD group. Inclusion in the pre-HD group was based on UHDRS total motor score <5 (Huntington Study Group 1996; Tabrizi, et al. 2009). The average estimated time to clinical onset for the pre-HD group was 16 ± 7 years, as determined by the Langbehn method, based on age and number of CAG repeats (Langbehn, et al. 2004). The symp-HD group had an average of 2 ± 2 years since diagnosis through symptom onset. All participants were right-handed and were free from brain injury, neurological, and/or severe diagnosed psychiatric conditions other than HD. Demographics, clinical information and neurocognitive measures of interest are provided in Table 6.2.

6.3.2 Measures

The complete battery of neurocognitive data collected for all participants as part of the IMAGE-HD study has been described elsewhere(Georgiou-Karistianis, et al. 2013a). These

were selected based on their sensitivity in detecting differences between groups (Stout, et al. 2011; Tabrizi, et al. 2009). Neurocognitive and motor tests were performed to assess visuomotor speed and attention (SDMT (Smith 1982)), speeded reading (Stroop Word Reading Test (Stroop 1935)), odour recognition (UPSIT (Doty, et al. 1984)), and motor speed and pacing (speeded tapping, and self-paced tapping slow (1.8Hz) and fast (3.0Hz) conditions) (Stout, et al. 2011). All of these tests showed significant differences between groups (Table 6.2). Tests were repeated at 18 months and 30 months after baseline, with 27 controls, 33 pre-HD and 29 symp-HD remaining enrolled at this time.

The IMAGE-HD study was approved by the Monash University and Melbourne Health Human Research Ethics Committees and informed written consent was obtained from each participant prior to testing in accord with the Helsinki Declaration. Scanning and testing were undertaken at the Royal Children's Hospital, Parkville, Melbourne, Australia. Ethics approval for the current sub-analysis was also obtained from both Monash University and from the Australian National University.

6.3.3 Imaging

Structural MR images were acquired with the Siemens Magnetom Tim Trio System 3 T MRI scanner (Siemens AG, Erlangen, Germany) and a 32-channel head coil at the Murdoch Children's Research Institute (Royal Children's Hospital, Victoria, Australia). High-resolution T_1-weighted images were acquired with the following parameters: 192 slices, slice thickness of 0.9 mm, 0.8 × 0.8 mm^2 in-plane resolution, 320 × 320 matrix, TI=900 ms ,TE=2.59 ms, TR=1900 ms, flip angle=9°.

6.3.4 Mid-sagittal thickness profiles

Thickness profiles for each midsagittal CC were generated from the 3D T1-weighted images using a fully automated pipeline (Adamson, et al. 2014). Briefly, the pipeline performed midsagittal plane extraction, CC segmentation and thickness profile generation based on the Laplace equation based method previously published (Adamson, et al. 2011). Midsagittal plane extraction was performed using alignment to a template. The CC segmentation method consisted of template-based initialisation followed by refinement using a cascade of mathematical morphology operations. Manual editing, blind to diagnosis, was performed to correct errors. Thickness profiles were generated using 100 nodes taken along an anterior-posterior trajectory.

6.3.5 Statistics

Thickness profiles were compared at 100 nodes along the length of the CC (Adamson, et al. 2011) for controls versus pre-HD; pre-HD versus symp-HD; and controls versus symp-HD utilising two-sample Welch's T-test, with age and intracranial volume (ICV) accounted for via regression. Sex differences in CC volume are largely due to variation in brain size, which was controlled for using ICV (Luders, et al. 2014). Multiple comparisons were corrected for via correction for the FDR. Correlations were performed between thickness profiles at each of the nodes with clinical and neurocognitive outcomes, utilising FDR to correct for multiple comparisons. The pipeline for this is available at www.nitrc.org/projects/ccsegthickness.

6.4 Results

6.4.1 Neurocognitive and motor testing

Symp-HD participants performed significantly worse on all of the neurocognitive and motor tests compared to controls ($p < 0.001$) and pre-HD ($p < 0.001$) (Georgiou-Karistianis, et al. 2013a). Significantly poorer performance was also seen in pre-HD compared to controls in self-paced tapping slow ($p < 0.05$) and fast conditions ($p < 0.05$) (Table 6.2).

Table 6.2: Demographic, clinical, motor and baseline neurocognitive data.

	Mean ± SD, (Range)		
	Controls	Pre-HD	Symp-HD
N (sample sizes)	36	36	37
Age	42 ± 13 (24-73)	42 ± 10 (24-65)$^{+++}$	52 ± 9 (37-71)***
Verbal IQ	118 ± 10	117 ± 11	113 ± 12
Total ICV (cm^3)	1457 ± 144	1415 ± 157	1401 ± 156
CAG repeats		42 ± 2 (39-46)	43 ± 2 (40-50)
Estimated YtO		16 ± 7 (3-39)	
Duration of illness (years)			2 ± 2 (0-5)
SDMT	56 ± 10	52 ± 9^{+++}	36 ± 12***
UPSIT	34 ± 3	33 ± 5^{+++}	26 ± 7***
Stroop	110 ± 17	104 ± 18^{+++}	82 ± 22***
Speeded tapping (ITI, ms)	220 ± 38	244 ± 45^{+++}	364 ± 162***
Self-paced tapping (slow condition)	24 ± 8	20 ± 7*$^{+++}$	11 ± 4***
Self-paced tapping (fast condition)	29 ± 8	24 ± 9*$^{+++}$	11 ± 6***
UHDRS (motor)		1 ± 1 (0-4)	19 ± 12 (6-60)

SD, standard deviation; ICV, intracranial volume; YtO, estimated years to disease onset; SDMT, Single Digit Modalities Test; UPSIT, University of Pennsylvania Smell Identification Test; Stroop, Stroop speeded word reading task; ITI, intertrial interval; Self-paced tapping

(slow condition), 1.8Hz self-paced tapping, 1/SD ITI; Self-paced tapping (fast condition), 3.0Hz self-paced tapping, 1/SD ITI; UHDRS, United Huntington Disease Rating Scale, motor subscore. Symp-HD or pre-HD versus controls: *$p \leq 0.05$; ** $p \leq 0.01$; *** $p \leq 0.001$; symp-HD versus pre-HD: $^{+}p \leq 0.05$; $^{++}p \leq 0.01$; $^{+++}p \leq 0.001$.

6.4.2 CC Thickness

Participants with symp-HD showed significantly decreased CC thickness, compared to controls and to pre-HD (Figure 6.2). Post-hoc tests showed lower CC thickness in symp-HD, compared to controls, in posterior regions of CC, extending to anterior regions by 30 months. This pattern of difference was the same between pre-HD and symp-HD. There were no significant differences in CC thickness between controls and pre-HD.

The three groups showed different patterns of raw CC thickness change over time, prior to FDR adjustment for multiple comparisons, representing inflation and deflation of thickness of the CC over the three time points depending on region (Figure 6.3). Both control and pre-HD groups showed some thickness expansion over time in posterior regions, as well as some small reductions in thickness anteriorly and near the splenium, whereas the symp-HD group tended to show thickness reductions across the entire callosal profile.

Figure 6.2: Cross-sectional analysis of CC thickness, corrected for multiple comparisons and controlling for age and ICV (next page)**.** The anterior callosum is on the right of each image. Significant changes are in colour. The colour bar displays the *p*-value and level of significance, after FDR correction: hotter colours (red) show the left named comparator group is larger in size with darker colours correspond to smaller, more significant p-values.

Control vs pre-HD | Pre-HD vs symp-HD | Control vs symp-HD

a) Baseline

b) 18 months

c) 30 months

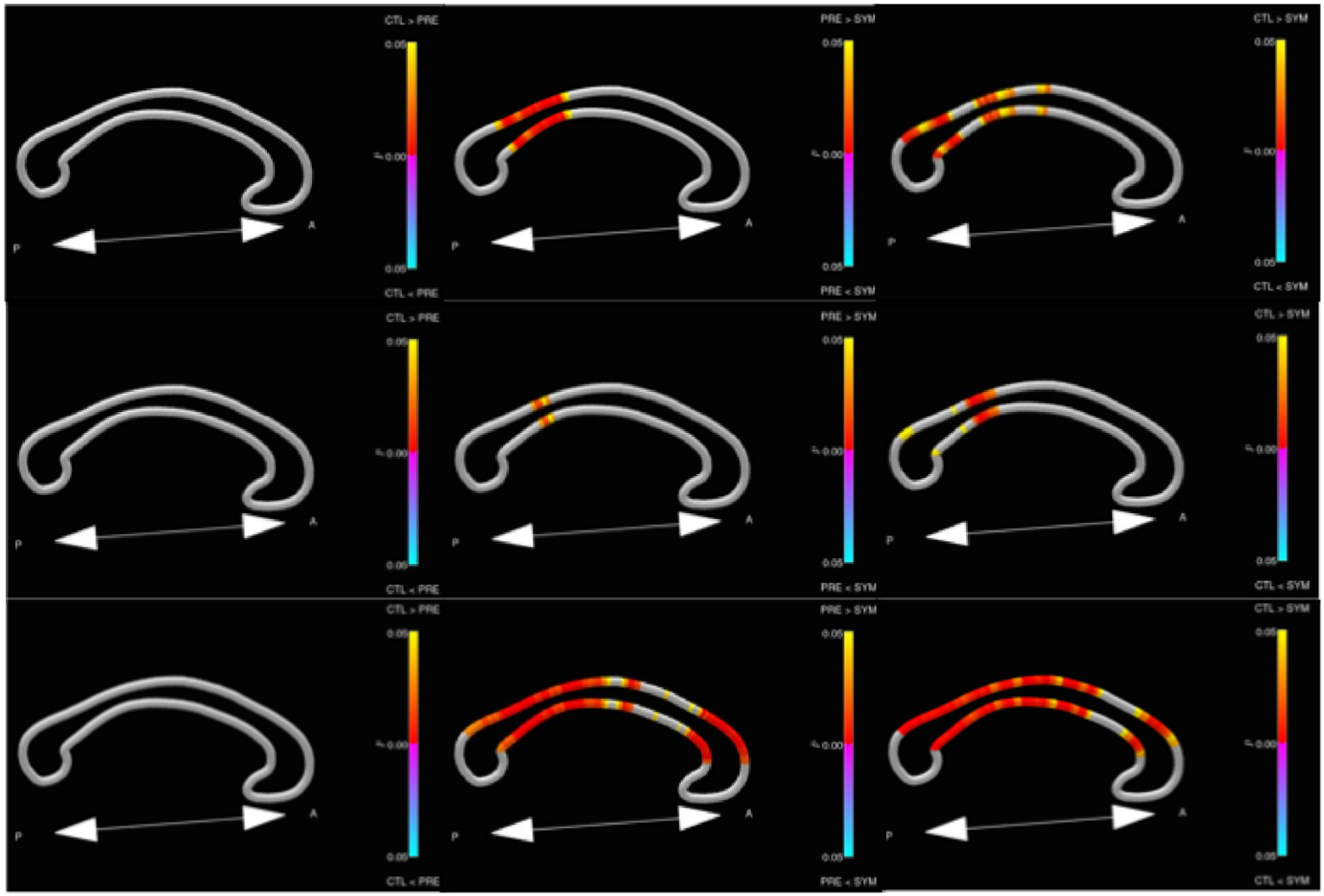

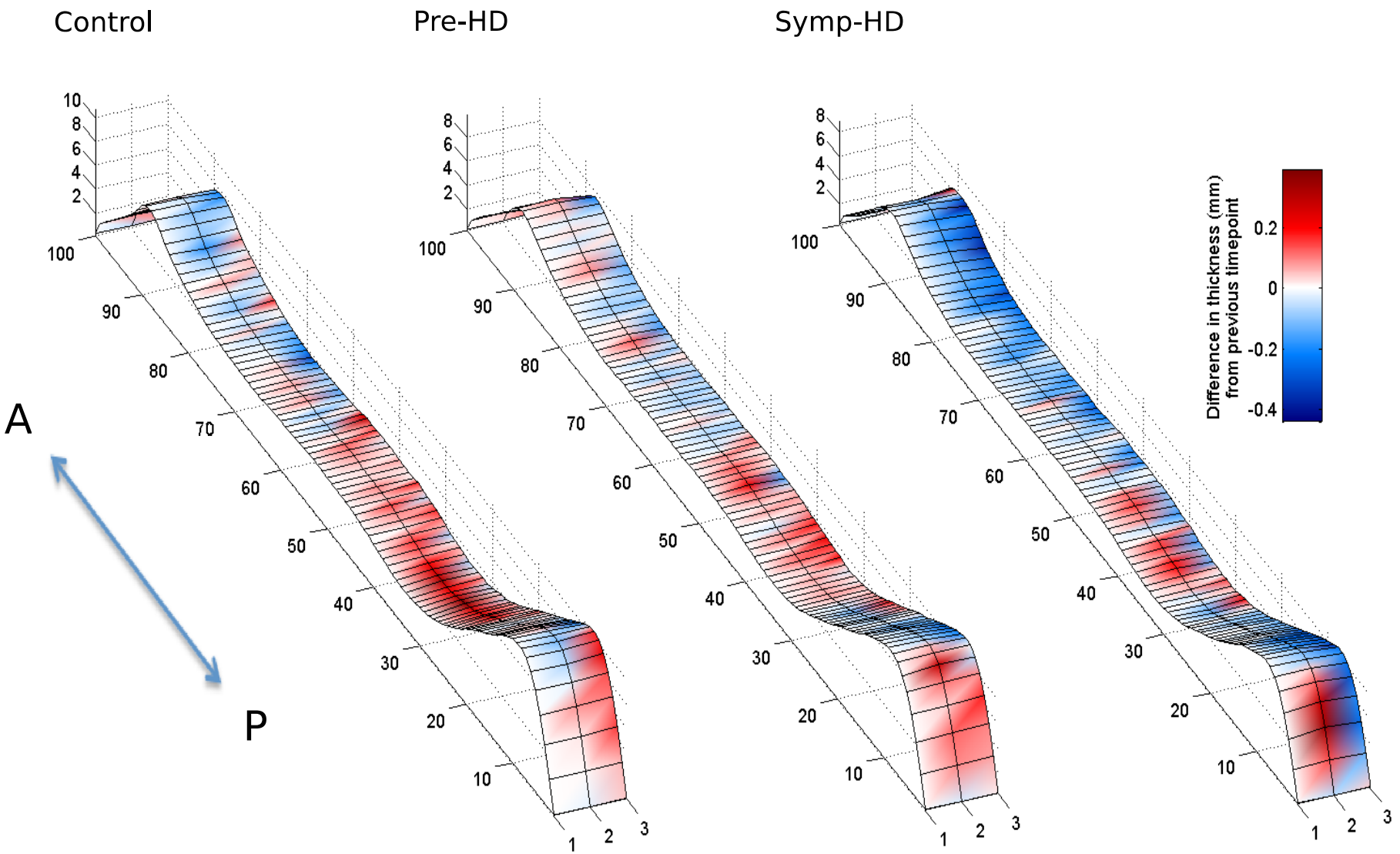
Control
Pre-HD
Symp-HD
A
P
Difference in thickness (mm) from previous timepoint
0.2
0
-0.2
-0.4

Figure 6.3: Ribbon plots showing mean change in callosal thickness. Change between time-points 1 (baseline), 2 (18 months) and 3 (30 months) is shown as expansions (red) or contractions (blue). For these ribbon plots, raw mean change for callosal thickness is shown (without correction for multiple comparisons), exploring expansion or contraction of thickness represented by colour coding of blue for contraction and red for expansion, with darker colours corresponding to larger values.

After controlling for age, ICV and multiple comparisons, symp-HD patients showed significant decreases in CC thickness over 30 months, while no significant changes were seen in controls or pre-HD (Figure 6.4). This reduction in thickness was in the posterior CC at the splenium.

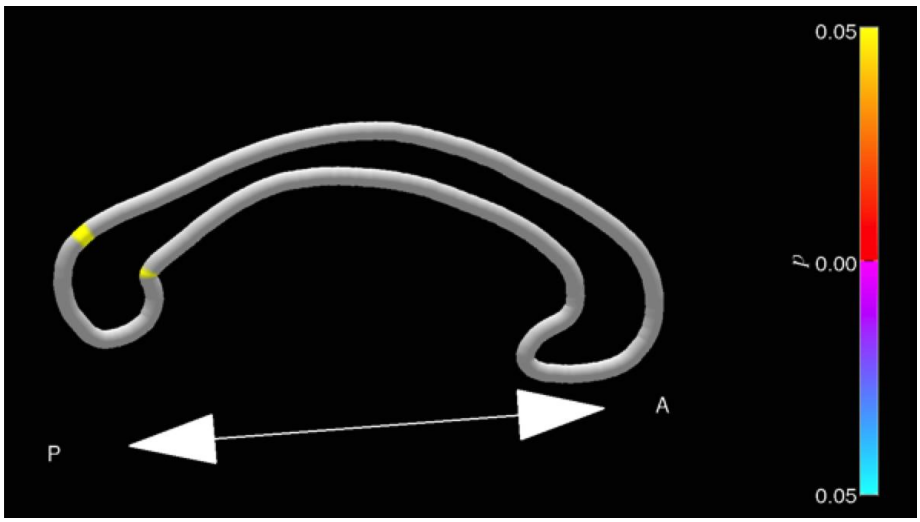

Figure 6.4: Longitudinal change in CC thickness in symp-HD after 30 months, corrected for multiple comparisons and controlling for age and ICV. Significant changes are shown in colour. The colour bar displays the *p*-value and level of significance, after FDR correction: warmer colours show the baseline scan is larger.

6.4.3 Group Correlations with Clinical and Neurocognitive Measures

We examined correlations between CC thickness and SDMT, Stroop, UPSIT, speeded tapping, self-paced tapping slow and fast conditions, CAG repeats and UHDRS motor subscores. After correcting for multiple comparisons and adjusting for age and ICV, a small negative correlation was seen in controls at 30 months between thickness in anterior CC and scores on SDMT (Figure 6.5).

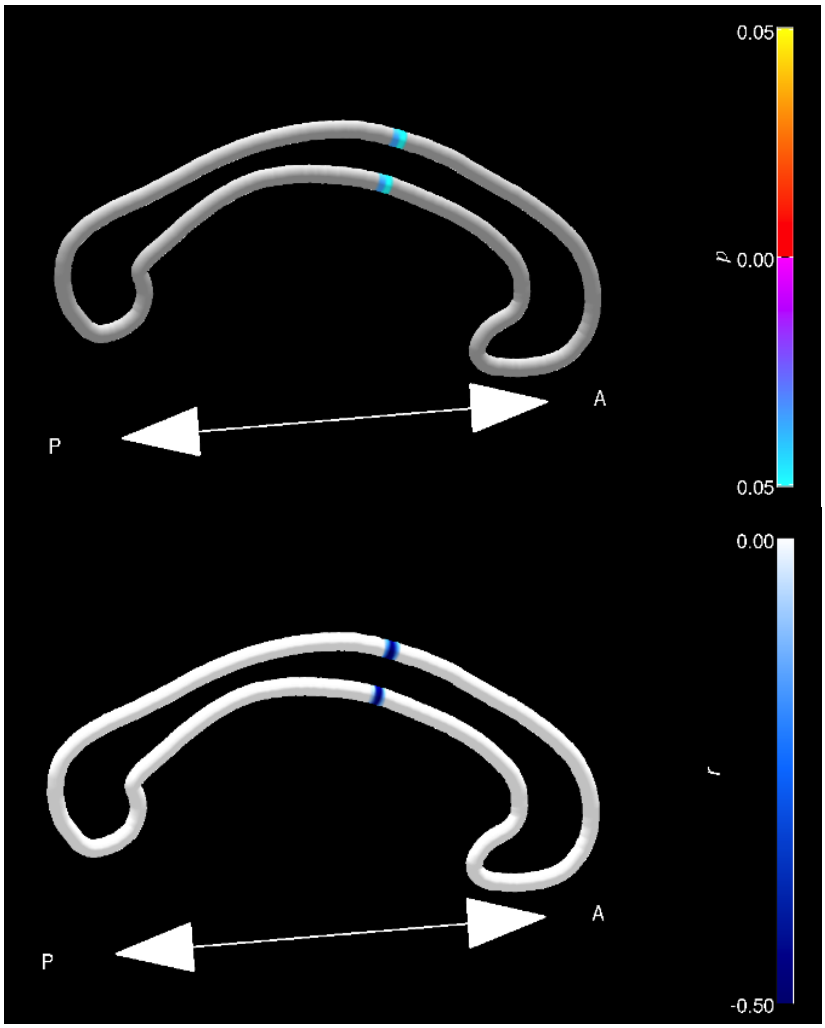

Figure 6.5: Correlation between CC thickness in controls at Time 3 and scores on SDMT. Significant correlations are in the panel on the top, and on the bottom is value of the correlation (r) at that position. The colour bar on the top displays the p-value and level of significance, after FDR correction: cooler colours (blue) show the correlation is negative.

6.5 Discussion

We found significantly decreased CC thickness in early symp-HD, a finding which is consistent with previous studies (Di Paola, et al. 2012; Rosas, et al. 2010). We also found a significant decrease in CC thickness over time in symp-HD, in a region confined to the splenium. While one previous study has found longitudinal changes in overall CC volume in HD (Crawford, et al. 2013), to our knowledge this is the first study to show longitudinal change in this level of anatomical detail.

6.5.1 Changes in CC thickness as a marker of loss of connectivity

Reductions in CC thickness in symp-HD were in areas connecting prefrontal, premotor, primary motor, motor association, primary sensory, temporal and parietal cortex. It may be that reductions in CC thickness, in the extensive regions identified, correspond to loss of homotopic cortical connectivity; this finding is in accord with a previous study in HD (Di Paola, et al. 2012) and concurs with the cortical volumetric changes seen in pre-HD in posterior and superior cerebral regions, particularly closer to disease onset, as well as with widespread cortical changes in symp-HD (Nopoulos, et al. 2010; Rosas, et al. 2008). This supports CC thickness as a proxy biomarker for more complex homotopic cortical regions (Hampel, et al. 1998; Mangalore, et al. 2021; Teipel, et al. 2003; Teipel, et al. 2002; Walterfang, et al. 2014). Our results also concur with more recent work on the spread of neural degeneration in HD occurring in a transneuronal pattern out from the striatum (Poudel, et al. 2019); hence the CC would not be expected to be affected at a macroscopic level early in the HD process.

We did not find any significant difference in callosal thickness between our sample of pre-HD and control participants. This corresponds with a previous study with a similar number of participants, who also did not find any changes in callosal thickness in pre-HD (Rosas, et al. 2010). More extensive changes have been found by other authors in individuals closer to expected time of disease onset (Crawford, et al. 2013; Hobbs, et al. 2010; Rosas, et al. 2010). For example, using the larger TRACK-HD dataset, Crawford and colleagues found a decrease in thickness in pre-HD participants who had less than 10 years to estimated disease onset (Crawford, et al. 2013). In contrast, our sample averaged 16 years to estimated motor onset of disease and may have been too early in the disease process to show a change in CC morphology. Lack of CC changes in pre-HD compared to controls points to the CC as less sensitive to pathology early in the disease, then becoming involved with disease progression and the spread of neurodegeneration from the striatum.

6.5.2 Bidirectional changes in the CC suggest ongoing plasticity

Of interest, the raw un-FDR corrected data demonstrated some inflation and deflation in callosal thickness over time in all groups, although after correcting for multiple comparisons significant changes (i.e., deflation) occurred only in symp-HD after 30 months. While callosal atrophy is seen in other disorders, such as schizophrenia (Walterfang, et al. 2008), various dementias (Walterfang, et al. 2014), and multiple sclerosis (Granberg, et al. 2015), other studies have shown bidirectional changes. For example, expansion in the posterior body and isthmus of the CC is seen in currently depressed patients but not those in remission (Walterfang, et al. 2009b), while global reduction in thickness is seen in bipolar affective disorder but depends on duration of illness and possibly lithium treatment (Walterfang, et al. 2009a). Together, these results suggest dynamic changes in callosal thickness may be related to disease status and potentially, treatment. Our results suggest mid-sagittal CC thickness may

be a potential biomarker for treatment effects in early symp-HD since changes are seen only in the symptomatic stage.

A minor negative correlation was found between a thickness in small region of anterior CC in controls and scores on SDMT. This correlation was only seen at Timepoint 3. The reason for this negative correlation, indicating better performance on SDMT with decreased CC thickness, is unclear: perhaps it is artefactual. No significant correlations were found in any group between CC thickness and any of the other clinical or neurocognitive measures tested. Of those other studies examining macrostructural changes, Rosas and colleagues found no correlation between CC thickness and SDMT, Stroop, age or CAG repeat number (Rosas, et al. 2010), while Della Nave et al. found a correlation between CC volume in the genu and SDMT and Stroop scores (Della Nave, et al. 2010). A number of DTI studies have shown correlations between various diffusivity measures and Stroop (Della Nave, et al. 2010; Rosas, et al. 2010; Rosas, et al. 2006), SDMT (Della Nave, et al. 2010; Dumas, et al. 2012; Rosas, et al. 2010), speeded finger tapping (Dumas, et al. 2012) and UHDRS motor subscore (Bohanna, et al. 2011b; Della Nave, et al. 2010; Phillips, et al. 2013), suggesting that DTI may be a more sensitive marker of white matter change and its functional concomitants.

6.6 Limitations

A limitation of this study is the reliance on previous tractography maps for inferences about structural connectivity of the CC. However, structural connectivity research has been replicated and extended in a number of cases and should be considered as reliable (Chao, et al. 2009; Hofer and Frahm 2006). The mapping of mid-sagittal thickness is a proxy measure for the entirety of the CC and necessarily loses some of the detail of measuring the entire

volume. Against this must be balanced the relative complexity of measuring the entire CC, as well as measuring change over time, which in context may make our method more practicable. Our method of measuring CC thickness is also one of the very few methods that explicitly corrects statistically for the non-independence of adjacent callosal measures and for multiple comparisons(Adamson, et al. 2014; Adamson, et al. 2011). This rigorous method gives high specificity albeit low sensitivity given the difficulty in reaching threshold for statistical significance. Consequently we believe that the results presented in this study offer a more robust and conservative statistical analysis.

6.7 Conclusion

Using a novel method to detect regional CC change across 100 anteroposterior points, we have reported for the first time decreased CC thickness in symp-HD with progressive decrease in thickness over time. These changes were observed in areas that are related to affected cortical regions and provide new information about disease progression. The ease of application of this method, and its application to existing MRI datasets, provides an important new tool in investigating the spread of structural change in neurodegenerative disease. In using this method we have shown that the CC is a potentially sensitive biomarker in HD and by extension, a potential and easily measured proxy for cortical volume changes.

7. General discussion

This thesis presents an investigation into subcortical changes in HD in specific neuroanatomical "hubs and spokes", i.e. the caudate, putamen, hippocampus, and corpus callosum, and their relationship with clinical, motor, neurocognitive and neuropsychiatric outcomes. The central questions were:

- Is there a difference between subcortical morphology in symp-HD, pre-HD, and controls?
- Do these change over time and progress in a determined pattern?
- Is there a relationship between shape change and motor and neurocognitive outcomes?
- Do these follow the expected relationships with known subcortical circuits in a topographical pattern?
- Can the picture of the above give a better understanding of the pathogenesis of HD and help with the development of a biomarker and endophenotype of HD?

Table 7.1: Scope of thesis. Investigation of the subcortical connectome in HD, with view to development of an endophenotype.

Study	Investigation	Rationale	Endophenotype components
Study One	Baseline analysis of neostriatum and relationship with functional outcomes	Key structure in HD and hub in frontostriatal circuitry	Genetics Morphology Function
Study Two	Longitudinal analysis of neostriatal change	Morphological change over time, investigating potential biomarkers	Genetics Morphology Spatiotemporal signature

Study Three	Baseline analysis of hippocampus and relationship with functional outcomes	Further extension of subcortical connectome in a different but related hub, potential for compensation	Genetics Morphology Function
Study Four	Baseline and longitudinal analysis of the corpus callosum	Major spoke within the connectome, complementary information regarding degeneration	Genetics Morphology Spatiotemporal signature

Investigation in this thesis focused on specific "hubs and spokes" within the brain, providing a more comprehensive picture of HD as a whole and the interrelationship between neuroanatomical changes and functional outcomes. This thesis found changes in subcortical morphology in pre-HD and symp-HD, which progressed in a determined pattern and related to genetic changes. This thesis also found correlations between shape changes in the striatum and motor and neurocognitive outcomes, in areas related to the appropriate frontostriatal circuitry. Further characterisation of changes in HD increases knowledge of neurodegenerative pathways and the relationship between quantitative measures of morphology (morphometry) and function *in vivo*, constituting endophenotypes, and aims towards developing biomarkers for prognostication and use in HD treatment trials.

7.1 Brief summary of findings

Study One investigated the baseline morphology of the neostriatum in pre-HD and symp-HD, and how this related to functional outcomes. Study One hypothesised that neostriatal morphology would differ significantly between controls and individuals with pre-HD and symp-HD, and that changes would be associated with cognitive, neuropsychiatric and motor

outcomes according to known functional connections. Significant shape differences were detected between all groups, with caudate and putamen being largest in controls, then in pre-HD, and then in symp-HD. Higher CAG repeats, DBS, and UHDRS total motor score were associated with striatal shape deflation and decreasing striatal thickness. In pre-HD, there were widespread correlations between decreasing striatal thickness and surface contraction in caudate and putamen and greater CAG repeat number and DBS. These associations were detected to a much lesser extent in symp-HD, with only small areas of association between lower surface area shape measures and increasing DBS in patches of bilateral caudate, as well as left anterior putamen. Increasing CAG repeat number was only associated with lower surface area shape measures in left caudate head and anterior tail in symp-HD. In symp-HD, UPSIT scores were correlated with greater thickness in left caudate tail and surface dilation ratio in left posterior putamen; Stroop scores were positively correlated with the thickness of left putamen head and body. Better scores in self-paced tapping (slow) were correlated with greater thickness and surface dilation in bilateral putamen in pre-HD and in right caudate in symp-HD, reflecting some element of network compensation. Self-paced tapping (fast) was correlated with higher surface dilation ratio in the right anterior putamen in symp-HD. Shape changes correlated with functional measures subserved by corticostriatal circuits, and were also correlated with genetic changes in HD, providing evidence towards the striatum as an endophenotype of HD.

Study Two aimed to extend the literature on morphological change in HD using a new method of longitudinal shape analysis. Study Two hypothesised that there would be longitudinal shape changes in the caudate and putamen, visualised in greater detail than previously due to the new method of analysis, and that this would help towards development of a biomarker for HD. Study Two found significant differences in shape of the striatum between groups.

Significant group-by-time interaction was observed for the putamen bilaterally, but not for caudate, with a differential rate of shape change between groups over time and deflation more pronounced in the symp-HD group. The main effect of CAG repeats on shape in pre-HD and symp-HD occurred for the entire bilateral striatum and there was no significant group-by-CAG-repeat interaction effect. In contrast to the lack of group-by-CAG-repeat interaction effect, there was a significant time-by-CAG-repeat interaction effect: later time points in pre-HD and symp-HD demonstrated an association between increased CAG repeats and increased deflation in the caudate.

Study Three extended the investigation of HD from the neostriatum to the hippocampus, another key neuronal hub which also has a relationship with clinical symptoms seen in HD, but which has been less extensively studied in this field. Study Three hypothesised that there would be subtle shape changes in the hippocampus in pre-HD and symp-HD, and that these would be related to psychiatric and cognitive scores related to the hippocampus, as well as to SSRI use as this alters hippocampal neurogenesis. No differences were found in baseline hippocampal volume between groups after controlling for age and intracranial volume. There was also no relationship between hippocampal volume and scores on UPSIT, BDI-II, HADS-A or HADS-D, all of which have links to the hippocampus. Unexpectedly, a significant difference in both right and left hippocampal volume was found in SSRI users, despite there being no significant changes between anxiety or depressive symptoms or motor incapacity. Significant shape contraction was seen in the right hippocampal head in symp-HD in a pattern consistent with later spread of neurodegeneration from the striatum. No longitudinal changes in shape were found in any group.

Study Four extended the hubs and spokes model of neuronal circuitry further to examine the largest "spoke" in the brain, the corpus callosum, which provides a unique opportunity to investigate a proxy marker of widespread neurodegeneration in HD. Study Four investigated mid-sagittal callosal thickness and aimed to correlate changes with functional outcomes. Study Four hypothesised that subtle changes would be seen in pre-HD and symp-HD over time, reflecting spread of neurodegeneration. Participants with symp-HD showed significant reductions in callosal thickness and significant decreases were seen in callosal thickness over time. There were no significant correlations between regional callosal thickness and clinical or neurocognitive outcomes in either pre-HD or symp-HD. While CC thickness was not impacted early in the disease process, it became affected after symptom onset, reflecting the spread of neurodegeneration to other structures.

7.2 Insights into progression of neurodegeneration in HD and implications for treatment

This thesis investigated structural changes to brain "hubs and spokes" and how these changes were related to motor, neurocognitive and psychiatric outcomes in HD. Using structural MRI and shape analysis techniques, this thesis demonstrated that changes to brain "hubs", particularly the neostriatum, occur in early disease stages, followed later by changes in the major "spoke" of the corpus callosum. "Hub" changes in the neostriatum were also reflected in correlations with functional outcomes related to underlying frontostriatal circuitry. In addition, changes reflected areas of both functional and structural compensation for neurodegeneration in HD. Neuroanatomical changes, compensation, and the implications for development of an endophenotype of HD are discussed below.

7.2.1 Neuroanatomical changes in HD, network spread, and potential for neural and functional compensation.

HD has its most marked effects on the neostriatum, but also has more subtle effects on other subcortical areas. This thesis also showed areas of surface contraction in symp-HD in the hippocampus compared to controls. Areas of change within the hippocampus were in regions which are topographically related to striatum and which receive inputs from other areas of the brain (rather than internal circuitry or output regions). Unlike these "hubs", this thesis found that the large "spoke" of the corpus callosum was not impacted early in the HD process but became affected after symptom onset. These converging lines of evidence highlight the spread of neurodegeneration from striatum to other structures (Poudel, et al. 2019), rather than supporting the competing hypothesis of multiple foci of cell autonomous degeneration (Tang, et al. 2019).

The two areas of potential neurogenesis in the adult human brain are within the hippocampus (SGZ) and next to the caudate (SVZ). New neurons from the SVZ can integrate into the striatum in adult humans: this is depleted in HD and postnatally generated neurons are absent in advanced stages of the disease (Ernst, et al. 2014), even though some early studies showed increased cell proliferation in the SVZ in HD and potential compensation (Curtis, et al. 2003). Similarly, a large subpopulation of hippocampal neurons are subject to turnover in the adult human brain, with neurogenesis continuing throughout the lifespan (Spalding, et al. 2013). Cell proliferation in the hippocampus is reduced in mouse models of HD but reportedly not in humans with advanced HD, although there are limited human histopathological studies (Low, et al. 2011). Well-defined maps of shape change in the neostriatum and hippocampus in HD are crucial towards recognising and tracking where potential compensation and neurogenesis can occur with treatment.

Recent studies investigating children and adolescents with pre-HD many years before motor onset have found a number of interesting changes in neurodevelopment. The recent Kids-HD study (Tereshchenko, et al. 2020; van der Plas, et al. 2019) investigated a cohort of young people age 6-18 with a parent or grandparent with symp-HD, and so therefore potentially at risk of later developing symp-HD themselves. The study excluded children with juvenile onset HD, and on average the estimated time to onset of symp-HD was 35 years. Given the ethical considerations with testing for genetic changes indicative of HD, genetic results were blinded to all participants and to everyone who was involved in working directly with participants. Abnormal neurodevelopment was found in the striatum in children who had pre-HD, with early hypertrophy (van der Plas, et al. 2019). In HD gene non-expanded individuals, the striatum grows in size until approximately age 14, followed by a decline in striatal volume (Herting, et al. 2018; van der Plas, et al. 2019). In pre-HD however, there is initial hypertrophy of the striatum prior to the age of 10, followed by a steady early decrease in volume. From age 14, volume loss occurs in a similar pattern in both pre-HD and gene non-expanded individuals. Children with CAG repeat lengths greater than 50 had both greater initial hypertrophy and faster rates of subsequent volume decline.

Resting-state fMRI was also used in this cohort to investigate possible compensation from the cerebellum for abnormal striatal neurodevelopment (Tereshchenko, et al. 2020). The cerebellum is integrated into the indirect pathway of the basal ganglia through outputs from the dorsocaudal putamen, globus pallidus externa, subthalamic nucleus, and pontine nuclei, and reciprocal inputs come from the dentate nucleus of the cerebellum to the ventrolateral thalamus and dorsocaudal putamen (Milardi, et al. 2016; Tereshchenko, et al. 2020). By calculating seed-to-seed correlations among these regions, significantly different trajectories of connectivity were found between all regions except the dorsocaudal putamen. In children

with pre-HD, hyperconnectivity is seen in early years (while hypertrophy of the striatum is occurring), with later linear decline. This hyperconnectivity is thought to be a compensatory measure for abnormal neurodevelopment in the striatum (Tereshchenko, et al. 2020), and cerebellar compensation has also been proposed during later striatal degeneration (Franklin, et al. 2020; Gaura, et al. 2017). This is in line with a number of other functional imaging studies which have shown compensatory increases in other pathways for motor and cognitive tasks in pre-HD and symp-HD (Georgiou-Karistianis, et al. 2013b; Georgiou-Karistianis, et al. 2014; Gregory, et al. 2018; Kloppel, et al. 2009; Klöppel, et al. 2015; Poudel, et al. 2015c).

7.2.2 Development of an endophenotype of HD, implications for treatment

Researchers continue to search for improved ways to monitor progression of disease in HD, as there are no current disease-modifying treatments and an ongoing need for a biomarker to help with testing potential treatments. CAG repeat number in HD accounts for only 50-70% of age at onset, and has less of a role in disease progression once the motor symptoms become apparent, although this role may be somewhat masked by the process of ageing itself (Rosenblatt, et al. 2012; Rosenblatt, et al. 2006; Wexler, et al. 2004). Indeed, in Study One there were reduced areas of striatal shape correlation with CAG repeat length in symp-HD (controlling for age, sex and ICV), occurring only in the left caudate, compared to widespread correlations between shape and UHDRS. Extending this, Study Two demonstrated that while there was a significant correlation between increasing CAG repeat number and shape deflation in caudate and putamen, a significant effect of time on this effect was only found in the caudate and stronger in the left hemisphere. Group by time interactions, however, revealed correlations only with putamen, and not caudate, shape: change in putamen shape over time in

symp-HD appears to be somewhat independent of CAG repeat length. These results point specifically to the putamen as the better biomarker for progression in pre-HD and symp-HD.

As research moves towards searching in younger cohorts for potential biomarkers in HD, one recent study looking at young adults in their 20s found a few potential biomarkers at very early stages of pre-HD, with an average of 24 years to diagnosis (Scahill, et al. 2020). One of these was putamen volume, although volume was not correlated with CAG repeat numbers. The others were two CSF markers and one serum marker, with CSF neurofilament light protein being the most sensitive measure and correlated with CAG repeat number (Scahill, et al. 2020). From a practical standpoint however, regular lumbar punctures to siphon CSF has a number of disadvantages, as it is a painful procedure and carries significant risks. Importantly, this young adult study looked at putaminal volumes only and not shape. Results in this thesis would suggest that adding shape to the measure of putaminal changes could also increase sensitivity for a biomarker at early stages.

Establishment of an endophenotype, a "biological measure that correlates with, or predicts, clinical features of brain dysfunction" (Looi, et al. 2014b), is especially important in complex conditions like HD, given the issues described above. Research in this thesis confirms the neostriatum as a perfect candidate for an endophenotype in HD, as it sits central to the motor changes but also to other neurocognitive changes and is related to the known genetic changes in HD (Looi and Walterfang 2012). Knowledge of the anatomy of this circuitry, of its topographical nature, as well as the overall changes within the "hubs and spokes" of the brain in HD can help to guide potential treatments, whether these be targeting with surgery or novel molecular mechanisms.

7.3.3 Future directions

Studies in HD and in neuroscience more generally are moving towards pooling data with international collaborations, increasing power to find biomarkers, endophenotypes, and mechanisms of disease (Thompson, et al. 2020). This is particularly useful for rare diseases such as HD, which requires multicentre data even for Phase 1 trials (Wijeratne, et al. 2020). Amongst other benefits, larger data sets and international collaboration also facilitate the investigation of intriguing findings from smaller studies, such as the SSRI findings in this study.

Automated shape analysis is likely to take over from manual methods as automated methods improve, with longitudinal shape analysis also becoming increasingly available and detailed. The subcortical connectome should continue to be targeted by these methods as composite endpoints increase power further to investigate changes in HD (Wijeratne, et al. 2020), and morphological investigation of the subcortical connectome provides a clinically and practically useful intermediary step between mapping complicated large-scale networks and studying individual structures (Looi, et al. 2014b).

Given recent findings of early compensation by the cerebellum for abnormal striatal development (Tereshchenko, et al. 2020), the cerebellum should receive more research input, particularly from a morphological perspective due to the advantages of structural analysis discussed throughout this thesis. This could target the dentate gyrus in particular, as another hub in the connectome. As studies are looking towards younger cohorts, morphological analysis also has strong potential to provide a useful biomarker and endophenotype here, and has not yet been investigated in this group.

Psychiatric conditions in HD are increasingly receiving more research interest and recognition as an integral and disabling part of the condition (Goh, et al. 2018; Ho, et al. 2009; Sellers, et al. 2020). A recent study examined gene expression profiles from peripheral blood samples in pre-HD and symp-HD and found differential gene expression between depressed and non-depressed people with HD (Colpo, et al. 2020). While examining only a small number of people, as an exploratory study it reveals a number of interesting changes. 19 genes were differentially expressed between people with HD with and without depression, with 6 upregulated and 13 downregulated. Of note, several of the top differentially expressed genes were involved in nervous system development. Unfortunately however, there is no mention in this study of whether any of the participants were taking psychiatric or other medications. This has implications both from the findings in this thesis of altered hippocampal volumes with SSRIs, as well as the known epigenetic changes from a number of medications, including the mood stabiliser sodium valproate, which is sometimes used in HD (Bachoud-Levi, et al. 2019; de Campos Vidal and Mello 2020). Of great interest in this thesis is the never before noted association between SSRI use and decreased hippocampal volume in HD. Given the high proportion of people with HD with depression and on SSRIs, this warrants further investigation and may yield more information about abnormal molecular pathways and neurogenesis in HD.

7.4. Conclusion

This thesis demonstrates morphological change in several subcortical regions in pre-HD and symp-HD and correlates these with functional outcomes. It reveals neuronal degeneration in HD occurring largely in a pattern of spread from the neostriatum. Correlations between

striatal shape changes and functional outcomes occur in areas linked to subserving (frontostriatal) circuitry, adding to the growing weight of evidence pointing towards the neostriatum as an endophenotype of HD.

Spatiotemporal signatures developed from shape analysis of neuronal structures assist in understanding pathophysiology of disease, with the view to developing biomarkers for prognostication and analysis of potential disease-modifying treatments. This is the first time that such robust statistical analysis of longitudinal shape change in HD has been able to be performed and shows the neostriatum, particularly the putamen, as a potentially useful structural basis for the characterisation of an endophenotype of HD. This thesis provides a more comprehensive picture of neuroanatomical change in HD by using a "hubs and spokes" approach to analyse key areas, increasing knowledge about the pathogenesis of HD and network changes in neurodegenerative disease.

References

Adamson C, Beare R, Ball G, Walterfang M, Seal M. 2018. Callosal thickness profiles for prognosticating conversion from mild cognitive impairment to Alzheimer's disease: A classification approach. Brain Behav 8(12):e01142.

Adamson C, Beare R, Walterfang M, Seal M. 2014. Software pipeline for midsagittal corpus callosum thickness profile processing : automated segmentation, manual editor, thickness profile generator, group-wise statistical comparison and results display. Neuroinformatics 12(4):595-614.

Adamson CL, Wood AG, Chen J, Barton S, Reutens DC, Pantelis C, Velakoulis D, Walterfang M. 2011. Thickness profile generation for the corpus callosum using Laplace's equation. Human Brain Mapping 32:2131-40.

Ahveninen LM, Stout JC, Georgiou-Karistianis N, Lorenzetti V, Glikmann-Johnston Y. 2018. Reduced amygdala volumes are related to motor and cognitive signs in Huntington's disease: The IMAGE-HD study. Neuroimage Clin 18:881-887.

Alexander B, Georgiou-Karistianis N, Beare R, Ahveninen LM, Lorenzetti V, Stout JC, Glikmann-Johnston Y. 2020. Accuracy of automated amygdala MRI segmentation approaches in Huntington's disease in the IMAGE-HD cohort. Hum Brain Mapp 41(7):1875-1888.

Alexander GE, Delong MR, Strick PL. 1986. Parallel organization of functionally segregated circuits linking basal ganglia and cortex. Annual Review of Neuroscience 9:357-381.

Ament SA, Pearl JR, Cantle JP, Bragg RM, Skene PJ, Coffey SR, Bergey DE, Wheeler VC, MacDonald ME, Baliga NS and others. 2018. Transcriptional regulatory networks underlying gene expression changes in Huntington's disease. Mol Syst Biol 14(3):e7435.

Andre R, Carty L, Tabrizi SJ. 2016. Disruption of immune cell function by mutant huntingtin in Huntington's disease pathogenesis. Curr Opin Pharmacol 26:33-8.

Andrew SE, Goldberg YP, Kremer B, Telenius H, Theilmann J, Adam S, Starr E, Squitieri F, Lin B, Kalchman MA and others. 1993. The relationship between trinucleotide (CAG) repeat length and clinical features of Huntington's disease. Nat. Genet. 4(4):398-403.

Aylward E, Mills J, Liu D, Nopoulos P, Ross CA, Pierson R, Paulsen JS. 2011a. Association between Age and Striatal Volume Stratified by CAG Repeat Length in Prodromal Huntington Disease. PLoS Currents 3:RRN1235.

Aylward EH, Harrington DL, Mills JA, Nopoulos PC, Ross CA, Long JD, Liu D, Westervelt HK, Paulsen JS. 2013. Regional atrophy associated with cognitive and motor function in prodromal Huntington disease. J Huntingtons Dis 2(4):477-89.

Aylward EH, Liu DW, Nopoulos PC, Ross CA, Pierson RK, Mills JA, Long JD, Paulsen JS, Huntington Study Group. 2012. Striatal volume contributes to the prediction of onset of Huntington Disease in incident cases. Biol. Psychiatry 71(9):822-828.

Aylward EH, Nopoulos PC, Ross CA, Langbehn DR, Pierson RK, Mills JA, Johnson HJ, Magnotta VA, Juhl AR, Paulsen JS and others. 2011b. Longitudinal change in regional brain volumes in prodromal Huntington disease. Journal of Neurology Neurosurgery and Psychiatry 82(4):405-410.

Aylward EH, Rosenblatt A, Field K, Yallapragada V, Kieburtz K, McDermott M, Raymond LA, Almqvist EW, Hayden M, Ross CA. 2003. Caudate volume as an outcome measure in clinical trials for Huntington's disease: a pilot study. Brain Research Bulletin 62(2):137-141.

Aziz NA, van der Burg JMM, Tabrizi SJ, Landwehrmeyer GB. 2018. Overlap between age-at-onset and disease-progression determinants in Huntington disease. Neurol. 90(24):e2099-e2106.
Bachoud-Levi AC, Ferreira J, Massart R, Youssov K, Rosser A, Busse M, Craufurd D, Reilmann R, De Michele G, Rae D and others. 2019. International Guidelines for the Treatment of Huntington's Disease. Front Neurol 10:710.
Barani IJ, Benedict SH, Lin P-S. 2007. Neural stem cells: Implications for the conventional radiotherapy of central nervous system malignancies. International Journal of Radiation Oncology Biology Physics 68(2):324-333.
Bates G. 2003. Huntingtin aggregation and toxicity in Huntington's disease. Lancet 361(9369):1642-4.
Bechtel N, Scahill RI, Rosas HD, Acharya T, van den Bogaard SJA, Jauffret C, Say MJ, Sturrock A, Johnson H, Onorato CE and others. 2010. Tapping linked to function and structure in premanifest and symptomatic Huntington disease. Neurol. 75(24):2150-2160.
Beck AT, Steer, R.A., Brown, G. K. 1996. Manual for the Beck Depression Inventory - II. San Antonio: Psychol. Corp.
Begeti F, Schwab LC, Mason SL, Barker RA. 2016. Hippocampal dysfunction defines disease onset in Huntington's disease. J Neurol Neurosurg Psychiatry 87(9):975-81.
Berner LA, Wang Z, Stefan M, Lee S, Huo Z, Cyr M, Marsh R. 2019. Subcortical shape abnormalities in Bulimia Nervosa. Biol. Psychiatry Cogn. Neurosci. Neuroimaging.
Biglan KM, Ross CA, Langbehn DR, Aylward EH, Stout JC, Queller S, Carlozzi NE, Duff K, Beglinger LJ, Paulsen JS and others. 2009. Motor Abnormalities in Premanifest Persons with Huntington's Disease: The PREDICT-HD Study. Movement Disorders 24(12):1763-1772.
Blumenfeld H. 2010. Neuroanatomy Through Clinical Cases. Sunderland, Mass.: Sinauer Associates.
Bohanna I, Georgiou-Karistianis N, Egan GF. 2011a. Connectivity-based segmentation of the striatum in Huntington's disease: Vulnerability of motor pathways. Neurobiol. Dis. 42(3):475-481.
Bohanna I, Georgiou-Karistianis N, Hannan AJ, Egan GF. 2008. Magnetic resonance imaging as an approach towards identifying neuropathological biomarkers for Huntington's disease. Brain Research Reviews 58(1):209-225.
Bohanna I, Georgiou-Karistianis N, Sritharan A, Asadi H, Johnston L, Churchyard A, Egan G. 2011b. Diffusion Tensor Imaging in Huntington's disease reveals distinct patterns of white matter degeneration associated with motor and cognitive deficits. Brain Imaging and Behavior 5(3):171-180.
Boldrini M, Underwood MD, Hen R, Rosoklija GB, Dwork AJ, John Mann J, Arango V. 2009. Antidepressants increase neural progenitor cells in the human hippocampus. Neuropsychopharmacology 34(11):2376-89.
Burrus CJ, McKinstry SU, Kim N, Ozlu MI, Santoki AV, Fang FY, Ma A, Karadeniz YB, Worthington AK, Dragatsis I and others. 2020. Striatal Projection Neurons Require Huntingtin for Synaptic Connectivity and Survival. Cell Rep 30(3):642-657.e6.
Calabresi P, Centonze D, Pisani A, Bernardi G. 1999. Metabotropic glutamate receptors and cell-type-specific vulnerability in the striatum: implication for ischemia and Huntington's disease. Exp Neurol 158(1):97-108.
Calabresi P, Centonze D, Pisani A, Sancesario G, Gubellini P, Marfia GA, Bernardi G. 1998. Striatal spiny neurons and cholinergic interneurons express differential ionotropic glutamatergic responses and vulnerability: implications for ischemia and Huntington's disease. Ann Neurol 43(5):586-97.

Canals JM, Pineda JR, Torres-Peraza JF, Bosch M, Martin-Ibanez R, Munoz MT, Mengod G, Ernfors P, Alberch J. 2004. Brain-derived neurotrophic factor regulates the onset and severity of motor dysfunction associated with enkephalinergic neuronal degeneration in Huntington's disease. Journal of Neuroscience 24(35):7727-7739.
Chaganti SS, McCusker EA, Loy CT. 2017. What do we know about Late Onset Huntington's Disease? J Huntingtons Dis 6(2):95-103.
Chao YP, Cho KH, Yeh CH, Chou KH, Chen JH, Lin CP. 2009. Probabilistic topography of human corpus callosum using cytoarchitectural parcellation and high angular resolution diffusion imaging tractography. Hum Brain Mapp 30(10):3172-87.
Choi JS, Kim SH, Yoo SY, Kang DH, Kim CW, Lee JM, Kim IY, Kim SI, Kim YY, Kwon JS. 2007. Shape deformity of the corpus striatum in obsessive-compulsive disorder. Psychiatry Res 155(3):257-64.
Chung MK, Dalton KM, Davidson RJ. 2008. Tensor-based cortical surface morphometry via weighted spherical harmonic representation. IEEE Trans Med Imaging 27(8):1143-51.
Ciarochi JA, Calhoun VD, Lourens S, Long JD, Johnson HJ, Bockholt HJ, Liu J, Plis SM, Paulsen JS, Turner JA. 2016. Patterns of Co-Occurring Gray Matter Concentration Loss across the Huntington Disease Prodrome. Front Neurol 7:147.
Colpo GD, Rocha NP, Furr Stimming E, Teixeira AL. 2020. Gene Expression Profiling in Huntington's Disease: Does Comorbidity with Depressive Symptoms Matter? Int J Mol Sci 21(22).
Coppen EM, Jacobs M, van den Berg-Huysmans AA, van der Grond J, Roos RAC. 2018. Grey matter volume loss is associated with specific clinical motor signs in Huntington's disease. Parkinsonism Relat Disord 46:56-61.
Crawford HE, Hobbs NZ, Keogh R, Langbehn DR, Frost C, Johnson H, Landwehrmeyer B, Reilmann R, Craufurd D, Stout JC and others. 2013. Corpus callosal atrophy in premanifest and early Huntington's disease. J Huntingtons Dis 2(4):517-26.
Cummings JL. 1993. Frontal-subcortical circuits and human-behavior. Archives of Neurology 50(8):873-880.
Curtis MA, Low VF, Faull RLM. 2012. Neurogenesis and progenitor cells in the adult human brain: A comparison between hippocampal and subventricular progenitor proliferation. Developmental Neurobiology 72(7):990-1005.
Curtis MA, Penney EB, Pearson AG, van Roon-Mom WMC, Butterworth NJ, Dragunow M, Connor B, Faull RLM. 2003. Increased cell proliferation and neurogenesis in the adult human Huntington's disease brain. Proceedings of the National Academy of Sciences of the United States of America 100(15):9023-9027.
de Campos Vidal B, Mello MLS. 2020. Sodium valproate (VPA) interactions with DNA and histones. Int J Biol Macromol 163:219-231.
Della Nave R, Ginestroni A, Tessa C, Giannelli M, Piacentini S, Filippi M, Mascalchi M. 2010. Regional distribution and clinical correlates of white matter structural damage in Huntington Disease: A tract-based spatial statistics study. American Journal of Neuroradiology 31:1675-81.
Delmaire C, Dumas E, Sharman M, van den Bogaard S, Valabregue R, Jauffret C, Justo D, Reilmann R, Stout J, Craufurd D and others. 2012. The structural correlates of functional deficits in early Huntington's disease. Hum. Brain Mapp. 34(9):2141-2153.
Di Paola M, Luders E, Cherubini A, Sanchez-Castaneda C, Thompson PM, Toga AW, Caltagirone C, Orobello S, Elifani F, Squitieri F and others. 2012. Multimodal MRI analysis of the corpus callosum reveals white matter differences in presymptomatic and early Huntington's disease. Cereb Cortex 22(12):2858-66.

DiFiglia M, Sapp E, Chase KO, Davies SW, Bates GP, Vonsattel JP, Aronin N. 1997. Aggregation of huntingtin in neuronal intranuclear inclusions and dystrophic neurites in brain. Science 277(5334):1990-3.
Dominguez DJ, Egan GF, Gray MA, Poudel GR, Churchyard A, Chua P, Stout JC, Georgiou-Karistianis N. 2013. Multi-modal neuroimaging in premanifest and early Huntington's disease: 18 month longitudinal data from the IMAGE-HD study. PLOS ONE 8(9).
Domínguez DJ, Poudel G, Stout JC, Gray M, Chua P, Borowsky B, Egan GF, Georgiou-Karistianis N. 2017. Longitudinal changes in the fronto-striatal network are associated with executive dysfunction and behavioral dysregulation in Huntington's disease: 30 months IMAGE-HD data. Cortex 92:139-149.
Domínguez JF, Ng AC, Poudel G, Stout JC, Churchyard A, Chua P, Egan GF, Georgiou-Karistianis N. 2016. Iron accumulation in the basal ganglia in Huntington's disease: cross-sectional data from the IMAGE-HD study. J Neurol Neurosurg Psychiatry 87(5):545-9.
Dominguez JF, Stout JC, Poudel G, Churchyard A, Chua P, Egan GF, Georgiou-Karistianis N. 2016. Multimodal imaging biomarkers in premanifest and early Huntington's disease: 30-month IMAGE-HD data. Br. J. Psychiatry 208(6):571-8.
Doty RL, Shaman P, Kimmelman CP, Dann MS. 1984. University of Pennsylvania Smell Identification Test: a rapid quantitative olfactory function test for the clinic. Laryngoscope 94(2 Pt 1):176-8.
Douaud G, Gaura V, Ribeiro MJ, Lethimonnier F, Maroy R, Verny C, Krystkowiak P, Damier P, Bachoud-Levi AC, Hantraye P and others. 2006. Distribution of grey matter atrophy in Huntington's disease patients: A combined ROI-based and voxel-based morphometric study. Neuroimage 32(4):1562-1575.
Draganski B, Kherif F, Kloeppel S, Cook PA, Alexander DC, Parker GJM, Deichmann R, Ashburner J, Frackowiak RSJ. 2008. Evidence for segregated and integrative connectivity patterns in the human basal ganglia. J. Neurosci. 28(28):7143-7152.
Duan WZ, Peng Q, Masuda N, Ford E, Tryggestad E, Ladenheim B, Zhao M, Cadet JL, Wong J, Ross CA. 2008. Sertraline slows disease progression and increases neurogenesis in N171-82Q mouse model of Huntington's disease. Neurobiology of Disease 30(3):312-322.
Dumas EM, van den Bogaard SJA, Ruber ME, Reilman RR, Stout JC, Craufurd D, Hicks SL, Kennard C, Tabrizi SJ, van Buchem MA and others. 2012. Early changes in white matter pathways of the sensorimotor cortex in premanifest Huntington's disease. Human Brain Mapping 33(1):203-212.
Erickson KI, Voss MW, Prakash RS, Basak C, Szabo A, Chaddock L, Kim JS, Heo S, Alves H, White SM and others. 2011. Exercise training increases size of hippocampus and improves memory. Proceedings of the National Academy of Sciences of the United States of America 108(7):3017-3022.
Ernst A, Alkass K, Bernard S, Salehpour M, Perl S, Tisdale J, Possnert G, Druid H, Frisén J. 2014. Neurogenesis in the striatum of the adult human brain. Cell 156(5):1072-83.
Fanselow MS, Dong HW. 2010. Are the dorsal and ventral hippocampus functionally distinct structures? Neuron 65(1):7-19.
Faria AV, Ratnanather JT, Tward DJ, Lee DS, van den Noort F, Wu D, Brown T, Johnson H, Paulsen JS, Ross CA and others. 2016. Linking white matter and deep gray matter alterations in premanifest Huntington disease. Neuroimage Clin. 11:450-460.
Ferrante RJ, Beal MF, Kowall NW, Richardson EP, Jr., Martin JB. 1987a. Sparing of acetylcholinesterase-containing striatal neurons in Huntington's disease. Brain Res 411(1):162-6.

Ferrante RJ, Kowall NW, Beal MF, Martin JB, Bird ED, Richardson EP, Jr. 1987b. Morphologic and histochemical characteristics of a spared subset of striatal neurons in Huntington's disease. J Neuropathol Exp Neurol 46(1):12-27.
Fouquet C, Babayan BM, Watilliaux A, Bontempi B, Tobin C, Rondi-Reig L. 2013. Complementary Roles of the Hippocampus and the Dorsomedial Striatum during Spatial and Sequence-Based Navigation Behavior. Plos One 8(6).
Franklin GL, Camargo CHF, Meira AT, Lima NSC, Teive HAG. 2020. The Role of the Cerebellum in Huntington's Disease: a Systematic Review. Cerebellum.
Fung YL, Ng KET, Vogrin SJ, Meade C, Ngo M, Collins SJ, Bowden SC. 2019. Comparative Utility of Manual versus Automated Segmentation of Hippocampus and Entorhinal Cortex Volumes in a Memory Clinic Sample. J Alzheimers Dis 68(1):159-171.
Furlong LS, Jakabek D, Power BD, Owens-Walton C, Wilkes FA, Walterfang M, Velakoulis D, Egan G, Looi JC, Georgiou-Karistianis N. 2020. Morphometric in vivo evidence of thalamic atrophy correlated with cognitive and motor dysfunction in Huntington's disease: The IMAGE-HD study. Psychiatry Res Neuroimaging 298:111048.
Gabery S, Georgiou-Karistianis N, Lundh SH, Cheong RY, Churchyard A, Chua P, Stout JC, Egan GF, Kirik D, Petersén Å. 2015. Volumetric analysis of the hypothalamus in Huntington Disease using 3T MRI: the IMAGE-HD Study. PLoS One 10(2):e0117593.
Gaura V, Lavisse S, Payoux P, Goldman S, Verny C, Krystkowiak P, Damier P, Supiot F, Bachoud-Levi AC, Remy P. 2017. Association Between Motor Symptoms and Brain Metabolism in Early Huntington Disease. JAMA Neurol 74(9):1088-1096.
Gauthier LR, Charrin BC, Borrell-Pages M, Dompierre JP, Rangone H, Cordelieres FP, De Mey J, MacDonald ME, Lessmann V, Humbert S and others. 2004. Huntingtin controls neurotrophic support and survival of neurons by enhancing BDNF vesicular transport along microtubules. Cell 118(1):127-138.
Georgiou-Karistianis N, Gray MA, Dominguez JF, Dymowski AR, Bohanna I, Johnston LA, Churchyard A, Chua P, Stout JC, Egan GF. 2013a. Automated differentiation of pre-diagnosis Huntington's disease from healthy control individuals based on quadratic discriminant analysis of the basal ganglia: The IMAGE-HD study. Neurobiol. Dis. 51:82-92.
Georgiou-Karistianis N, Poudel GR, Domínguez DJ, Langmaid R, Gray MA, Churchyard A, Chua P, Borowsky B, Egan GF, Stout JC. 2013b. Functional and connectivity changes during working memory in Huntington's disease: 18 month longitudinal data from the IMAGE-HD study. Brain Cogn 83(1):80-91.
Georgiou-Karistianis N, Scahill R, Tabrizi SJ, Squitieri F, Aylward E. 2013c. Structural MRI in Huntington's disease and recommendations for its potential use in clinical trials. Neurosci. and Biobehav. Rev. 37(3):480-490.
Georgiou-Karistianis N, Stout JC, Domínguez DJ, Carron SP, Ando A, Churchyard A, Chua P, Bohanna I, Dymowski AR, Poudel G and others. 2014. Functional magnetic resonance imaging of working memory in Huntington's disease: cross-sectional data from the IMAGE-HD study. Hum Brain Mapp 35(5):1847-64.
Gerig G, Fishbaugh J, Sadeghi N. 2016. Longitudinal modeling of appearance and shape and its potential for clinical use. Medical Image Analysis 33:114-121.
Germeyan SC, Kalikhman D, Jones L, Theodore WH. 2014. Automated versus manual hippocampal segmentation in preoperative and postoperative patients with epilepsy. Epilepsia 55(9):1374-9.
Gil-Mohapel J, Simpson JM, Ghilan M, Christie BR. 2011. Neurogenesis in Huntington's disease: Can studying adult neurogenesis lead to the development of new therapeutic strategies? Brain Research 1406:84-105.

Goh AM, Wibawa P, Loi SM, Walterfang M, Velakoulis D, Looi JC. 2018. Huntington's disease: Neuropsychiatric manifestations of Huntington's disease. Australas Psychiatry 26(4):366-375.
Gonzalez V, Cif L, Biolsi B, Garcia-Ptacek S, Seychelles A, Sanrey E, Descours I, Coubes C, de Moura AM, Corlobe A and others. 2014. Deep brain stimulation for Huntington's disease: long-term results of a prospective open-label study. J Neurosurg 121(1):114-22.
Gottesman II, Gould TD. 2003. The endophenotype concept in psychiatry: etymology and strategic intentions. Am. J. Psychiatry 160(4):636-45.
Granberg T, Bergendal G, Shams S, Aspelin P, Kristoffersen-Wiberg M, Fredrikson S, Martola J. 2015. MRI-Defined Corpus Callosal Atrophy in Multiple Sclerosis: A Comparison of Volumetric Measurements, Corpus Callosum Area and Index. J Neuroimaging 25(6):996-1001.
Gray MA, Egan GF, Ando A, Churchyard A, Chua P, Stout JC, Georgiou-Karistianis N. 2013. Prefrontal activity in Huntington's disease reflects cognitive and neuropsychiatric disturbances: the IMAGE-HD study. Exp Neurol 239:218-28.
Gregory S, Long JD, Klöppel S, Razi A, Scheller E, Minkova L, Johnson EB, Durr A, Roos RAC, Leavitt BR and others. 2018. Testing a longitudinal compensation model in premanifest Huntington's disease. Brain 141(7):2156-2166.
Gregory S, Scahill RI, Seunarine KK, Stopford C, Zhang H, Zhang J, Orth M, Durr A, Roos RA, Langbehn DR and others. 2015. Neuropsychiatry and White Matter Microstructure in Huntington's Disease. J Huntingtons Dis 4(3):239-49.
Grote HE, Bull ND, Howard ML, van Dellen A, Blakemore C, Bartlett PF, Hannan AJ. 2005. Cognitive disorders and neurogenesis deficits in Huntington's disease mice are rescued by fluoxetine. European Journal of Neuroscience 22(8):2081-2088.
Gusella JF, MacDonald ME, Lee JM. 2014. Genetic modifiers of Huntington's disease. Mov Disord 29(11):1359-65.
Gutman BA, Jahanshad N, Ching CR, Wang Y, Kochunov PV, Nichols TE, Thompson PM. 2015. Medial Demons Registration localizes the degree of genetic influence over subcortical shape variability: An N= 1480 Meta-Analysis. Proc. I.E.E.E. Int. Symp. Biomed. Imaging 2015:1402-1406.
Gutman BA, Wang Y, Rajagopalan P, Toga AW, Thompson PM. Shape matching with medial curves and 1-D group-wise registration; 2012 2-5 May 2012. p 716-719.
Haber SN. 2003. The primate basal ganglia: parallel and integrative networks. J Chem. Neuroanat. 26(4):317-30.
Haber SN, Fudge JL, McFarland NR. 2000. Striatonigrostriatal pathways in primates form an ascending spiral from the shell to the dorsolateral striatum. J Neurosci 20(6):2369-82.
Hampel H, Teipel SJ, Alexander GE, Horwitz B, Teichberg D, Schapiro MB, Rapoport SI. 1998. Corpus callosum atrophy is a possible indicator of region- and cell type-specific neuronal degeneration in Alzheimer disease: a magnetic resonance imaging analysis. Arch Neurol 55(2):193-8.
Heemskerk A, Roos R. 2012. Aspiration pneumonia and death in Huntington's disease. PLOS Currents Huntington Disease.
Herting MM, Johnson C, Mills KL, Vijayakumar N, Dennison M, Liu C, Goddings AL, Dahl RE, Sowell ER, Whittle S and others. 2018. Development of subcortical volumes across adolescence in males and females: A multisample study of longitudinal changes. Neuroimage 172:194-205.
Hervas-Corpion I, Guiretti D, Alcaraz-Iborra M, Olivares R, Campos-Caro A, Barco A, Valor LM. 2018. Early alteration of epigenetic-related transcription in Huntington's disease mouse models. Sci Rep 8(1):9925.

Ho AK, Gilbert AS, Mason SL, Goodman AO, Barker RA. 2009. Health-related quality of life in Huntington's disease: Which factors matter most? Mov Disord 24(4):574-8.
Hobbs NZ, Barnes J, Frost C, Henley SM, Wild EJ, Macdonald K, Barker RA, Scahill RI, Fox NC, Tabrizi SJ. 2010. Onset and progression of pathologic atrophy in Huntington disease: a longitudinal MR imaging study. AJNR Am J Neuroradiol 31(6):1036-41.
Hobbs NZ, Cole JH, Farmer RE, Rees EM, Crawford HE, Malone IB, Roos RA, Sprengelmeyer R, Durr A, Landwehrmeyer B and others. 2012. Evaluation of multi-modal, multi-site neuroimaging measures in Huntington's disease: Baseline results from the PADDINGTON study. Neuroimage Clin 2:204-11.
Hobbs NZ, Henley SMD, Wild EJ, Leung KK, Frost C, Barker RA, Scahill RI, Barnes J, Tabrizi SJ, Fox NC. 2009. Automated quantification of caudate atrophy by local registration of serial MRI: Evaluation and application in Huntington's disease. Neuroimage 47(4):1659-1665.
Hofer S, Frahm J. 2006. Topography of the human corpus callosum revisited--comprehensive fiber tractography using diffusion tensor magnetic resonance imaging. Neuroimage 32(3):989-94.
Hong S, Fishbaugh J, Rezanejad M, Siddiqi K, Johnson H, Paulsen J, Kim EY, Gerig G. 2017. Subject-Specific Longitudinal Shape Analysis by Coupling Spatiotemporal Shape Modeling with Medial Analysis. Proc SPIE Int Soc Opt Eng 10133.
Hong Y, O'Donnell LJ, Savadjiev P, Zhang F, Wassermann D, Pasternak O, Johnson H, Paulsen J, Vonsattel JP, Makris N and others. 2018. Genetic load determines atrophy in hand cortico-striatal pathways in presymptomatic Huntington's disease. Hum Brain Mapp 39(10):3871-3883.
Horn A, Fox MD. 2020. Opportunities of connectomic neuromodulation. Neuroimage 221:117180.
Huntington Study Group. 1996. Unified Huntington's Disease Rating Scale: reliability and consistency. Mov. Disord. 11(2):136-42.
Jin KL, LaFevre-Bernt M, Sun YJ, Chen S, Gafni J, Crippen D, Logvinova A, Ross CA, Greenberg DA, Ellerby LM. 2005. FGF-2 promotes neurogenesis and neuroprotection and prolongs survival in a transgenic mouse model of Huntington's disease. Proceedings of the National Academy of Sciences of the United States of America 102(50):18189-18194.
Julien CL, Thompson JC, Wild S, Yardumian P, Snowden JS, Turner G, Craufurd D. 2007. Psychiatric disorders in preclinical Huntington's disease. J Neurol Neurosurg Psychiatry 78(9):939-43.
Kachian ZR, Cohen-Zimerman S, Bega D, Gordon B, Grafman J. 2019. Suicidal ideation and behavior in Huntington's disease: Systematic review and recommendations. J Affect Disord 250:319-329.
Kassubek J, Juengling FD, Kioschies T, Henkel K, Karitzky J, Kramer B, Ecker D, Andrich J, Saft C, Kraus P and others. 2004. Topography of cerebral atrophy in early Huntington's disease: a voxel based morphometric MRI study. Journal of Neurology Neurosurgery and Psychiatry 75(2):213-220.
Kieburtz K, Penney JB, Como P, Ranen N, Shoulson I, Feigin A, Abwender D, Greenamyre JT, Higgins D, Marshall FJ and others. 1996. Unified Huntington's disease rating scale: Reliability and consistency. Movement Disorders 11(2):136-142.
Kiernan JA. 2005. Barr's The human nervous system: an anatomical viewpoint: Lippincott Williams and Wilkins.
Kiernan JA. 2012. Anatomy of the temporal lobe. Epilepsy Res Treat 2012:176157.

Kim H, Kim JH, Possin KL, Winer J, Geschwind MD, Xu D, Hess CP. 2017. Surface-based morphometry reveals caudate subnuclear structural damage in patients with premotor Huntington disease. Brain Imaging Behav. 11(5):1365-1372.
Kim S, Kim KT. 2014. Therapeutic Approaches for Inhibition of Protein Aggregation in Huntington's Disease. Exp Neurobiol 23(1):36-44.
Kipps CM, Duggins AJ, Mahant N, Gomes L, Ashburner J, McCusker EA. 2005. Progression of structural neuropathology in preclinical Huntington's disease: a tensor based morphometry study. Journal of Neurology Neurosurgery and Psychiatry 76(5):650-655.
Kirkwood S, Su J, Conneally P, Foroud T. 2001. Progression of symptoms in the early and middle stages of Huntington Disease. Archives of Neurology 58:273-278.
Kloppel S, Draganski B, Golding CV, Chu C, Nagy Z, Cook PA, Hicks SL, Kennard C, Alexander DC, Parker GJ and others. 2008. White matter connections reflect changes in voluntary-guided saccades in pre-symptomatic Huntington's disease. Brain 131(Pt 1):196-204.
Kloppel S, Draganski B, Siebner HR, Tabrizi SJ, Weiller C, Frackowiak RS. 2009. Functional compensation of motor function in pre-symptomatic Huntington's disease. Brain 132(Pt 6):1624-32.
Klöppel S, Gregory S, Scheller E, Minkova L, Razi A, Durr A, Roos RA, Leavitt BR, Papoutsi M, Landwehrmeyer GB and others. 2015. Compensation in Preclinical Huntington's Disease: Evidence From the Track-On HD Study. EBioMedicine 2(10):1420-9.
Knierim JJ, Neunuebel JP, Deshmukh SS. 2014. Functional correlates of the lateral and medial entorhinal cortex: objects, path integration and local-global reference frames. Philos Trans R Soc Lond B Biol Sci 369(1635):20130369.
Koutsis G, Karadima G, Kladi A, Panas M. 2013. The challenge of juvenile Huntington disease: to test or not to test. Neurology 80(11):990-6.
Langbehn DR, Brinkman RR, Falush D, Paulsen JS, Hayden MR, International Huntingtons Disease Collaborative Group. 2004. A new model for prediction of the age of onset and penetrance for Huntington's disease based on CAG length. Clin. Gen. 65(4):267-277.
Langbehn DR, Stout JC, Gregory S, Mills JA, Durr A, Leavitt BR, Roos RAC, Long JD, Owen G, Johnson HJ and others. 2019. Association of CAG Repeats With Long-term Progression in Huntington Disease. JAMA Neurol.
Lee JK, Mathews K, Schlaggar B, Perlmutter J, Paulsen JS, Epping E, Burmeister L, Nopoulos P. 2012. Measures of growth in children at risk for Huntington disease. Neurology 79(7):668-674.
Lee JM, Ivanova EV, Seong IS, Cashorali T, Kohane I, Gusella JF, MacDonald ME. 2007. Unbiased gene expression analysis implicates the huntingtin polyglutamine tract in extra-mitochondrial energy metabolism. PLoS Genet 3(8):e135.
Levitt JJ, Styner M, Niethammer M, Bouix S, Koo MS, Voglmaier MM, Dickey CC, Niznikiewicz MA, Kikinis R, McCarley RW and others. 2009. Shape abnormalities of caudate nucleus in schizotypal personality disorder. Schizophrenia Research 110(1-3):127-139.
Li XJ, Li S. 2011. Proteasomal dysfunction in aging and Huntington disease. Neurobiol Dis 43(1):4-8.
Li Y, Yui DS, Luikart BW, McKay RM, Li YJ, Rubenstein JL, Parada LF. 2012. Conditional ablation of brain-derived neurotrophic factor-TrkB signaling impairs striatal neuron development. Proceedings of the National Academy of Sciences of the United States of America 109(38):15491-15496.

Lindberg O, Walterfang M, Looi JCL, Malykhin N, Ostberg P, Zandbelt B, Styner M, Paniagua B, Velakoulis D, Orndahl E and others. 2012. Hippocampal Shape Analysis in Alzheimer's Disease and Frontotemporal Lobar Degeneration Subtypes. Journal of Alzheimers Disease 30(2):355-365.

Liston C, Watts R, Tottenham N, Davidson MC, Niogi S, Ulug AM, Casey BJ. 2006. Frontostriatal microstructure modulates efficient recruitment of cognitive control. Cereb. Cortex 16(4):553-60.

Loi SM, Walterfang M, Velakoulis D, Looi JC. 2018. Huntington's disease: Managing neuropsychiatric symptoms in Huntington's disease. Australas Psychiatry 26(4):376-380.

Looi JC, Velakoulis D, Walterfang M, Georgiou-Karistianis N, Macfarlane MD, Power BD, Nilsson C, Styner M, Thompson PM, Van Westen D and others. 2014a. The Australian, US, Scandinavian Imaging Exchange (AUSSIE): an innovative, virtually-integrated health research network embedded in health care. Australas Psychiatry 22(3):260-265.

Looi JC, Walterfang M, Styner M, Niethammer M, Svensson LA, Lindberg O, Ostberg P, Botes L, Orndahl E, Chua P and others. 2011. Shape analysis of the neostriatum in subtypes of frontotemporal lobar degeneration: neuroanatomically significant regional morphologic change. Psychiatry Res 191(2):98-111.

Looi JCL, Lindberg O, Liberg B, Tatham V, Kumar R, Maller J, Millard E, Sachdev P, Hogberg G, Pagani M and others. 2008. Volumetrics of the caudate nucleus: Reliability and validity of a new manual tracing protocol. Psychiatry Res.: Neuroimaging 163(3):279-288.

Looi JCL, Rajagopalan P, Walterfang M, Madsen SK, Thompson PM, Macfarlane MD, Ching C, Chua P, Velakoulis D. 2012. Differential putaminal morphology in Huntington's disease, frontotemporal dementia and Alzheimer's disease. Aust. N.Z. J. Psychiatry.

Looi JCL, Santillo AF. 2017. Time and relative dimensions in syndromology: Towards endophenotypes in neurology, psychiatry and in-between. Aust. N. Z. J. Psychiatry 51(11):1079-1081.

Looi JCL, Svensson L, Lindberg O, Zandbelt BB, Ostberg P, Orndahl E, Wahlund LO. 2009. Putaminal volume in frontotemporal lobar degeneration and Alzheimer disease: differential volumes in dementia subtypes and controls. Am. J. Neuroradiology 30(8):1552-1560.

Looi JCL, Walterfang M. 2012. Striatal morphology as a biomarker in neurodegenerative disease. Mol. Psychiatry 18(4):417-424.

Looi JCL, Walterfang M, Nilsson C, Power BD, van Westen D, Velakoulis D, Wahlund LO, Thompson PM. 2014b. The subcortical connectome: hubs, spokes and the space between - a vision for further research in neurodegenerative disease. Aust. N. Z. J. Psychiatry 48(4):306-9.

Low VF, Dragunow M, Tippett LJ, Faull RL, Curtis MA. 2011. No change in progenitor cell proliferation in the hippocampus in Huntington's disease. Neuroscience 199:577-88.

Luders E, Toga AW, Thompson PM. 2014. Why size matters: differences in brain volume account for apparent sex differences in callosal anatomy: the sexual dimorphism of the corpus callosum. Neuroimage 84:820-4.

Mackay-Sim A, Doty, R.L. 2001. The University of Pennsylvania Smell Identification Test: Normative adjustment for Australian subjects. Australian Journal of Oto-Laryngology 4:174-177.

MacLeod CM, MacDonald PA. 2000. Interdimensional interference in the Stroop effect: uncovering the cognitive and neural anatomy of attention. Trends Cogn. Sci. 4(10):383-391.
Maguire EA, Gadian DG, Johnsrude IS, Good CD, Ashburner J, Frackowiak RS, Frith CD. 2000. Navigation-related structural change in the hippocampi of taxi drivers. Proc Natl Acad Sci U S A 97(8):4398-403.
Majid DSA, Aron AR, Thompson W, Sheldon S, Hamza S, Stoffers D, Holland D, Goldstein J, Corey-Bloom J, Dale AM. 2011. Basal ganglia atrophy in prodromal Huntington's disease is detectable over one year using automated segmentation. Movement Disorders 26(14):2544-2551.
Mangalore S, Mukku SSR, Vankayalapati S, Sivakumar PT, Varghese M. 2021. Shape Profile of Corpus Callosum As a Signature to Phenotype Different Dementia. J Neurosci Rural Pract 12(1):185-192.
Mangin JF, Rivière D, Duchesnay E, Cointepas Y, Gaura V, Verny C, Damier P, Krystkowiak P, Bachoud-Lévi AC, Hantraye P and others. 2020. Neocortical morphometry in Huntington's disease: Indication of the coexistence of abnormal neurodevelopmental and neurodegenerative processes. Neuroimage Clin 26:102211.
Marrakchi-Kacem L, Delmaire C, Guevara P, Poupon F, Lecomte S, Tucholka A, Roca P, Yelnik J, Durr A, Mangin JF and others. 2013. Mapping cortico-striatal connectivity onto the cortical surface: a new tractography-based approach to study Huntington disease. PLoS One 8(2):e53135.
McColgan P, Gregory S, Seunarine KK, Razi A, Papoutsi M, Johnson E, Durr A, Roos RAC, Leavitt BR, Holmans P and others. 2018. Brain Regions Showing White Matter Loss in Huntington's Disease Are Enriched for Synaptic and Metabolic Genes. Biol Psychiatry 83(5):456-465.
McColgan P, Tabrizi SJ. 2018. Huntington's disease: a clinical review. Eur J Neurol 25(1):24-34.
McDonald RJ, White NM. 1994. Parallel information processing in the water maze: evidence for independent memory systems involving dorsal striatum and hippocampus. Behav Neural Biol 61(3):260-70.
McKinnon MC, Yucel K, Nazarov A, MacQueen GM. 2009. A meta-analysis examining clinical predictors of hippocampal volume in patients with major depressive disorder. J Psychiatry Neurosci 34(1):41-54.
Medina L, Figueredo-Cardenas G, Reiner A. 1996. Differential abundance of superoxide dismutase in interneurons versus projection neurons and in matrix versus striosome neurons in monkey striatum. Brain Res 708(1-2):59-70.
Milardi D, Arrigo A, Anastasi G, Cacciola A, Marino S, Mormina E, Calamuneri A, Bruschetta D, Cutroneo G, Trimarchi F and others. 2016. Extensive Direct Subcortical Cerebellum-Basal Ganglia Connections in Human Brain as Revealed by Constrained Spherical Deconvolution Tractography. Front Neuroanat 10:29.
Misiura MB, Lourens S, Calhoun VD, Long J, Bockholt J, Johnson H, Zhang Y, Paulsen JS, Turner JA, Liu J and others. 2017. Cognitive control, learning, and clinical motor ratings are most highly associated with basal ganglia brain volumes in the premanifest Huntington's Disease phenotype. J. Int. Neuropsychol. Soc. 23(2):159-170.
Molina-Ruiz RM, Looi JCL, Walterfang M, García-Saiz T, Wilkes FA, Liu LL, Velakoulis D, Perera JLC, Diaz-Marsa M. 2020. Striatal volumes as potential biomarkers in Eating Disorders: A pilot study. Rev Psiquiatr Salud Ment.
Morey RA, Petty CM, Xu Y, Hayes JP, Wagner HR, 2nd, Lewis DV, LaBar KS, Styner M, McCarthy G. 2009. A comparison of automated segmentation and manual tracing for quantifying hippocampal and amygdala volumes. Neuroimage 45(3):855-66.

Morigaki R, Goto S. 2017. Striatal Vulnerability in Huntington's Disease: Neuroprotection Versus Neurotoxicity. Brain Sci 7(6).
Moser MB, Moser EI. 1998. Functional differentiation in the hippocampus. Hippocampus 8(6):608-19.
Muirhead N, Benjamin E, Saleh H. 2013. Is the University of Pennsylvania Smell Identification Test (UPSIT) valid for the UK population? The Otorhinolaryngologist 6(2):99-103.
Muralidharan P, Fishbaugh J, Johnson HJ, Durrleman S, Paulsen JS, Gerig G, Fletcher PT. 2014. Diffeomorphic shape trajectories for improved longitudinal segmentation and statistics. Med Image Comput Comput Assist Interv 17(Pt 3):49-56.
Muralidharan P, Fishbaugh J, Kim EY, Johnson HJ, Paulsen JS, Gerig G, Fletcher PT. 2016. Bayesian Covariate Selection in Mixed-Effects Models For Longitudinal Shape Analysis. Proc IEEE Int Symp Biomed Imaging 2016:656-659.
Nasir J, Floresco SB, O'Kusky JR, Diewert VM, Richman JM, Zeisler J, Borowski A, Marth JD, Phillips AG, Hayden MR. 1995. Targeted disruption of the Huntington's disease gene results in embryonic lethality and behavioral and morphological changes in heterozygotes. Cell 81(5):811-23.
Nelson HE, Willison J. 1991. National adult reading test, 2nd Edition. Windsor: NFER-Nelson.
Nogovitsyn N, Muller M, Souza R, Hassel S, Arnott SR, Davis AD, Hall GB, Harris JK, Zamyadi M, Metzak PD and others. 2020. Hippocampal tail volume as a predictive biomarker of antidepressant treatment outcomes in patients with major depressive disorder: a CAN-BIND report. Neuropsychopharmacology 45(2):283-291.
Nolan M, Roman E, Nasa A, Levins KJ, O'Hanlon E, O'Keane V, Willian Roddy D. 2020. Hippocampal and Amygdalar Volume Changes in Major Depressive Disorder: A Targeted Review and Focus on Stress. Chronic Stress (Thousand Oaks) 4:2470547020944553.
Nopoulos PC, Aylward EH, Ross CA, Johnson HJ, Magnotta VA, Juhl AR, Pierson RK, Mills J, Langbehn DR, Paulsen JS and others. 2010. Cerebral cortex structure in prodromal Huntington disease. Neurobiology of Disease 40(3):544-554.
Nopoulos PC, Aylward EH, Ross CA, Mills JA, Langbehn DR, Johnson HJ, Magnotta VA, Pierson RK, Beglinger LJ, Nance MA and others. 2011. Smaller intracranial volume in prodromal Huntington's disease: evidence for abnormal neurodevelopment. Brain 134:137-142.
Ong D, Walterfang M, Malhi GS, Styner M, Velakoulis D, Pantelis C. 2012. Size and shape of the caudate nucleus in individuals with bipolar affective disorder. Aust N Z J Psychiatry 46(4):340-51.
Paulsen JS, Langbehn DR, Stout JC, Aylward E, Ross CA, Nance M, Guttman M, Johnson S, MacDonald M, Beglinger LJ and others. 2008. Detection of Huntington's disease decades before diagnosis: the Predict-HD study. J. Neurol. Neurosurg. Psychiatry 79(8):874-880.
Paulsen JS, Miller AC, Hayes T, Shaw E. 2017. Cognitive and behavioral changes in Huntington disease before diagnosis. Handb Clin Neurol 144:69-91.
Paulsen JS, Ready RE, Hamilton JM, Mega MS, Cummings JL. 2001. Neuropsychiatric aspects of Huntington's disease. J Neurol Neurosurg Psychiatry 71(3):310-4.
Peltsch A, Hoffman A, Armstrong I, Pari G, Munoz DP. 2008. Saccadic impairments in Huntington's disease. Exp Brain Res 186(3):457-69.
Peng Q, Masuda N, Jiang M, Li Q, Zhao M, Ross CA, Duan W. 2008. The antidepressant sertraline improves the phenotype, promotes neurogenesis and increases BDNF levels

in the R6/2 Huntington's disease mouse model. Experimental Neurology 210(1):154-163.
Phillips JL, Batten LA, Tremblay P, Aldosary F, Blier P. 2015. A Prospective, Longitudinal Study of the Effect of Remission on Cortical Thickness and Hippocampal Volume in Patients with Treatment-Resistant Depression. Int J Neuropsychopharmacol 18(8).
Phillips O, Sanchez-Castaneda C, Elifani F, Maglione V, Di Pardo A, Caltagirone C, Squitieri F, Sabatini U, Di Paola M. 2013. Tractography of the corpus callosum in Huntington's disease. Plos One 8(9).
Possin KL, Kim H, Geschwind MD, Moskowitz T, Johnson ET, Sha SJ, Apple A, Xu D, Miller BL, Finkbeiner S and others. 2017. Egocentric and allocentric visuospatial working memory in premotor Huntington's disease: A double dissociation with caudate and hippocampal volumes. Neuropsychologia 101:57-64.
Poudel GR, Driscoll S, Domínguez DJ, Stout JC, Churchyard A, Chua P, Egan GF, Georgiou-Karistianis N. 2015a. Functional Brain Correlates of Neuropsychiatric Symptoms in Presymptomatic Huntington's Disease: The IMAGE-HD Study. J Huntingtons Dis 4(4):325-32.
Poudel GR, Egan GF, Churchyard A, Chua P, Stout JC, Georgiou-Karistianis N. 2014a. Abnormal synchrony of resting state networks in premanifest and symptomatic Huntington disease: the IMAGE-HD study. J Psychiatry Neurosci 39(2):87-96.
Poudel GR, Harding IH, Egan GF, Georgiou-Karistianis N. 2019. Network spread determines severity of degeneration and disconnection in Huntington's disease. Hum Brain Mapp 40(14):4192-4201.
Poudel GR, Stout JC, Domínguez DJ, Churchyard A, Chua P, Egan GF, Georgiou-Karistianis N. 2015b. Longitudinal change in white matter microstructure in Huntington's disease: The IMAGE-HD study. Neurobiol Dis 74:406-12.
Poudel GR, Stout JC, Domínguez DJ, Gray MA, Salmon L, Churchyard A, Chua P, Borowsky B, Egan GF, Georgiou-Karistianis N. 2015c. Functional changes during working memory in Huntington's disease: 30-month longitudinal data from the IMAGE-HD study. Brain Struct Funct 220(1):501-12.
Poudel GR, Stout JC, Dominguez DJ, Salmon L, Churchyard A, Chua P, Georgiou-Karistianis N, Egan GF. 2014b. White matter connectivity reflects clinical and cognitive status in Huntington's disease. Neurobiol Dis 65:180-7.
Power BD, Looi JC. 2015. The thalamus as a putative biomarker in neurodegenerative disorders. Aust N Z J Psychiatry 49(6):502-18.
Purves P, Cabeza R., Huettel, S., LaBar, K., Platt, M., Woldorff, M. 2012. Principles of Cognitive Neuroscience. Sunderland, MA.: Sinauer Associates, Inc. .
Qiu A, Brown T, Fischl B, Ma J, Miller MI. 2010. Atlas generation for subcortical and ventricular structures with its applications in shape analysis. IEEE Trans Image Process 19(6):1539-47.
Ramirez-Garcia G, Galvez V, Diaz R, Bayliss L, Fernandez-Ruiz J, Campos-Romo A. 2020. Longitudinal atrophy characterization of cortical and subcortical gray matter in Huntington's disease patients. Eur J Neurosci 51(8):1827-1843.
Ransome MI, Renoir T, Hannan AJ. 2012. Hippocampal Neurogenesis, Cognitive Deficits and Affective Disorder in Huntington's Disease. Neural Plasticity.
Ratovitski T, Chighladze E, Arbez N, Boronina T, Herbrich S, Cole RN, Ross CA. 2012. Huntingtin protein interactions altered by polyglutamine expansion as determined by quantitative proteomic analysis. Cell Cycle 11(10):2006-21.
Rawlins MD, Wexler NS, Wexler AR, Tabrizi SJ, Douglas I, Evans SJ, Smeeth L. 2016. The Prevalence of Huntington's Disease. Neuroepidemiology 46(2):144-53.

Reiner A, Deng YP. 2018. Disrupted striatal neuron inputs and outputs in Huntington's disease. CNS Neurosci Ther 24(4):250-280.
Rigamonti D, Bauer JH, De-Fraja C, Conti L, Sipione S, Sciorati C, Clementi E, Hackam A, Hayden MR, Li Y and others. 2000. Wild-type huntingtin protects from apoptosis upstream of caspase-3. J Neurosci 20(10):3705-13.
Rigamonti D, Sipione S, Goffredo D, Zuccato C, Fossale E, Cattaneo E. 2001. Huntingtin's neuroprotective activity occurs via inhibition of procaspase-9 processing. J Biol Chem 276(18):14545-8.
Roos R, Pruyt J, de Vries J, Bots G. 1985. Neuronal distribution in the putamen in Huntington's disease. Journal of Neurology, Neurosurgery and Psychiatry 48(5):422-5.
Rosas HD, Lee SY, Bender AC, Zaleta AK, Vangel M, Yu P, Fischl B, Pappu V, Onorato C, Cha JH and others. 2010. Altered white matter microstructure in the corpus callosum in Huntington's disease: Implications for cortical "disconnection". Neuroimage 49(4):2995-3004.
Rosas HD, Reuter M, Doros G, Lee SY, Triggs T, Malarick K, Fischl B, Salat DH, Hersch SM. 2011. A Tale of Two Factors: What Determines the Rate of Progression in Huntington's Disease? A Longitudinal MRI Study. Movement Disorders 26(9):1691-1697.
Rosas HD, Salat DH, Lee SY, Zaleta AK, Pappu V, Fischl B, Greve D, Hevelone N, Hersch SM. 2008. Cerebral cortex and the clinical expression of Huntington's disease: complexity and heterogeneity. Brain 131:1057-1068.
Rosas HD, Tuch DS, Hevelone ND, Zaleta AK, Vangel M, Hersch SM, Salat DH. 2006. Diffusion tensor imaging in presymptomatic and early Huntington's disease: Selective white matter pathology and its relationship to clinical measures. Movement Disorders 21(9):1317-1325.
Rosen AC, Sugiura L, Kramer JH, Whitfield-Gabrieli S, Gabrieli JD. 2011. Cognitive Training Changes Hippocampal Function in Mild Cognitive Impairment: A Pilot Study. Journal of Alzheimers Disease 26:349-357.
Rosenblatt A, Kumar BV, Mo A, Welsh CS, Margolis RL, Ross CA. 2012. Age, CAG repeat length, and clinical progression in Huntington's disease. Movement Disorders 27(2):272-276.
Rosenblatt A, Liang KY, Zhou H, Abbott MH, Gourley LM, Margolis RL, Brandt J, Ross CA. 2006. The association of CAG repeat length with clinical progression in Huntington disease. Neurology 66(7):1016-1020.
Ross CA, Tabrizi SJ. 2011. Huntington's disease: from molecular pathogenesis to clinical treatment. Lancet Neurol. 10(1):83-98.
Rossi S, Prosperetti C, Picconi B, De Chiara V, Mataluni G, Bernardi G, Calabresi P, Centonze D. 2006. Deficits of glutamate transmission in the striatum of toxic and genetic models of Huntington's disease. Neurosci Lett 410(1):6-10.
Rowe KC, Paulsen JS, Langbehn DR, Wang C, Mills J, Beglinger LJ, Smith MM, Epping EA, Fiedorowicz JG, Duff K and others. 2012. Patterns of serotonergic antidepressant usage in prodromal Huntington disease. Psychiatry Research 196(2-3):309-314.
Rubinsztein DC, Leggo J, Coles R, Almqvist E, Biancalana V, Cassiman JJ, Chotai K, Connarty M, Craufurd D, Curtis A and others. 1996. Phenotypic characterization of individuals with 30-40 CAG repeats in the Huntington disease (HD) gene reveals HD cases with 36 repeats and apparently normal elderly individuals with 36-39 repeats. American Journal of Human Genetics 59(1):16-22.
Ruocco HH, Bonilha L, Li LM, Lopes-Cendes I, Cendes F. 2008. Longitudinal analysis of regional grey matter loss in Huntington disease: effects of the length of the expanded CAG repeat. J Neurol Neurosurg Psychiatry 79(2):130-5.

Sadeh T, Shohamy D, Levy DR, Reggev N, Maril A. 2011. Cooperation between the hippocampus and the striatum during episodic encoding. J Cogn Neurosci 23(7):1597-608.
Sassone J, Colciago C, Cislaghi G, Silani V, Ciammola A. 2009. Huntington's disease: the current state of research with peripheral tissues. Exp Neurol 219(2):385-97.
Saudou F, Humbert S. 2016. The Biology of Huntingtin. Neuron 89(5):910-26.
Scahill RI, Hobbs NZ, Say MJ, Bechtel N, Henley SM, Hyare H, Langbehn DR, Jones R, Leavitt BR, Roos RA and others. 2013. Clinical impairment in premanifest and early Huntington's disease is associated with regionally specific atrophy. Hum Brain Mapp 34(3):519-29.
Scahill RI, Zeun P, Osborne-Crowley K, Johnson EB, Gregory S, Parker C, Lowe J, Nair A, O'Callaghan C, Langley C and others. 2020. Biological and clinical characteristics of gene carriers far from predicted onset in the Huntington's disease Young Adult Study (HD-YAS): a cross-sectional analysis. Lancet Neurol 19(6):502-512.
Sellers J, Ridner SH, Claassen DO. 2020. A Systematic Review of Neuropsychiatric Symptoms and Functional Capacity in Huntington's Disease. J Neuropsychiatry Clin Neurosci 32(2):109-124.
Seredenina T, Luthi-Carter R. 2012. What have we learned from gene expression profiles in Huntington's disease? Neurobiol Dis 45(1):83-98.
Shishegar R, Rajapakse S, Georgiou-Karistianis N. 2019. Altered Cortical Morphometry in Pre-manifest Huntington's Disease: Cross-sectional Data from the IMAGE-HD Study. Conf Proc IEEE Eng Med Biol Soc 2019:2844-2847.
Smarr KL, Keefer AL. 2011. Measures of depression and depressive symptoms: Beck Depression Inventory-II (BDI-II), Center for Epidemiologic Studies Depression Scale (CES-D), Geriatric Depression Scale (GDS), Hospital Anxiety and Depression Scale (HADS), and Patient Health Questionnaire-9 (PHQ-9). Arthritis Care Res (Hoboken) 63 Suppl 11:S454-66.
Smith A. 1982. Symbol Digit Modality Test (SDMT): Manual (Revised). Los Angeles: Psychological Services.
Soloveva MV, Jamadar SD, Velakoulis D, Poudel G, Georgiou-Karistianis N. 2020. Brain compensation during visuospatial working memory in premanifest Huntington's disease. Neuropsychologia 136:107262.
Solowij N, Walterfang M, Lubman DI, Whittle S, Lorenzetti V, Styner M, Velakoulis D, Pantelis C, Yuecel M. 2013. Alteration to hippocampal shape in cannabis users with and without schizophrenia. Schizophrenia Research 143(1):179-184.
Sørensen S, Fenger K. 1992. Causes of death in patients with Huntington's disease and in unaffected first degree relatives. Journal of Medical Genetics 29(12):911-14.
Spalding KL, Bergmann O, Alkass K, Bernard S, Salehpour M, Huttner HB, Boström E, Westerlund I, Vial C, Buchholz BA and others. 2013. Dynamics of hippocampal neurogenesis in adult humans. Cell 153(6):1219-1227.
Sritharan A, Egan GF, Johnston L, Horne M, Bradshaw JL, Bohanna I, Asadi H, Cunnington R, Churchyard AJ, Chua P and others. 2010. A longitudinal diffusion tensor imaging study in symptomatic Huntington's disease. Journal of Neurology Neurosurgery and Psychiatry 81(3):257-262.
Stahl CM, Feigin A. 2020. Medical, Surgical, and Genetic Treatment of Huntington Disease. Neurol Clin 38(2):367-378.
Stout JC, Paulsen JS, Queller S, Solomon AC, Whitlock KB, Campbell JC, Carlozzi N, Duff K, Beglinger LJ, Langbehn DR and others. 2011. Neurocognitive signs in prodromal Huntington Disease. Neuropsychol. 25(1):1-14.

Stout JC, Ready RE, Grace J, Malloy PF, Paulsen JS. 2003. Factor analysis of the frontal systems behavior scale (FrSBe). Assessment 10(1):79-85.
Strange BA, Witter MP, Lein ES, Moser EI. 2014. Functional organization of the hippocampal longitudinal axis. Nat Rev Neurosci 15(10):655-69.
Stroop JR. 1935. Studies of interference in serial verbal reactions. J. Exp. Psychol. 18(6):643-662.
Styner M, Oguz I, Xu S, Brechbühler C, Pantazis D, Levitt J, Shenton M, Gerig G. 2006. Framework for the statistical shape analysis of brain structures using SPHARM-PDM. Insight Journal 1071:242-50.
Subramaniam S, Sixt KM, Barrow R, Snyder SH. 2009. Rhes, a striatal specific protein, mediates mutant-huntingtin cytotoxicity. Science 324(5932):1327-30.
Sun YM, Zhang YB, Wu ZY. 2017. Huntington's Disease: Relationship Between Phenotype and Genotype. Mol Neurobiol 54(1):342-348.
Tabrizi SJ, Langbehn DR, Leavitt BR, Roos RAC, Durr A, Craufurd D, Kennard C, Hicks SL, Fox NC, Scahill RI and others. 2009. Biological and clinical manifestations of Huntington's disease in the longitudinal TRACK-HD study: cross-sectional analysis of baseline data. Lancet Neurol. 8(9):791-801.
Tabrizi SJ, Scahill RI, Durr A, Roos RAC, Leavitt BR, Jones R, Landwehrmeyer GB, Fox NC, Johnson H, Hicks SL and others. 2011. Biological and clinical changes in premanifest and early stage Huntington's disease in the TRACK-HD study: the 12-month longitudinal analysis. Lancet Neurology 10(1):31-42.
Tabrizi SJ, Workman J, Hart PE, Mangiarini L, Mahal A, Bates G, Cooper JM, Schapira AH. 2000. Mitochondrial dysfunction and free radical damage in the Huntington R6/2 transgenic mouse. Ann Neurol 47(1):80-6.
Tang X, Ross CA, Johnson H, Paulsen JS, Younes L, Albin RL, Ratnanather JT, Miller MI. 2019. Regional subcortical shape analysis in premanifest Huntington's disease. Hum. Brain Mapp. 40(5):1419-1433.
Tate DF, Wade BS, Velez CS, Drennon AM, Bolzenius J, Gutman BA, Thompson PM, Lewis JD, Wilde EA, Bigler ED and others. 2016. Volumetric and shape analyses of subcortical structures in United States service members with mild traumatic brain injury. J Neurol 263(10):2065-79.
Tate DF, Wade BSC, Velez CS, Drennon AM, Bolzenius JD, Cooper DB, Kennedy JE, Reid MW, Bowles AO, Thompson PM and others. 2019. Subcortical shape and neuropsychological function among U.S. service members with mild traumatic brain injury. Brain Imaging Behav. 13(2):377-388.
Teipel SJ, Bayer W, Alexander GE, Bokde AL, Zebuhr Y, Teichberg D, Müller-Spahn F, Schapiro MB, Möller HJ, Rapoport SI and others. 2003. Regional pattern of hippocampus and corpus callosum atrophy in Alzheimer's disease in relation to dementia severity: evidence for early neocortical degeneration. Neurobiol Aging 24(1):85-94.
Teipel SJ, Bayer W, Alexander GE, Zebuhr Y, Teichberg D, Kulic L, Schapiro MB, Möller HJ, Rapoport SI, Hampel H. 2002. Progression of corpus callosum atrophy in Alzheimer disease. Arch Neurol 59(2):243-8.
Teisberg P. 1995. The genetic background of anticipation. J R Soc Med 88(4):185-7.
Tereshchenko AV, Schultz JL, Bruss JE, Magnotta VA, Epping EA, Nopoulos PC. 2020. Abnormal development of cerebellar-striatal circuitry in Huntington disease. Neurology 94(18):e1908-e1915.
The Huntington's Disease Research Group. 1993. A novel gene containing a trinucleotide repeat that is expanded and unstable on Huntington's disease chromosomes. . Cell 72(6):971-83.

Thompson JC, Harris J, Sollom AC, Stopford CL, Howard E, Snowden JS, Craufurd D. 2012. Longitudinal evaluation of neuropsychiatric symptoms in Huntington's disease. J Neuropsychiatry Clin Neurosci 24(1):53-60.
Thompson PM, Hayashi KM, De Zubicaray GI, Janke AL, Rose SE, Semple J, Hong MS, Herman DH, Gravano D, Doddrell DM and others. 2004. Mapping hippocampal and ventricular change in Alzheimer disease. Neuroimage 22(4):1754-66.
Thompson PM, Jahanshad N, Ching CRK, Salminen LE, Thomopoulos SI, Bright J, Baune BT, Bertolín S, Bralten J, Bruin WB and others. 2020. ENIGMA and global neuroscience: A decade of large-scale studies of the brain in health and disease across more than 40 countries. Transl Psychiatry 10(1):100.
Tulving E. 2002. Episodic memory: from mind to brain. Annu Rev Psychol 53:1-25.
Turner LM, Jakabek D, Wilkes FA, Croft RJ, Churchyard A, Walterfang M, Velakoulis D, Looi JC, Georgiou-Karistianis N, Apthorp D. 2016. Striatal morphology correlates with frontostriatal electrophysiological motor processing in Huntington's disease: an IMAGE-HD study. Brain Behav. 6(12):e00511.
van den Bogaard SJA, Dumas EM, Acharya TP, Johnson H, Langbehn DR, Scahill RI, Tabrizi SJ, van Buchem MA, van der Grond J, Roos RAC and others. 2011a. Early atrophy of pallidum and accumbens nucleus in Huntington's disease. J. Neurol. 258(3):412-420.
van den Bogaard SJA, Dumas EM, Ferrarini L, Milles J, van Buchem MA, van der Grond J, Roos RAC. 2011b. Shape analysis of subcortical nuclei in Huntington's disease, global versus local atrophy - Results from the TRACK-HD study. J. Neurol. Sci. 307(1-2):60-68.
van der Plas E, Langbehn DR, Conrad AL, Koscik TR, Tereshchenko A, Epping EA, Magnotta VA, Nopoulos PC. 2019. Abnormal brain development in child and adolescent carriers of mutant huntingtin. Neurology 93(10):e1021-e1030.
van Duijn E, Craufurd D, Hubers AA, Giltay EJ, Bonelli R, Rickards H, Anderson KE, van Walsem MR, van der Mast RC, Orth M and others. 2014. Neuropsychiatric symptoms in a European Huntington's disease cohort (REGISTRY). J Neurol Neurosurg Psychiatry 85(12):1411-8.
van Duijn E, Kingma EM, van der Mast RC. 2007. Psychopathology in verified Huntington's disease gene carriers. J. Neuropsychiatry Clin. Neurosci. 19(4):441-448.
Velakoulis D, Pantelis C, McGorry PD, Dudgeon P, Brewer W, Cook M, Desmond P, Bridle N, Tierney P, Murrie V and others. 1999. Hippocampal volume in first-episode psychoses and chronic schizophrenia - A high-resolution magnetic resonance imaging study. Archives of General Psychiatry 56(2):133-141.
Voermans NC, Petersson KM, Daudey L, Weber B, van Spaendonck KP, Kremer HPH, Fernandez G. 2004. Interaction between the human hippocampus and the caudate nucleus during route recognition. Neuron 43(3):427-435.
Vonsattel JP, Myers RH, Stevens TJ, Ferrante RJ, Bird ED, Richardson EP, Jr. 1985. Neuropathological classification of Huntington's disease. J Neuropathol Exp Neurol 44(6):559-77.
Vonsattel JPG, DiFiglia M. 1998. Huntington disease. Journal of Neuropathology and Experimental Neurology 57(5):369-384.
Wachinger C, Salat DH, Weiner M, Reuter M. 2016. Whole-brain analysis reveals increased neuroanatomical asymmetries in dementia for hippocampus and amygdala. Brain 139(12):3253-3266.
Walker FO. 2007. Huntington's disease. Lancet 369(9557):218-28.

Walterfang M, Looi JC, Styner M, Walker RH, Danek A, Niethammer M, Evans A, Kotschet K, Rodrigues GR, Hughes A and others. 2011. Shape alterations in the striatum in chorea-acanthocytosis. Psychiatry Res 192(1):29-36.
Walterfang M, Luders E, Looi JC, Rajagopalan P, Velakoulis D, Thompson PM, Lindberg O, Ostberg P, Nordin LE, Svensson L and others. 2014. Shape analysis of the corpus callosum in Alzheimer's disease and frontotemporal lobar degeneration subtypes. J Alzheimers Dis 40(4):897-906.
Walterfang M, Wood AG, Barton S, Velakoulis D, Chen J, Reutens DC, Kempton MJ, Haldane M, Pantelis C, Frangou S. 2009a. Corpus callosum size and shape alterations in individuals with bipolar disorder and their first-degree relatives. Prog Neuropsychopharmacol Biol Psychiatry 33(6):1050-7.
Walterfang M, Wood AG, Reutens DC, Wood SJ, Chen J, Velakoulis D, McGorry PD, Pantelis C. 2008. Morphology of the corpus callosum at different stages of schizophrenia: cross-sectional study in first-episode and chronic illness. British Journal of Psychiatry 192(6):429-434.
Walterfang M, Yucel M, Barton S, Reutens DC, Wood AG, Chen J, Lorenzetti V, Velakoulis D, Pantelis C, Allen NB. 2009b. Corpus callosum size and shape in individuals with current and past depression. J Affect Disord 115(3):411-20.
Wang Y, Song Y, Rajagopalan P, An T, Liu K, Chou YY, Gutman B, Toga AW, Thompson PM. 2011. Surface-based TBM boosts power to detect disease effects on the brain: an N=804 ADNI study. Neuroimage 56(4):1993-2010.
Watson C, Andermann F, Gloor P, Jones-Gotman M, Peters T, Evans A, Olivier A, Melanson D, Leroux G. 1992. Anatomic basis of amygdaloid and hippocampal volume measurement by magnetic resonance imaging. Neurology 42(9):1743-50.
Watson D, Wu KD. 2005. Development and validation of the Schedule of Compulsions, Obsessions, and Pathological Impulses (SCOPI). Assessment 12(1):50-65.
Weaver KE, Richards TL, Liang O, Laurino MY, Samii A, Aylward EH. 2009. Longitudinal diffusion tensor imaging in Huntington's Disease. Exp Neurol 216(2):525-9.
Wexler A, Wild EJ, Tabrizi SJ. 2016. George Huntington: a legacy of inquiry, empathy and hope. Brain 139(Pt 8):2326-33.
Wexler NS, Lorimer J, Porter J, Gomez F, Moskowitz C, Shackell E, Marder K, Penchaszadeh G, Roberts SA, Gayan J and others. 2004. Venezuelan kindreds reveal that genetic and environmental factors modulate Huntington's disease age of onset. Proc Natl Acad Sci U S A 101(10):3498-503.
White NM. 2009. Some highlights of research on the effects of caudate nucleus lesions over the past 200 years. Behav Brain Res 199(1):3-23.
White NM, McDonald RJ. 2002. Multiple parallel memory systems in the brain of the rat. Neurobiol Learn Mem 77(2):125-84.
Wijeratne PA, Johnson EB, Eshaghi A, Aksman L, Gregory S, Johnson HJ, Poudel GR, Mohan A, Sampaio C, Georgiou-Karistianis N and others. 2020. Robust Markers and Sample Sizes for Multicenter Trials of Huntington Disease. Ann Neurol 87(5):751-762.
Wijeratne PA, Young AL, Oxtoby NP, Marinescu RV, Firth NC, Johnson EB, Mohan A, Sampaio C, Scahill RI, Tabrizi SJ and others. 2018. An image-based model of brain volume biomarker changes in Huntington's disease. Ann Clin Transl Neurol 5(5):570-582.
Wilkes FA, Abaryan Z, Ching CRK, Gutman BA, Madsen SK, Walterfang M, Velakoulis D, Stout JC, Chua P, Egan GF and others. 2019. Striatal morphology and neurocognitive dysfunction in Huntington disease: The IMAGE-HD study. Psychiatry Res Neuroimaging 291:1-8.

Wilson CJ, Kawaguchi Y. 1996. The origins of two-state spontaneous membrane potential fluctuations of neostriatal spiny neurons. J Neurosci 16(7):2397-410.
Winograd-Gurvich CT, Georgiou-Karistianis N, Evans A, Millist L, Bradshaw JL, Churchyard A, Chiu E, White OB. 2003. Hypometric primary saccades and increased variability in visually-guided saccades in Huntington's disease. Neuropsychologia 41(12):1683-1692.
Wood SJ, Kennedy D, Phillips LJ, Seal ML, Yuecel M, Nelson B, Yung AR, Jackson G, McGorry PD, Velakoulis D and others. 2010. Hippocampal pathology in individuals at ultra-high risk for psychosis: A multi-modal magnetic resonance study. Neuroimage 52(1):62-68.
Yamashita T, Ninomiya M, Acosta PH, Garcia-Verdugo JM, Sunabori T, Sakaguchi M, Adachi K, Kojima T, Hirota Y, Kawase T and others. 2006. Subventricular zone-derived neuroblasts migrate and differentiate into mature neurons in the post-stroke adult striatum. Journal of Neuroscience 26(24):6627-6636.
Younes L, Ratnanather T, Brown T, Aylward E, Nopoulos P, Johnson H, Magnotta VA, Paulsen JS, Margolis RL, Albin RL and others. 2012. Regionally selective atrophy of subcortical structures in prodromal HD as revealed by statistical shape analysis. Hum. Brain Mapp.
Young AB, Shoulson I, Penney JB, Starosta-Rubinstein S, Gomez F, Travers H, Ramos-Arroyo MA, Snodgrass SR, Bonilla E, Moreno H and others. 1986. Huntington's disease in Venezuela: neurologic features and functional decline. Neurology 36(2):244-9.
Zeng HM, Han HB, Zhang QF, Bai H. 2021. Application of modern neuroimaging technology in the diagnosis and study of Alzheimer's disease. Neural Regen Res 16(1):73-79.
Zigmond AS, Snaith RP. 1983. The hospital anxiety and depression scale. Acta Psychiatr. Scand. 67(6):361-70.
Zuccato C, Cattaneo E. 2007. Role of brain-derived neurotrophic factor in Huntington's disease. Progress in Neurobiology 81(5-6):294-330.
Zuccato C, Ciammola A, Rigamonti D, Leavitt BR, Goffredo D, Conti L, MacDonald ME, Friedlander RM, Silani V, Hayden MR and others. 2001. Loss of huntingtin-mediated BDNF gene transcription in Huntington's disease. Science 293(5529):493-498.
Zuccato C, Marullo M, Conforti P, MacDonald ME, Tartari M, Cattaneo E. 2008. Systematic assessment of BDNF and its receptor levels in human cortices affected by Huntington's disease. Brain Pathology 18(2):225-238.
Zuccato C, Tartari M, Crotti A, Goffredo D, Valenza M, Conti L, Cataudella T, Leavitt BR, Hayden MR, Timmusk T and others. 2003. Huntingtin interacts with REST/NRSF to modulate the transcription of NRSE-controlled neuronal genes. Nature Genetics 35(1):76-83.